MODELING, SIMULATION AND OPTIMIZATION OF FLASHED-STEAM GEOTHERMAL POWER PLANTS FROM THE POINT OF VIEW OF NONCONDENSABLE GAS REMOVAL SYSTEMS

A Thesis Submitted to
The Graduate School of Engineering and Sciences of
İzmir Institute of Technology
In Partial Fulfillment of the Requirements for the Degree of

Doctor of Philosophy

in Mechanical Engineering

by
Nurdan YILDIRIM ÖZCAN

June 2010
İZMİR

We approve the thesis of **Nurdan YILDIRIM ÖZCAN**

Assoc. Prof. Dr. Gülden GÖKÇEN AKKURT
Supervisor

Prof. Dr. Macit TOKSOY
Committee Member

Prof. Dr. Mehmet Barış ÖZERDEM
Committee Member

Prof. Dr. Mehmet KANOĞLU
Committee Member

Assoc. Prof. Dr. Harun Kemal ÖZTÜRK
Committee Member

7 June 2010

Prof. Dr. Metin TANOĞLU
Head of the Department of
Mechanical Engineering

Assoc. Prof. Dr. Talat YALÇIN
Dean of the Graduate School of
Engineering and Sciences

ACKNOWLEDGEMENTS

Foremost, I would like to express my sincere gratitude to my advisor Assoc. Prof. Dr. Gülden Gökçen Akkurt for the continuous support of my Ph.D. study. Her guidance helped me in all the time of research and writing of this Thesis. In private life, she acts like a sister to support and listen to me during my difficult times.

Besides my advisor, I would like to thank my thesis progress committee members: Prof. Dr. M. Barış Özerdem and Assoc. Prof. Dr. Harun Kemal Öztürk for their encouragement and insightful comments. Especially, Assoc. Prof. Dr. Harun Kemal Öztürk had to travel at several times from Denizli to Izmir because of my thesis progress meetings. I am really grateful to him.

My sincere thanks also go to Prof. Dr. Pall Valdimarsson, my supervisor in 2002, from United Nations University (UNU) Geothermal Training Programme, Reykjavik-Iceland. Until that time, he always has been in contact with me and visited several times in Turkey. He is always supported and helped me on my studies by sharing his immense knowledge and literature. In this point I would like to repeat my thanks to Dr. Ingvar B. Fridleifsson who is head of the UNU Geothermal Training Programme, Reykjavik-Iceland and all of the teachers and lecturers of the Programme. Because I learned lot of thinks about geothermal energy in during six-month education. Besides this, even after graduated they have always supported to me spiritually as well as financially to attend the World Geothermal Congress 2005 in Antalya, Turkey and World Geothermal Congress 2010 in Bali, Indonesia.

My special thanks also go to my friends for sharing their friendships with me and not forgetting to me best friends who always been there.

Last but not the least; I owe my loving thanks to my husband Orhan Özcan, my three-year old daughter Gül Hepsev Özcan. They have lost a lot due to my Ph.D. studies. My deepest gratitude goes to my family: my father, mother and brother for their unflagging love and support throughout my life; especially for looking after my little daughter most of the time throughout my studies. Without their encouragement and understanding it would not have been possible to finilise this dissertation.

ABSTRACT

MODELING, SIMULATION AND OPTIMIZATION OF FLASHED-STEAM GEOTHERMAL POWER PLANTS FROM THE POINT OF VIEW OF NONCONDENSABLE GAS REMOVAL SYSTEMS

Geothermal fluids contain noncondensable gases (NCGs) at various amounts. The presence of NCGs in geothermal steam results with a dramatic decrease in net power output increasing condenser pressure and total auxiliary power consumption. Hence, NCGs should be withdrawn by a gas removal equipment to improve the performance of geothermal power plants (GPPs). The flashed-steam GPPs (single-flash, double-flash) are a relatively simple way to convert geothermal energy into electricity when the geothermal wells produce a mixture of steam and liquid. The primary aim of the Thesis is to model and develop a code to simulate flashed-steam GPPs to examine the thermodynamic and economical performance of NCG removal systems, which are major concerns at planning and basic design stages of GPPs. The model is validated comparing model output with Kizildere GPP output, classified as deterministic and static. The model is simulated to identify the effects of input variables which are NCG fraction, separator pressure, condenser pressure, wet bulb temperature, interest rate, tax rate, O&M cost ratio and electricity sales price. Among the variables, NCG fraction is the most significant parameter affecting thermodynamic performance and profitability of flashed-steam GPPs. The net power output and overall exergetic efficiency of single-flash GPP is decreased 0.4% for compressor system (CS), 2.2% for hybrid system (HS), 2.5% for reboiler system (RS) and 2.7% for steam jet ejector system (SJES) by 1% increase in NCG fraction. Based on thermodynamic and economical simulations, SJES, HS and CS can be recommended to be used for a NCG fraction range of 0-2%, 2-10% and >10%, respectively. Furthermore, thermodynamic performance of single-flash plants can be improved by adding second flash by 45.5-127.9%.

ÖZET

FLAŞ BUHARLI JEOTERMAL ELEKTRİK SANTRALLARININ GAZ AYIRMA SİSTEMLERİ AÇISINDAN MODELLENMESİ, SİMÜLASYONU VE OPTİMİZASYONU

Jeotermal akışkanlar değişik miktarlarda yoğuşmayan gazlar (YGlar) içerir. Jeotermal buhardaki YGların varlığı kondenser basıncını ve santralın toplam iç tüketimi arttırarak santral net güç üretiminde önemli boyutlarda düşüşe neden olurlar. Bu nedenle, YGlar jeotermal elektrik santrallarının (JESlarının) performansını iyileştirmek için gaz ayırma ekipmanları ile sistemden uzaklaştırılmalıdır. Flaş-buharlı JESları (tek-flaşlı ve ikincil-flaşlı) jeotermal kuyulardan buhar ve sıvı karışımı üretilmesi durumunda, jeotermal enerjinin elektrik enerjisine çevrilmesindeki en basit yollardan biridir. Tezin ana amacı, flaş-buharlı JESlarının, dizayn ve planlama aşamalarında büyük önemi olan gaz ayırma sistemlerinin termodinamik ve ekonomik performansını belirlemek için modellenmesi ve simülasyonu için bir kod geliştirilmesidir. Modelden elde edilen sonuçların Kizildere JES verileri ile karşılaştırılması ile doğrulanan model, statik ve determinist olarak sınıflandırılır. YG oranı, separatör basıncı, kondenser basıncı, yaş termometre sıcaklığı, faiz oranı, vergi oranı, işletme ve bakım giderleri oranı ve elektrik satış fiyatı gibi model girdilerinin etkilerini belirleyebilmek için simülasyonlar yapılmıştır. Girdiler arasında, YG oranı, flaş-buharlı JESlarının performansını ve karlılığını etkileyen en önemli parametredir. Tek-flaşlı JESnın net güç üretimi ve çevrim ekserji verimi YG oranındaki %1'lik artış ile, kompresör sisteminde %0.4, hibrid sisteminde %2.2, reboyler sisteminde %2.5 ve buhar jet ejektörü sisteminde %2.7 oranında azalmaktadır. Termodinamik ve ekonomik simülasyon sonuçlarına bağlı olarak, buhar jet ejektörü, hibrid ve kompresör sistemlerinin YG oranlarına göre sırasıyla %0-2, %2-10 ve >%10 aralıklarında kullanılması tavsiye edilir. Ayrıca, tek-flaşlı JESnın termodinamik performansı, ikincil-flaş uygulanması durumunda %45.5-127.9 oranında arttırılabilir.

The Thesis is dedicated to my father Hamdi YILDIRIM, who always has been excited to see me as a doctor and my daughter, Gül Hepsev ÖZCAN, who had to live most of the time without me throughout my dissertation studies.

TABLE OF CONTENTS

LIST OF FIGURES

LIST OF TABLES

LIST OF SYMBOLS AND ABBREVIATIONS

AC : Amortization cost (USD/year)

AS : Air-steam ratio (-)

B : Benefit

BV : Book value (USD)

C : Cost

C_p : Constant pressure specific heat (kJ/kgK)

C_v : Constant volume specific heat (kJ/kgK)

E : Entrainment ratio (-)

Er : Expansion ratio

$\dot{E}x$: Exergy (kW)

f : Noncondensable gas fraction (% weigth od steam)

h : Enthalpy (kJ/kg)

i : Annual interest rate or discount rate

I : Exergy loss (kW)

IRR : Internal rate of return

k : The accomplishment date of a project (deadline of construction)

M : Molar mass (kg/kmol)

$\dot{m}$: Mass flowrate (kg/s)

NPV : Net present value

OM : Operation-Maintenance cost (USD/year)

P : Pressure (kPa)

Rev : Revenue (USD/year)

Ru : Universal gas constant, 8.314 kJ/(kmol K)

$\dot{Q}$: Heat load (kW)

s : Entropy (kJ/kgK)

t : The number of the periods for the project exploitation

T : Temperature (K)

TAE : Total air equivalent (kg/s)

Tax : Tax cost (USD)

TI : Taxable income (USD)

TR : Tax rate (%)

$\dot{V}$: Volume flowrate (m^3/s);

W : Mass of circulating water per unit mass of dry air (-);

$\dot{W}$: Power/Work (kW)

x : Quality (-)

Greek letters

η : Efficiency (%)

υ : the specific volume of the water vapor (m^3/kg)

ΔP : Pressure drop (Pa)

γ : Cp/Cv (-)

ΔT : Temperature difference (°C)

ω : Humidity ratio (-)

Subscripts

0 : Refers to the environmental state

a : Dry air

ac : After-condenser

air, A : Air inlet

air, B : Air outlet

aux : Auxiliary

CO_2 : Carbon dioxide

comp : Compressor

con : Condenser

ct : Cooling tower

cw : Cooling water

dem : Demister

desired : Desired

destroyed : Irreversibilities

Ex : Exergetic

exhaust : Exhaust

fan : Fan

gen : Generator

grs : Gas removal system

heatloss,pipe : Heatloss of pipe
HPC : High pressure compressor
i : Indice for steam jet ejectors
ic : Inter-condenser
in : Input/ inlet
is : Isentropic
l : liquid stream
LPC : Low pressure compressor
LRVP : Liquid ring vacuum pump
motor, fan : Motor fan
motor, pump : Motor pump
n : Number of the years
NCG : Noncondensable gases
net : Net
out : Output/ outlet
overall : Overall
pump : Pump
reboiler : Reboiler
s : Steam stream
sep : Separator
sje : Steam jet ejector
tur : Turbine
waste : Waste

Abbreviations

CS : Compressor system
EES : Engineering equation solver
EPDK : Energy market regulatory authority of Turkey
GPP : Geothermal power plant
HPC : High pressure compressor
HS : Hybrid system
IRR : Internal rate of return
LPC : Low pressure compressor
LRVP : Liquid ring vacuum pump

NCG : Noncondensable gas

NPV : Net present value

RS : Reboiler system

SJE : Steam jet ejector

SJES : Steam jet ejector system

SPT : Simple payback time

CHAPTER 1

INTRODUCTION

High temperature geothermal fluids are widely used for electricity production and total installed geothermal power plant (GPP) capacity in the World has reached to 10,715 MW and 520 units in 2010. An increase of approximately 20% in the five year term 2005-2010 has been achieved, following the rough standard linear trend of 350 MW/year, with an evident increment of the average value of about 200 MW/year in the precedent 2000-2005 period (Bertani, 2010). In Turkey, geothermal power development initiated with Kizildere GPP in 1984 and paused 22 years until 2006 due to lack of legislative framework. Since enaction of the Renewable Energy Law (2005) and the Law on Utilization of Renewable Energy Resources for the Purpose of Generating Electrical Energy (2007), investors have shown a significant interest on GPP construction. From 2006 to 2010 geothermal power installed capacity increased by 388% and an addition of 153 MW capacity license is issued by Energy Market Regulatory Authority of Turkey (EPDK) (EPDK, 2010).

Geothermal power can be produced by dry steam, flashed-steam, binary and Kalina plants depending on the temperature and state of the geothermal fluid. Flashed-steam (single and double-flash) GPPs are the most commonly used power generation systems with a total share of 61% within the installed capacity in the World, mainly because most geothermal reservoirs are formed by liquid dominated hydrothermal systems (Bertani, 2010). Similar to the global trends, flashed-steam GPPs constitute 68% of total GPP installed capacity in Turkey (Aksoy, 2007; Serpen et al., 2008; Durak, 2009; EPDK, 2010).

Geothermal steam, which flows through the entire cycle of conventional (dry and flashed-steam) GPPs, contains higher concentration of noncondensable gases (NCGs) (CO_2, H_2S, NH_3, N_2, CH_4 etc.) compared with conventional fossil-fueled power plants. The amount of NCGs contained in geothermal steam has significant impact on the power production performance of a GPP. Depending on the resource, the fraction of the NCGs varies over the World from almost zero to as much as 25% by weight of steam (Hall, 1996; Coury et al., 1996).

The NCGs in geothermal steam interfere with heat transfer in the condenser by forming a 'gas-blanketing' effect, which raises the condenser temperature and back-pressure on the turbine, reducing its output. In practice, the gases' effect can only be overcome by evacuating them, along with a portion of steam (Vorum and Fritzler, 2000). The power needed to extract the NCGs from the condensers and exhaust them to the atmosphere or an abatement system is supplied from the generated electricity; this seriously impairs the power production performance (Duthie and Nawaz, 1989). NCGs also decrease the exergy of the fluid reducing the available work in the plant. Thus, evaluation of the net work of the turbine should consider the NCG content (Montero, 1990). Comparing with fossil-fuelled power plants, GPPs require larger capacity NCG removal systems which occupy large portion in total plant cost. Therefore, selection of NCG removal system becomes a major concern at planning and basic design stages which aim to maximize net power output and minimize both investment and operation and maintenance (O&M) costs of GPPs in a long-term perspective (Tajima and Nomura, 1982; Hankin et al., 1984).

The commonly used conventional NCG removal systems are steam jet ejector (SJE)s, liquid ring vacuum pumps (LRVPs), centrifugal compressors and hybrid system (HS)s. Besides, innovative upstream RSs. are another approach to remove NCGs from geothermal steam before they enter the turbine. Recently, in GPPs hybrid NCG removal system (SJE and LRVP) are most common. Some flashed steam GPPs and the type of NCG removal systems employed are given in Table 1.1.

Table 1.1. Some flashed steam GPPs and the type of NCG removal systems employed. (Source: Kwambai, 2010; Horie et al., 2010; Moya and DiPippo, 2010; Wallace et al., 2009)

Name of GPP	Type of GPP	Number of Stage	Type of NCG Removal System
Miravalles Unit-3, Costa-Rica	Single-flash	3	2-SJE and LRVP
Kawerau, New Zealand	Double-flash	3	2-SJE and LRVP
Gurmat, Turkey	Double-flash	2	SJE and LRVP
Olkaria-1, Kenya	Single-flash	2	SJE
Kizildere-Turkey	Single-flash	3	Compressor

The complex and unique nature of GPPs reveals to use design and simulation software. The majority of existing commercial software are developed for reservoir and geothermal field modeling (Milicich, et al., 2010; Tanaka and Itoi, 2010; Holzbecher and Sauter, 2010), borehole heat exchangers and heat pumps (Kim et al., 2010; Cisarova et al., 2010), geochemical modeling of geothermal fluids (Hasse et al., 2006; Putten and Colonna, 2007) and direct use applications (HeatMap, 2010). There exists several software to design and simulate GPPs. The oldest known is GEOCOST (Bloomster et al., 1975), which includes only steam jet ejectors as NCG removal system, not applicable to high NCG fields. The other software is RetScreen is a power plant design software includes GPP module (RetScreen, 2010). GPP module of RetScreen does not include information of NCG removal system information. GETEM determines the performance of flashed-steam GPPs considering only steam jet ejector and LRVP as NCG removal system (GETEM, 2010). The most comprehensive and costly software, is ASPEN-HYSYS, which is a modeling tool for conceptual design, optimization, business planning, asset management, and performance monitoring of energy systems It is possible to make mass and energy balance with software but there is no information about NCG removal system (Aspen-HYSYS, 2010). Since there is a substantial lack of design and simulation software of GPPs including NCG gas removal alternatives, the Thesis aims to develop a model to provide a guide or reference which could quickly and easily be used to determine the GPP gas removal system which maximizes the power output at minimum cost. The model includes mass, energy and exergy balances, and economical analysis under steady-state, steady-flow conditions.

Systems and processes that degrade the quality of energy resources can only be identified through a detailed thermodynamic analysis of the whole system. Most cases of thermodynamic imperfection cannot be detected by an energy balance. A careful evaluation of processes using exergy balance enables the identification of the source of inefficiencies and waste, which leads to improved designs and resultant savings. Exergy balance is a tool for identifying the types, locations and magnitudes of thermal losses. Identifying and quantifying these losses allows for the evaluation and improvement of the designs of thermodynamic systems (Rosen, 1999; 2002; Rosen and Dincer, 2001; Kwambai, 2005).

The prime objective of every project is to be profitable. For a geothermal project, profits are related to the difference between the price obtained for power and the cost of producing it. The financial structure, conditions and capital, operational and

maintenance (O&M) and financial costs are important factors influencing the levelized cost of energy and profitability of the project. The economical viability of GPPs can be evaluated by various methods including net present value (NPV), internal rate of return (IRR) and simple payback time (SPT) methods, and cost of electricity production.

The aim of the Thesis is manifold:

a. Modeling of flashed-steam GPPs with particular emphasis on NCG removal systems,
b. Development of a code based on mass, energy and exergy balances, and economical analysis,
c. Validation of the model for Kizildere GPP, which is a single-flash plant,
d. Thermodynamic simulation of flashed-steam GPPs depending on geothermal field (NCG fraction, separator pressure), plant (condenser pressure and turbine inlet temperature), and environmental parameters (wet bulb temperature),
e. Economical simulation of flashed-steam GPPs depending on interest rate, tax rate, O&M cost ratio, electricity sales price,

The static model is developed for flashed-steam (single and double-flash) GPPs with different NCG removal system options which are compressor system (CS), steam jet ejector system (SJES), hybrid (steam jet ejector and LRVP) system (HS) and reboiler system (RS). A code is developed by Engineering Equation Solver (EES) (F-Chart, 2010) including mass, energy and exergy balances for each plant component. Economical model consists of NPV, IRR and SPT methods, and cost of electricity production. The model is validated by Kizildere GPP data. Then the simulation is performed on the disturbances of input parameters which are geothermal field (NCG fraction, separator pressure), plant (condenser pressure and turbine inlet temperature), environmental (wet bulb temperature) and economical (interest rate, tax rate, O&M cost ratio, electricity sales price) parameters.

In the Thesis, in Chapter 2, geothermal power production and NCG removal systems are introduced. General literature survey on NCG removal systems are summarized in Chapter 3. While the detailed information about mass, energy and exergy balances, and economical analysis in the model are given in Chapter 4, the methodology of the model is explained in Chapter 5. The results of the modeling and simulation given in Chapter 6, are summarized in Chapter 7. Finally, Conclusions take place in Chapter 8.

CHAPTER 2

GEOTHERMAL POWER PRODUCTION AND NCG REMOVAL SYSTEMS

The word **geothermal** comes from the Greek words geo (earth) and therme (heat). Geothermal energy is energy from the depths of the earth. It originates from the earth's molten interior and from the decay of radioactive materials in underground rocks. The heat is brought near the surface by crustal plate movements, by deep circulation of groundwater and by intrusion of molten magma. In some places the heat rises to the surface in natural streams of steam or hot water. In the history, geothermal resources have been used in many ways, including healing and physical therapy, cooking, space heating, and bathing. One of the first known human use of geothermal resources was more than 10,000 years ago with the settlement of Paleo-Indians at hot springs as bathing and cooking. Geothermal resources have since been developed for many applications as given in Lindal diagram such as electricity production and direct use applications. The Lindal diagram (Figure 2.1) shows examples of current and potential uses of geothermal energy in terms of resource temperature.

Prince Piero Ginori Conti invented the first GPP in 1904, at the Larderello dry steam field in Italy (Dickson and Fanelli, 2004). In 1958 a small GPP began operating in New Zealand. The first GPPs in the United States were operated in 1960 at The Geysers in Sonoma County, California, with a capacity of 11 MW (World Energy Council, 2010; Crest, 2008).

Direct use applications include space and district heating, industrial process heating, snow melting, drying, greenhouse heating, aquaculture.

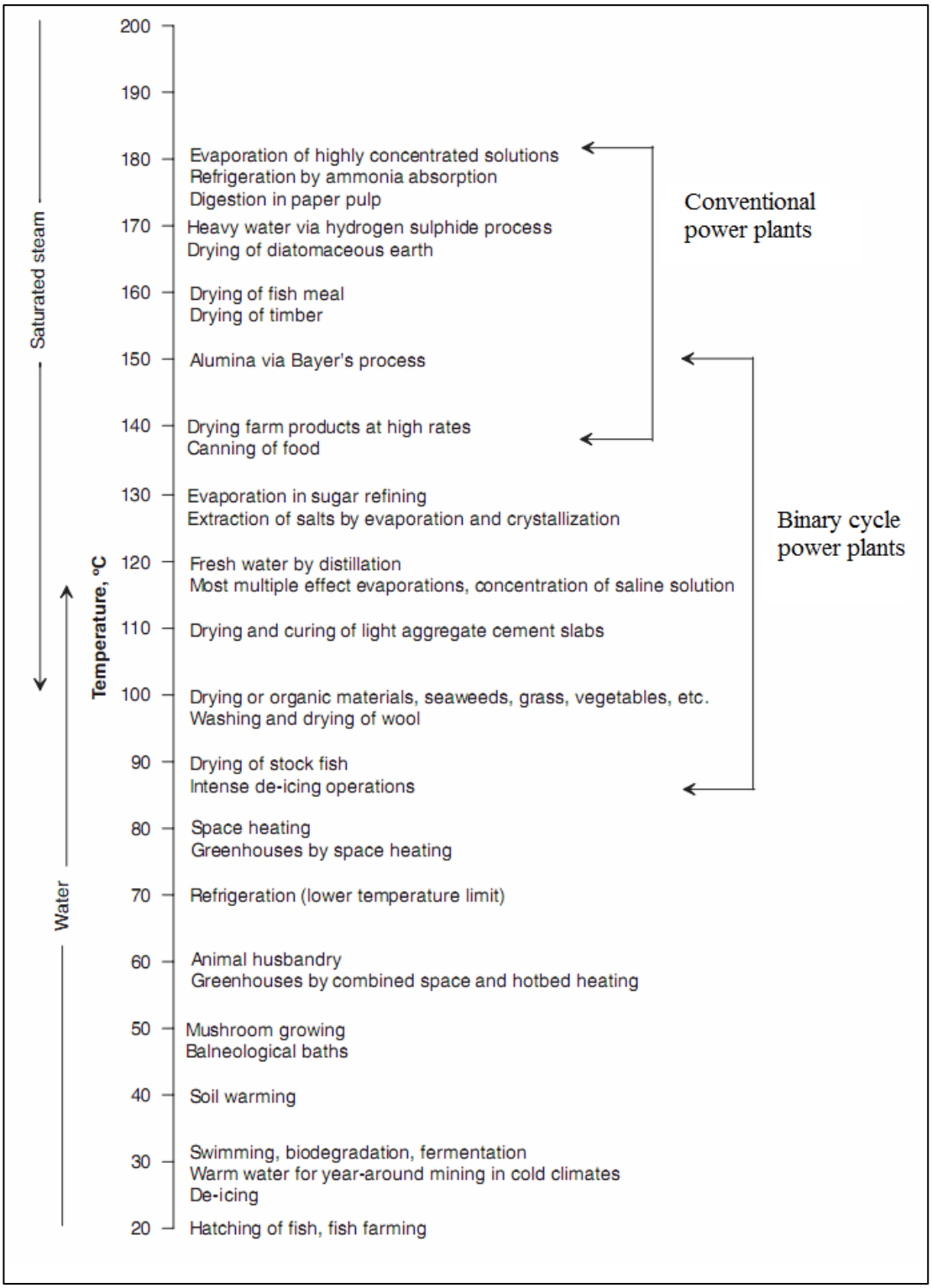

Figure 2.1. Lindal diagram.
(Source: Gupta and Roy, 2007)

2.1. Geothermal Power Production

Geothermal resources are like human fingerprints, no two are exactly alike. A geothermal resource may have geothermal fluid in the following thermodynamic states: (1) saturated or superheated vapor (dry steam), (2) saturated liquid-steam mixture (wet steam) and (3) saturated or compressed liquid (brine). Different technologies are used to produce power depending on the state of geothermal fluid extracted. GPPs operating in the World are basically of four types: dry steam, flashed-steam, binary and Kalina power plants (Kanoglu, 1999).

The simplest and cheapest GPPs are dry steam GPPs (Figure 2.2-a). Steam from the geothermal well is simply passed through a steam turbine, which convert the thermal energy extracted from pressurized steam into useful mechanical energy. Then mechanical energy is then converted into electricity by the generator. Dry steam GPPs have a condenser at the exit of the turbines and cooling towers. The Geysers GPPs in The United States and the Larderello GPP in Italy are example for dry steam GPPs in the World.

A hot water reservoir (such as Wairakei in New Zealand) is used in a flashed-steam power plant, in which hot fluids with temperatures usually in excess of 180^{o}C are brought up to the surface through a production well where, upon being released from the pressure of the deep reservoir, some of the water flashes into steam in a separator (Figure 2.2-b). The steam powers the turbines then is cooled, condensed and either used in the cooling system of the plant or injected back into the reservoir. Since most geothermal reservoirs are formed by liquid dominated hydrothermal systems, flashed-steam GPPs are the most commonly used GPPs in the World.

Low-to-medium temperature geothermal reservoirs which are between about 85 and 150^{o}C are not hot enough to flash enough steam but can still be used to produce electricity in a binary power plant (also, referred as Organic Rankine Cycle (ORC) power plants). In a binary GPP (Figure 2.2-c), the geothermal fluid is passed through a heat exchanger, where its heat is transferred into a low-boiling point binary (secondary) fluid such as propane, iso-butane, iso-pentane or ammonia. When heated, the binary liquid flashes into vapor, expands and powers the turbines. The vapor is then re-condensed and used repeatedly (Gupta and Roy, 2007).

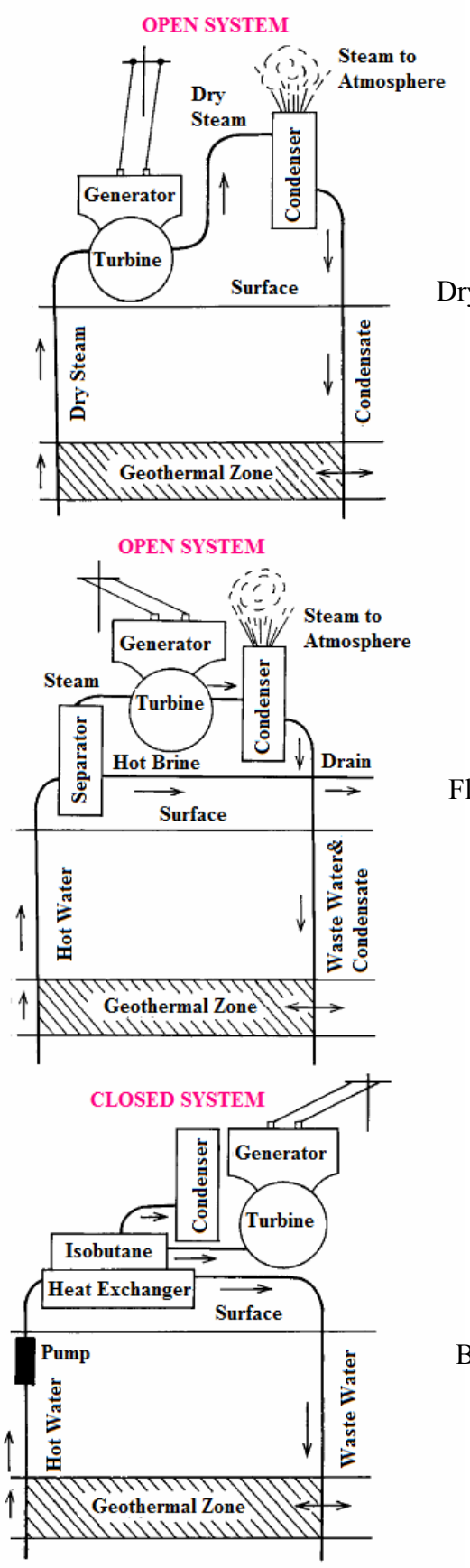

Dry Steam GPPs

(a)

Flashed-Steam GPPs

(b)

Binary GPPs

(c)

Figure 2.2. Basic GPP types.
(Source: Gupta and Roy, 2007)

Kalina cycle (Figure 2.3) is another cycle used in GPPs for low temperature resources.

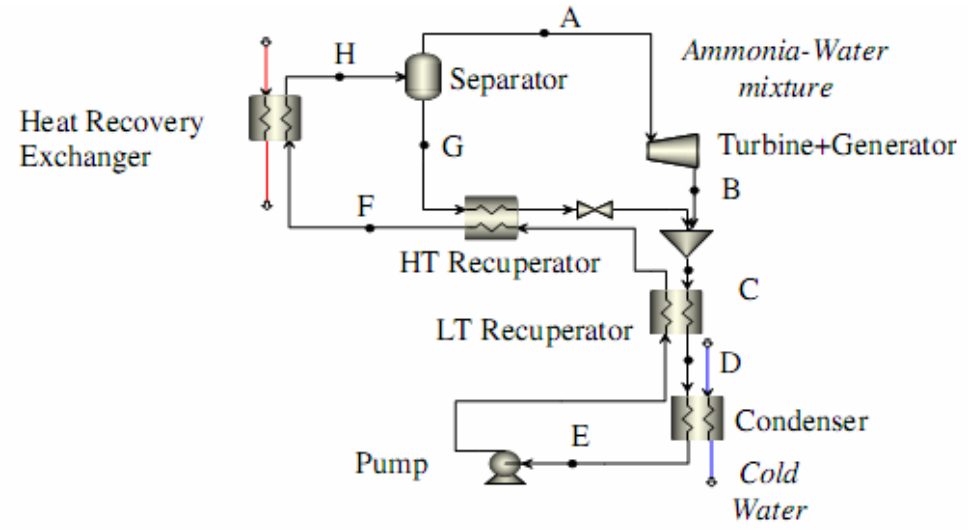

Figure 2.3. Kalina cycle.
(Source: Bombarda et al., 2010)

The Kalina cycle is principally a modified Rankine cycle. The transformation starts with an important process change to the Rankine cycle, changing the working fluid in the cycle from a pure component (typically water) to a mixture of ammonia and water. In comparison with binary GPPs, the main advantages of Kalina GPPs lie in higher thermodynamic efficiency, producing less emission and requiring less energy. The Kalina cycle technology is presently undergoing active testing in Iceland, and it will take some more time to demonstrate the actual improvement in efficiency resulting from its use (Mlcak, 1996; Kalina, 2003; Gupta and Roy, 2007; Swandaru, 2009; Geothermania, 2010; DiPippo, 2005; Kanoglu, 1999).

There are some geothermal resources that demand more sophisticated energy conversion systems than the basic ones explained before. Furthermore, energy conversion systems have evolved to fit the needs of specific developing fields by integrating different types of power plant into a unified, complex enterprise such as double-flash, combined single and double flash, combined flash and binary, combined flash and kalina etc. As an example in Figure 2.4 a simplified schematic diagram of a double-flash plant, is an improvement on the single-flash plant design, is illustrated. Main equipment of double-flash GPPs are a high and low pressure separator, a high and low pressure turbine, a condenser, a cooling tower and circulation water pump and a

NCG removal system. In the double-flash plant, the steam from the single-flash turbine exhaust is directed to the low pressure turbine instead of directly to the condenser. Then, it is combined with the steam from the low pressure separator (DiPippo, 2005; Swandaru, 2009).

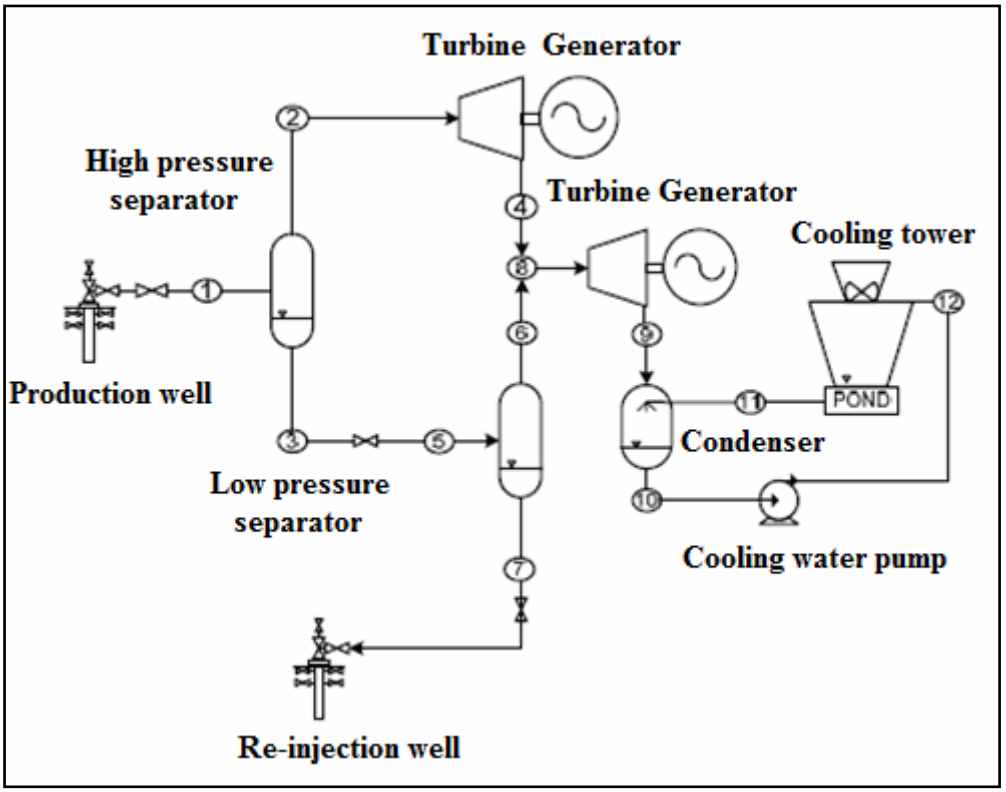

Figure 2.4. Simplified flow diagram of a double-flash GPP.
(Source: Swandaru, 2009)

2.1.1. Geothermal Power Production in the World

An acceleration of power production from geothermal resources continues to increase in recent years (Figure 2.5). By the year of 2010, 35 countries are engaged in producing electric power from geothermal energy resources. The total installed capacity is about 10,715 MW from 526 power generating units (Bertani, 2005; 2010).

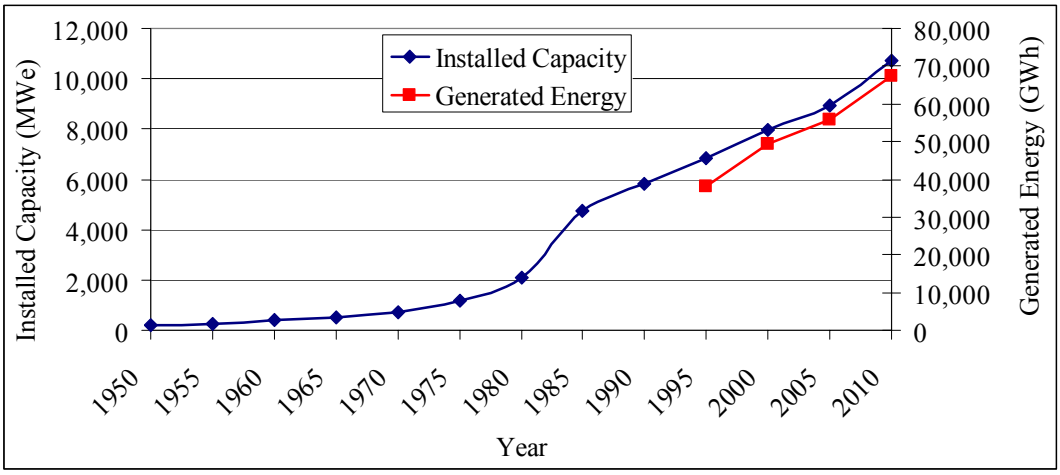

Figure 2.5. Growth of installed capacity of GPPs during the period 1950–2010 and generated electricity of last 20 years from GPPs. (Source: Bertani, 2010)

Contribution of installed geothermal electric capacity to overall national electric power capacity (all sources) for major geothermal power-producing countries is shown in Figure 2.6. Although USA is the leading country based on installed geothermal power capacity, El Salvador has the highest ratio of installed geothermal electric capacity to overall national electric power capacity (all sources).

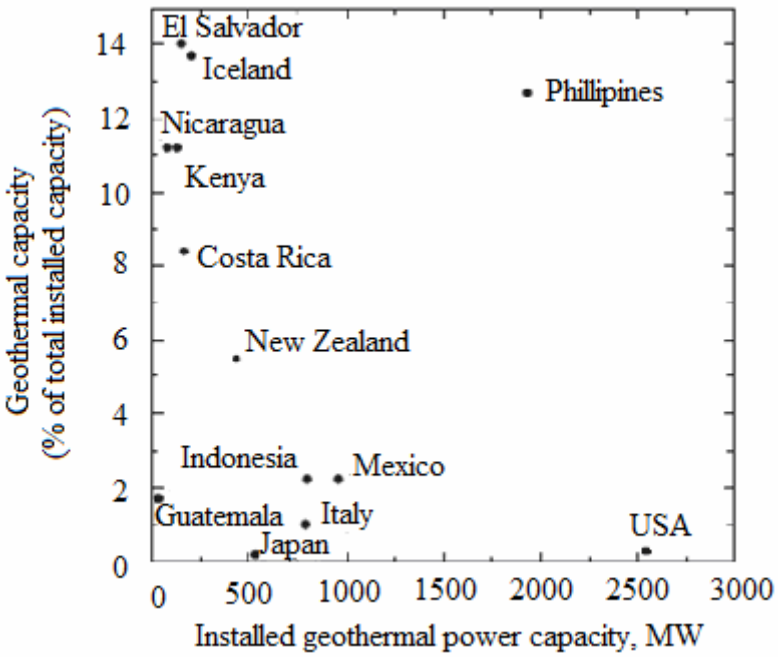

Figure 2.6. Contribution of installed geothermal electric capacity to overall national electric power capacity (all sources) for major geothermal power-producing countries. (Source: Gupta and Roy, 2007)

Worldwide GPP distribution by plant type is given in Table 2.1, which indicates that the largest installed capacities correspond to single and double-flash plants, covering 2/3 of the total (Bertani, 2005; 2010).

Table 2.1. Power plant distribution by plant type (early 2010 data).
(Source: Bertani, 2010)

Plant type		Installed capacity			
		(MW)	(%)	(number of units)	(%)
Dry steam		2878	27	62	12
Flashed-Steam	Single-flash	4421	41	141	27
	Double-flash	2092	20	61	12
	TOTAL	**6513**	**61**	**202**	**39**
Binary combined cycle/hybrid		1178	11	236	45
Back pressure		145	1	25	5
TOTAL		**10715**	**100**	**525**	**100**

2.1.2. Geothermal Power Production in Turkey

The first geothermal exploration and exploitation studies in Turkey started by Turkish Mineral Research and Exploration Institute (MTA) in 1960s. Since then, about 170 geothermal fields have been discovered by MTA, where 95% of them are low-medium enthalpy fields, which are suitable mostly for direct-use applications. Table 2.2 presents high-temperature geothermal fields suitable for electricity generation in Turkey (Erdogdu, 2009).

Kizildere GPP, which is the first GPP of Turkey, constructed in 1984 with an installed and average gross capacity of 20.4 MW and 10 MW, respectively. Kizildere GPP had been the only one GPP until 2006. After the Renewable Energy Law (2005) and Law on Utilization of Renewable Energy Resources for the Purpose of Generating Electrical Energy (2007) were released, GPP investment became attractive. Since then 79.2 MW GPP has been constructed and by 2010 GPP capacity of Turkey increased by 388% (Figure 2.7). An addition of 153 MW capacity licence for 8 GPPs at 6 different locations is issued by EPDK.

Table 2.2. Geothermal fields suitable for electricity generation in Turkey. (Source: Erdogdu, 2009)

Geothermal Field	Temperature (°C)
Denizli-Kizildere	243
Aydın-Germencik	232
Manisa-Salihli-Gobekli	182
Canakkale-Tuzla	174
Aydın-Salavatli	171
Kutahya-Simav	162
Izmir-Seferihisar	153
Manisa-Salihli-Caferbeyli	150
Aydın-Yilmazkoy	142
Izmir-Balcova	136
Izmir-Dikili	130

A list of existing and planned GPPs in Turkey and is given in Table 2.3 and 2.4, respectively (Aksoy, 2007; Serpen, et al., 2008; Durak, 2009; EPDK, 2010).

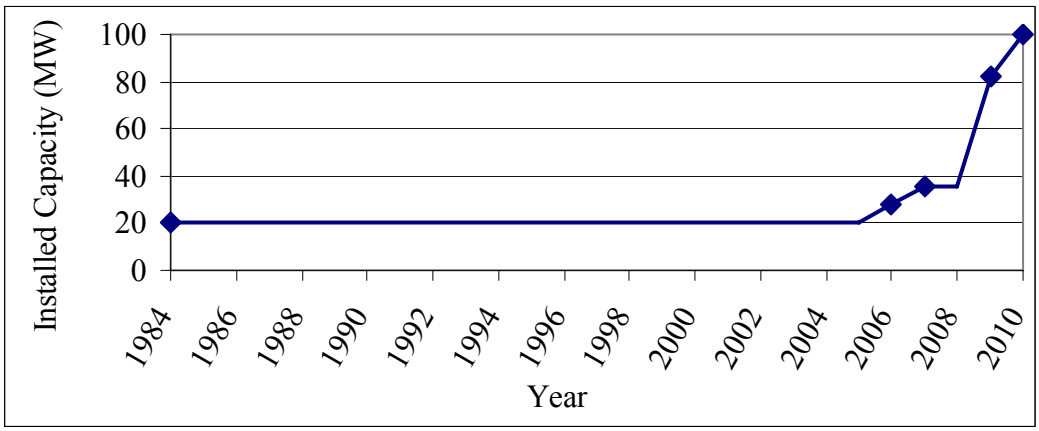

Figure 2.7. Cumulative installed capacity of GPPs in Turkey.

Table 2.3. GPPs installed in Turkey.
(Source: Aksoy, 2007; Serpen et al., 2008; EPDK, 2010)

Power Plant Type		Location	Year	Installed Capacity	
				(MW)	(%)
Flashed-Steam	Single-flash	Kizildere-Denizli	1984	20.4	20.5
	Double-flash	Germencik-Aydın	2009	47.4	47.5
	TOTAL			**67.8**	68
Binary		Salavatlı-Aydın	2006	7.95	8
		Denizli	2007	6.85	6.9
		Tuzla-Çanakkale	2010	7.5	7.5
		Salavatli-Aydın	2010	9.5	9.6
		TOTAL		**31.8**	32
GRAND TOTAL				**99.6**	100

Table 2.4. GPPs have and/or applied to electricity production license in Turkey.
(Source: EPDK, 2010)

Location	**Power Plant Capacity (MW)**	**Maximum Temperature (^{o}C)**
Caferbeyli-1, Salihli-Manisa	15	168
Caferbeyli-2, Salihli-Manisa	15	168
Atça, Nazilli, Sultanhisar-Aydın	9.5	124
Salavatlı,Sultanhisar - Aydın	34	171
Germencik-Aydın	9.5	143
Sarayköy-Kizildere-Denizli	60	242
Umurlu-1-Aydın	5	131
Umurlu-2-Aydın	5	131
TOTAL	**153**	

2.2. NCGs and NCG Removal Systems

Geothermal steam, which flows through the entire cycle of conventional GPPs contains NCGs such as CO_2, H_2S, NH_3, N_2, CH_4 and air. Depending on the resource, the concentration of NCGs can very from less than 0.5% to greater than 25% by weight of steam (Duthie and Nawaz, 1989). NCG concentration in some geothermal fields in the World is presented in Table 2.5.

Table 2.5. NCG concentration of some geothermal fields in the World.
(Source: Gokcen and Ozcan, 2007; Coury, 1987; Siregar, 2004; Swandaru, 2006)

Geothermal Field	NCG Concentration (% by weight of steam)
Kizildere, Turkey	10-21
Larderello, Italy	10
Broadlands, Ohaaki, New Zealand	3-6
BacMan, Philippines	5
Sibayak, Indonesia	3.1
Tongonan, Philippines	3
Geysers, USA	0.5-2
Patuha, Indonesia	1.1-1.8
Palinpinon, Philippines	1.3
Wairakei, New Zealand	0.2
China Lake, California	0.2
Puna field, Hawaii	0.1

The practical problems associated with elevated levels of NCGs in GPPs are:

- NCG collects in the sub-atmospheric pressure steam condensers by forming a 'gas-blanketing' effect, which raises the condenser temperature and back-pressure on the turbine, reducing its output
- The gases reduce the heat transfer efficiency of the power plant condensers. The primary effect of this is to increase the condenser operating pressure, which reduces turbine power output. As a consequence, overcoming the gas effects requires larger condensers with greater total heat transfer area and higher costs.

- The gases contribute a partial pressure that adds to the backpressure on the turbine.
- If NCG removal systems under-perform, this has the effect of an under-designed condenser, increasing the power turbine backpressure.
- NCGs contain lower recoverable specific energy than does steam. The gases dilute the geothermal steam and reduce gross turbine output in the power plant.
- NCGs such as CO_2 and H_2S contribute to corrosion problems in piping and equipment that contact steam and condensate.
- Conversely, when volatile acid gases evolve from flashing geothermal brine, the pH of the brine increases. This raises the risk of scale formation in brine piping and equipment, creating a potentially expensive maintenance problem in the process systems that handle both the steam and spent brine, including brine re-injection wells. Geothermal steam also entrains brine mist that causes the build-up of scale in power turbines and in flow systems (Vorum and Fritzler, 2000).

Because of the elevated NCG levels, GPPs require large capacity NCG removal systems which play a vital role in power production occupying large portion in its total plant cost and total auxiliary power consumption. Therefore, selection of NCG removal system becomes a major concern at planning and basic design stages of geothermal power plants.

The conventional gas removal systems used in geothermal power plants are:

_ Jet ejectors, e.g. steam jet ejectors, which are suitable for low NCG flows (<3%).

_ Liquid ring vacuum pumps (LRVPs).

_ Roto-dynamic, e.g. radial blowers, centrifugal compressors, which are mainly used for large flows of NCG (>3%).

_ Hybrid systems (any combination of equipment above),

_ Reboilers (Hall, 1996).

2.2.1. Steam Jet Ejectors

An ejector is a type of vacuum pump or compressor, which removes the NCGs from the condenser. Since an ejector has no valves, rotors, pistons or other moving

parts, it is a relatively low-cost component, is easy to operate and requires relatively little maintenance.

Figure 2.8 shows a diagram of a single-stage steam jet ejector. A steam jet ejector operates on the venture principle. The motive steam is expanded through the nozzle to the design suction pressure. The pressure energy of the steam is converted to velocity energy and on leaving the nozzle at high supersonic velocities the steam passes through the suction chamber and enters the converging diffuser or entrainment, as gas and associated water vapor.

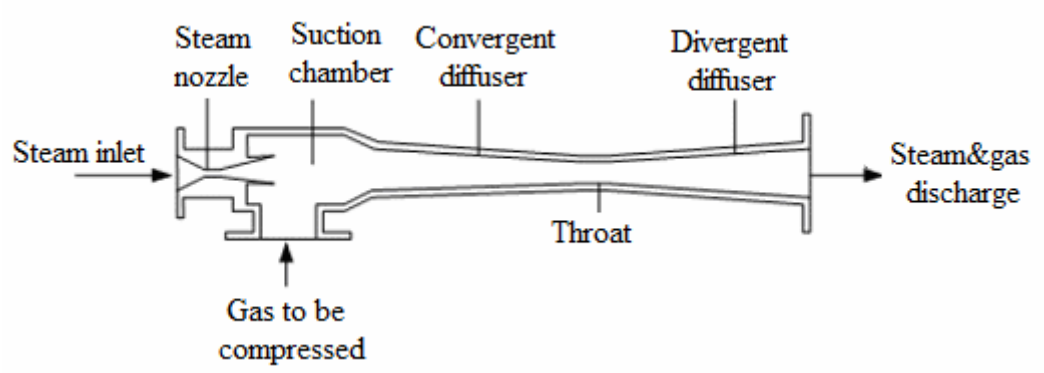

Figure 2.8. Single-stage steam jet ejector.
(Source: Swandaru, 2006)

Since the capacity is fixed by its dimensions, a single unit has practical limits on the total compression and throughput it can deliver. Two or more ejectors can be arranged in series for greater compression. Figure 2.9 shows a diagram of a two-stage system. Two stages of equal compression ratio gives a decrease in steam consumption compared to the single-stage ejector system (Birgenheier et al., 1993; Swandaru, 2006). In a multi-stage system, condensers are typically used between successive ejectors. By condensing the vapor before sending the stream onto the next stage, the vapor load is reduced. This allows smaller ejectors to be used, and reduces steam consumption. Pre-condensers (gas coolers) can be added to reduce the load on the first-stage ejector, and allow for a smaller unit. An after-condenser can also be added, to condense steam from the final stage. Adding an after-condenser will not affect overall system performance, but may ease disposal of steam (Birgenheier et al., 1993).

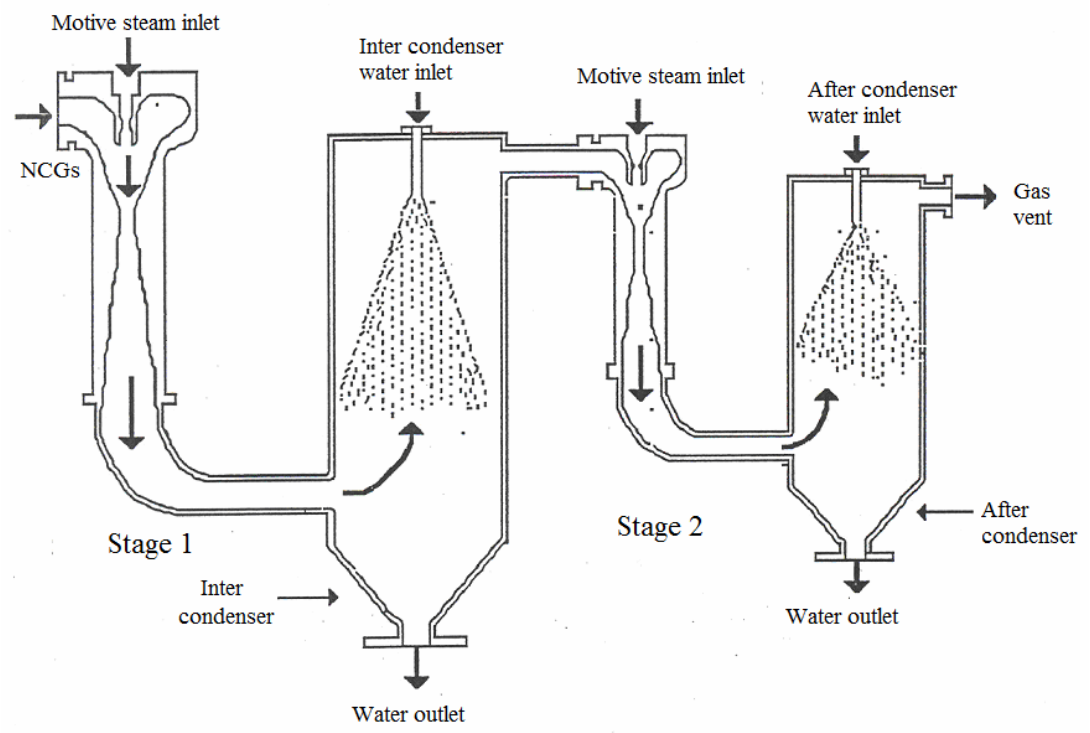

Figure 2.9. Two-stage SJES.
(Source: Geothermal Institute, 1996a)

2.2.2. Liquid Ring Vacuum Pumps

Liquid ring vacuum pumps (LRVPs) belong to the group of positive displacement pumps. The characteristic feature of this pump type is the energy transmission from the impeller to the fluid pumped by means of a liquid ring. The basic design of a LRVP is shown in Figure 2.10.

LRVP increases gas pressure by rotating a vaned impeller within an eccentric to a cylindrical casing. Liquid (usually water) is fed into the pump and, by centrifugal acceleration, forms a moving cylindrical ring against the inside of the casing. This liquid ring creates a series of seals in the space between the impeller vanes, which form compression chambers. The eccentricity between the impeller's axis of rotation and the casing geometric axis results in a cyclic variation of the volume enclosed by the vanes and the ring. Gas, is drawn into the pump via an inlet port in the end of the casing. The gas is trapped in the compression chambers formed by the impeller vanes and the liquid ring. The reduction in volume caused by the impeller rotation, increases gas pressure which forces to the discharge port (Lehmann, 1995).

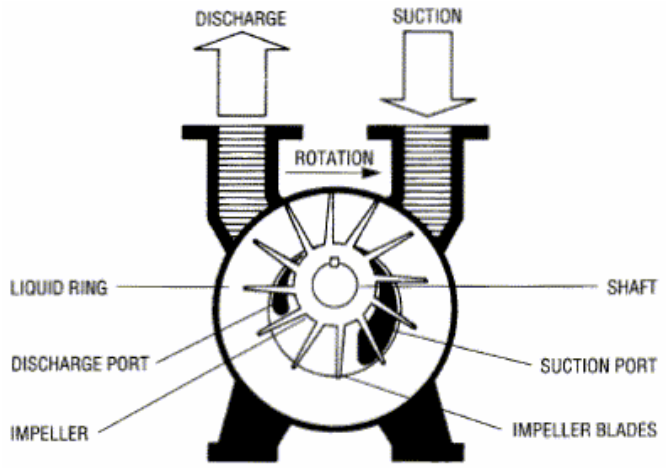

Figure 2.10. LRVP.
(Source: Sugar Engineers, 2010)

LRVPs have relatively high efficiency but high capital cost and are generally used alone in low flow applications where large pressure ratios are not required. It has been proposed to use LRVPs for geothermal applications in series with a steam jet ejector, which would provide the first stage of compression (Geothermal Institute, 1996b).

2.2.3. Centrifugal Compressors

Increasing NCG fraction increases steam consumption of steam jet ejectors and consequently operational cost becomes uneconomic. Centrifugal compressors (Figure 2.11) although expensive to install, have overall efficiencies in order of 75%.

When dealing with large quantities of NCGs this makes them the preferred option compared to the other systems. Centrifugal compressors are expensive to install and maintenance. In some cases, compression of NCG requires up to 20% of the power produced by the plant. But they are nearly 30% more efficient than LRVPs and 250% more efficient than SJEs (Barber-Nichols, 2010). Kizildere GPP employs the compressors as NCG removal system.

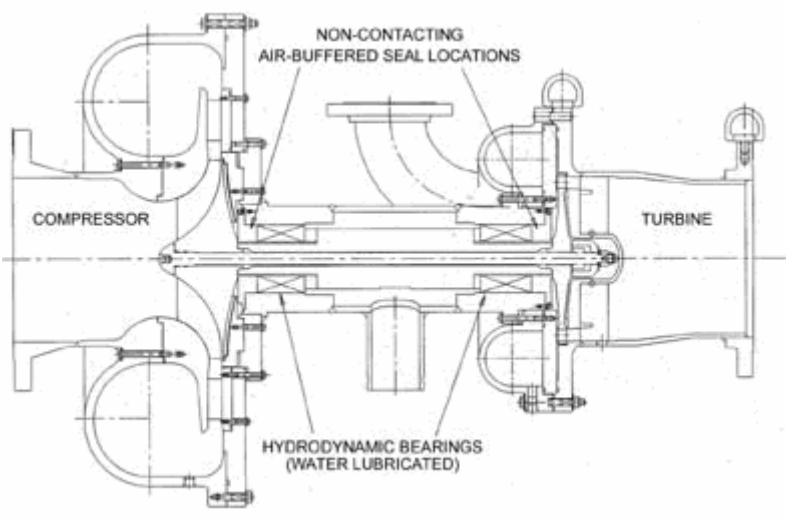

Figure 2.11. Centrifugal compressors.
(Source: Barber-Nichols, 2010)

2.2.4. Hybrid Systems

Integration of a SJE with a LRVP or centrifugal compressors is referred to as a HS. It is one of the more efficient methods for producing a process vacuum. HS having SJE and LRVP combination is commonly used in the World. The first and most recent cases of a LRVP being used in a GPP for removal of NCGs was in the Onikobe power plant, Japan (Geothermal Institute, 1996b) and Gurmat plant, Turkey.

2.2.5. Atmospheric Exhaust Turbines

The geothermal fluid produced by the wells is separated by separators, and the stream of steam and NCGs is scrubbed and expanded through a turbine to atmospheric pressure. Slightly higher than atmospheric pressure may be required if an H_2S abatement system is needed. Likewise, a condenser operating at essentially atmospheric pressure may be needed to condense steam and cool the NCGs prior to treatment by an H_2S abatement system. As shown in Figure 2.12, the liquid stream from the separator is flashed to generate steam for expansion in a low pressure steam turbine (Hankin et al., 1984).

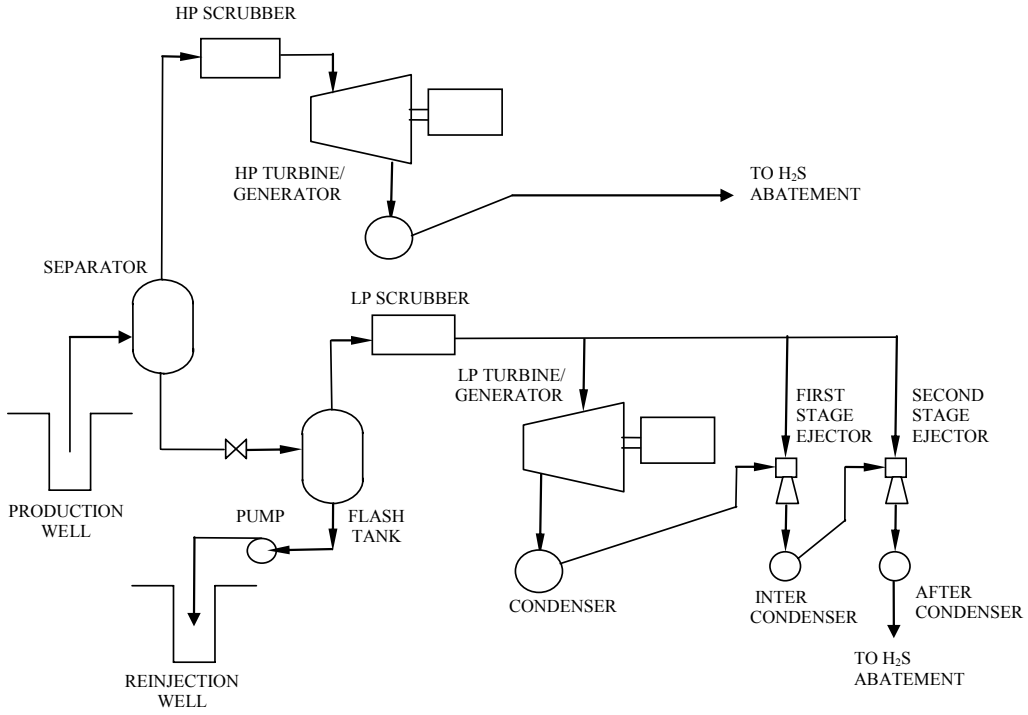

Figure 2.12. Atmospheric exhaust turbine.
(Source: Hankin et al., 1984)

2.2.6. Reboilers

RSs offer the only technology available for removing NCGs from geothermal steam upstream of the turbine. The advantages of the reboilers are;

- The stream feed to the turbine is less corrosive.
- Since NCGs concentration in the steam is reduced drastically, for certain resources, direct contact power plant condensers can be used rather than surface condensers which would be required if vent gas treatment is needed. Surface condensers may then still be needed but secondary H_2S abatement may not be required.
- Use of upstream reboilers allows H_2S abatement even during stacking operations.
- In case of high NCG content, the overall energy conversion process is more efficient (Awerbuch et al., 1984).

Upstream reboilers mainly are classified as two groups as indirect contact reboilers (vertical, horizontal and kettle types) and direct contact.

2.2.6.1. Vertical Tube Evaporator Reboilers

A vertical tube evaporator reboiler is a surface type heat exchanger shown in Figure 2.13.

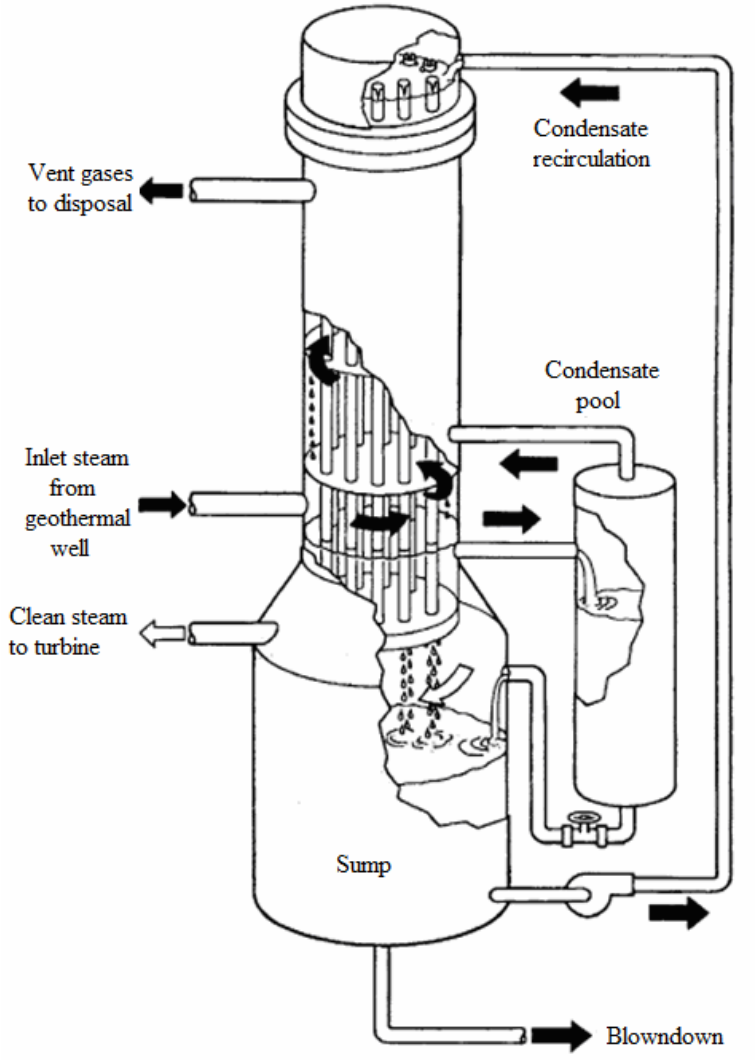

Figure 2.13. Vertical tube evaporator reboiler.
(Source: Hughes, 1987)

Wellhead steam enters the shell side of the exchanger near the bottom. The shell side is at a pressure and temperature slightly higher than the tube side. The temperature difference will result in steam condensing on the shell side and condensate evaporating on the tube side. Most of the NCGs will be exhausted in the vent stream. Condensate from the sump is pumped to the heat exchanger tubes where a fraction of the liquid flowing down will evaporate in a single pass (Awerbuch et al., 1984).

Vertical tube evaporator reboiler technology has been applied at the pilot level at the Geysers, California. During more than 1000h of accumulated test time, the average H_2S removal efficiency obtained as 94% (Coury and Associates, 1981).

2.2.6.2. Horizontal Tube Evaporator Reboilers

A horizontal tube evaporator reboiler is illustrated in Figure 2.14. Wellhead steam enters one of the tube boxes and flows into the tube side of the heat exchanger. The tube side temperature and pressure is higher than the shell side. Condensate is sprayed onto the shell side of the heat exchanger. The temperature difference will result in the steam condensing on the tube side and the condensate evaporating on the shell side. The condensate and the uncondensed vapor in the tubes will flow to a knockout chamber where the condensate and vent gases are separated. The condensate not evaporated is returned to the spray nozzles by a recirculation pump (Awerbuch et al., 1984).

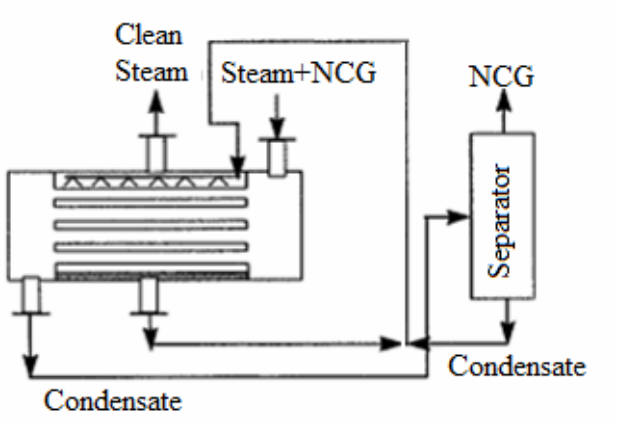

Figure 2.14. Horizontal tube evaporator reboiler.
(Source: Palen 1984; Gunerhan, 1999)

2.2.6.3. Kettle Type Reboilers

Kettle type reboilers basically consist of a bundle of U-tubes submerged in the condensate (Figure 2.15). The contaminated geothermal steam flows inside the tubes.

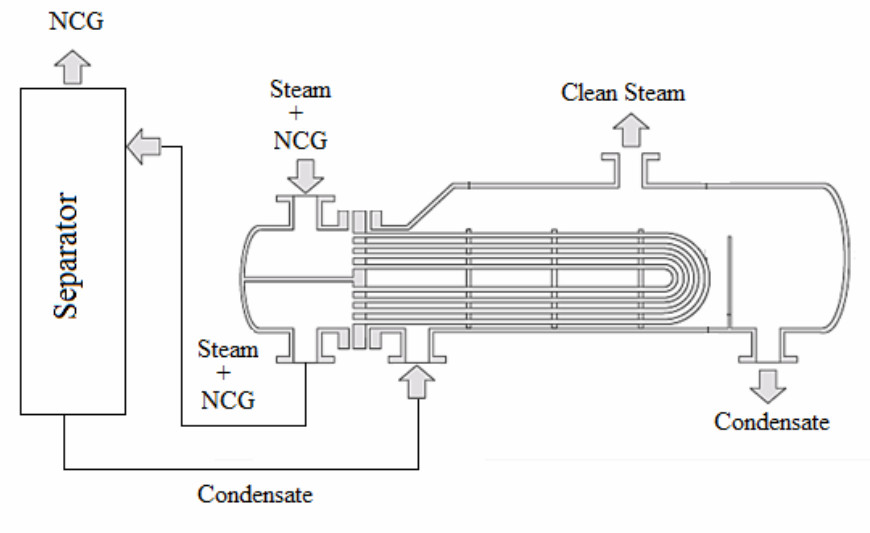

Figure 2.15. Kettle type reboiler.
(Source: Spirax Sarco, 2010; Gunerhan, 1999)

2.2.6.4. Direct Contact Reboilers

A direct contact heat exchanger vessel (e.g., packed bed column), flash vessels, and recirculation pump are the main components of a direct contact reboiler, shown in Figure 2.16.

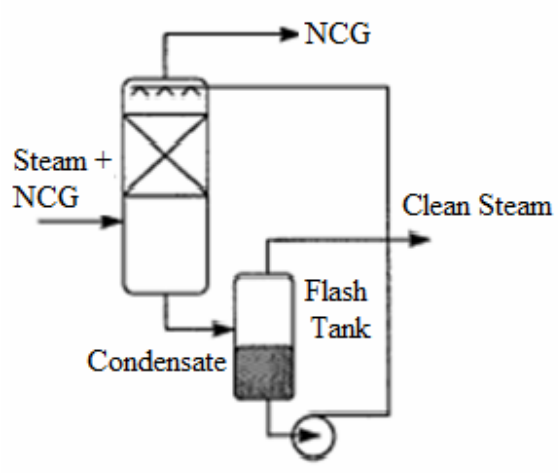

Figure 2.16. Direct contact reboiler.
(Source: Gunerhan, 1999)

Wellhead steam enters the direct contact heat exchanger near the bottom of the column. As the steam flows up the packed column, it condenses as it contacts

circulating colder condensate. At the top of the column, most of the NCGs will remain in the vapor stream which is vented. This hot liquid flows to a flash vessel where steam can be produced as feed to the turbines. A variation of the basic design is the use of two flash vessels to produce high and low pressure steam (Awerbuch et al., 1984).

The comparison of the reboiler types is given in Table 2.6.

Table 2.6. Comparison of upstream reboiler types.
(Source: Gunerhan, 1999).

Reboiler types	**Application in geothermal**	**Advantages**	**Disadvantages**
Vertical Tube	At pilot level in The Geysers (USA) and Cerro Prieto (Mexico)	Less fouling, Suitable for using Fouling liquids, low Residence time, low Liquid inventory, Low floor area	High head room (can cause stability problems), difficult to design, high differential pressure can cause tube collapse
Horizontal tube	No application	Capability of handling high Pressure difference, easier to Access for cleaning	
Kettle	Commercial Experience in New Zealand	Rugged construction, easy to design, negligible pressure drop	Expensive material, Control or stability problems, high liquid inventory, uneconomic for high pressure operation, unsuitable for fouling liquids, not easy to clean
Direct contact	Latera (Italy) (start-up in early 1999, abundant in 2003)	Suitable for fouling fluids, cheap to build, simple construction	Control problems

CHAPTER 3

LITERATURE SURVEY

The effects of NCGs on the performance of GPPs were first studied by Khalifa and Michaelides in 1978. In the study CO_2 was taken into consideration as NCGs and the influence of dissolved carbon dioxide on the performance of various components of GPP, such as turbine, flash tank, condenser and gas extraction system, had been analyzed in a simple, thermodynamically consistent manner. The study showed that, presence of 10% by weight of steam CO_2 in the geothermal steam results in as much as a 20-25% decrease in the net work output compared to a clean steam system (Khalifa and Michaelides, 1978).

Because of the NCGs heat transfer coefficient in the condenser is reduced. Therefore, Michaelides (1980) proposed a flash system at the wellhead to separate the NCGs before they enter the turbine and determined the flash temperature depending on the NCG content. It was emphasized that NCG content in the steam is an important factor for the estimation of the recoverable work. If the initial gas content was higher than 0.1% by weight of steam, the separation of the NCGs by flashing results in the recovery of higher amounts of work (Michaelides, 1980).

In another study of Michaelides (1982), different NCG removal systems, such as ejectors, pumps, compressors and combined system with steam jet ejectors and compressors were studied. It was explained that, the ejectors are simple, inexpensive devices and require little maintenance. However, they were inefficient and consume a great deal of available work. Compressors and pumps, although more efficient, were expensive and require frequent maintenance. In general, ejectors were used where the NCG content was relatively low and compressors are used where the gas content was high (Michaelides, 1982).

Optimization of NCG removal systems becomes extremely important if the geothermal steam contains large amount of NCGs. Tajima and Nomura (1982) and Hamano (1983) were studied four different NCG removal systems, which were steam jet ejectors, centrifugal gas compressors, combined systems of steam jet ejectors and centrifugal compressors, and back pressure turbine without NCG removal system.

Evaluation was made by comparison of electrical power generating cost, steam cost and capital cost for four alternative NCG removal systems. The study (Tajima and Nomura, 1982) showed that for 7.25% by volume NCG content, centrifugal compressors gave the highest capital cost and the lowest steam cost. Back pressure turbine gave the lowest capital cost and highest steam cost. If there was a large quantity of NCG content, more than 10% by weight of steam, the GPP may adopted a back pressure turbine without a condenser (Hamano, 1983). Because of the back pressure turbine caused a decrease of the total output or increases the steam consumption, for large capacity unit such as 50 MW, back pressure turbine was not recommended. The selection of the NCG removal systems depends on the condenser pressure. Consequently, centrifugal CSs were selected according to optimum condenser pressure. If the condenser pressure is below 11.77 kPa abs, combined system of steam jet ejector and centrifugal compressor became the most economical option (Tajima and Nomura, 1982).

Hankin, et al. (1984) studied, the performance of different NCG removal systems, which were condensing turbine with compressors, atmospheric exhaust turbine, tube type reboiler and direct contact reboiler, were examined and compared to the conventional process (condensing turbine with steam jet ejectors) for a 25% by weight of steam NCG content. Required flow rate of geothermal fluid, which relates directly to the number of the wells needed to operate the plant, was one of the comparison criteria. The better power plant processes were condensing turbine with compressor, tube type reboiler and direct contact reboiler require one-half to two-thirds the number of the wells as the conventional condensing turbine with steam jet ejectors for the optimum wellhead pressure (2.45 MPa). The first two required large, relatively expensive equipment to handle the high NCG. However, the direct contact reboiler process used relatively low cost direct contact heat exchangers for NCG separation. Thus, the direct contact reboiler process was promising for plant design where the steam contains high amount of NCG (Coury et al., 1980).

Although the use of upstream reboilers is not commonly practiced in GPPs to date, these reboilers can play a significant role in power plant design. Awerbuch, et al. (1984), described various upstream reboiler concepts, vertical tube evaporator (VTE), horizontal tube evaporator (HTE), kettle type and direct contact (DCR) reboilers, and application of these concepts for geothermal resources with low and high NCG content was discussed. According to the study, because of design constraints the VTE reboilers were generally most suitable for low concentrations of NCG steam where the pressure

differences between the shell and tube sides are relatively small. On the other hand, HTEs had some advantages over the VTE reboilers including capability of handling high pressure differences, and easier access for cleaning in case of fouling. The main concern with surface reboilers (VTE, HTE and Kettle) was selection of materials of construction and therefore capital cost. In view of the cost of surface reboilers, direct contact reboilers (DCR) had great promise since no heat transfer surfaces are required (Awerbuch, et al., 1984; Awerbuch and Van der Mast, 1985). Another study about upstream reboilers was conducted by Duthie and Nawaz in 1989. In the study direct contact and kettle reboilers were compared. This study has also shown that for large-scale projects based on a high NCG content resource, the direct contact reboiler had significant capital cost and levelized cost of power advantages over the kettle type reboiler (Duthie and Nawaz, 1989).

Gunerhan studied upstream RSs as an alternative to conventional gas extraction system for Kizildere GPP in Denizli, Turkey. Both vertical tube type (VTE) reboiler and direct contact reboiler (DCR) designed and evaluated. It was concluded that vertical tube type reboilers were not efficient for fields that contain high levels of NCG (>15% by weight of steam). Thus, the use of direct contact reboilers was recommended. The direct contact tests had been carried out in the field with a gas removal efficiency 76.3 ± 22.6 % at the base case (Gunerhan, 2000).

In June 2000, National Renewable Energy Laboratory (NREL) published a subcontractor report about removing NCGs from flashed steam GPPs (Vorum and Fritzler, 2000). In the study, six different methods of removing NCGs from GPPs were compared according to design and economic considerations. The studied NCG removal systems were, a two stage system of steam jet ejectors, a three-stage system using an innovative steam-driven turbo compressor, a HS using two stages of steam jet ejectors and a turbo compressor third stage, a HS using two stages of steam jet ejectors and a liquid ring vacuum pump third stage, a conceptual bi-phase eductor system and a reboiler process. It was concluded that, two gas removal options appeared to offer profitable economic potential. The hybrid vacuum system configurations and the reboiler process yield positive net present-value results over wide-ranging gas concentrations. The hybrid options looked favorable for both low-temperature and high-temperature resource applications. The reboiler looked profitable for low-temperature resource applications for NCG levels above about 20,000 parts per million by volume (ppmv). A vacuum system configuration using a three-stage turbo compressor battery

may be profitable for low temperature resources, but the results also showed that a HS is more profitable (Vorum and Fritzler, 2000).

A tray-type direct contact RS was applied to 40 MW Latera GPP in Italy where the NCG content is 3.5% at the wellhead. This was the first application to the geothermal industry in the world of the reboiler concept on a commercial scale. It was started up in early 1999 and abundant in 2003 because of the environmental problems (Sabatelli and Mannari, 1995).

Yildirim and Gokcen (2004) considered the NCG content on each step of energy and exergy analysis of Kizildere GPP. They emphasized the importance of NCGs on power plant performance and concluded that since GPPs contain a considerable amount of NCGs, the NCG content should not be omitted throughout the process and dead state properties should reflect the specified state properties.

In another study (NASH, 2006), NCG removal systems for GPPs were compared to each other depending on their capital cost, operating cost and electric power cost. Three different options were considered: Option A was three-stage all SJES, Option B was a three-stage HS with two stage steam jet ejector and third stage vacuum pump, Option C was a two-stage HS with first stage ejector and third stage vacuum pump. The study showed that, Option A, the all SJES, shows an attractively low initial investment. However, the annual operating costs are far higher than either of the other two cases. Option B balances operating costs savings against initial investment. Option C has the lowest operating costs. The higher initial investment to gain this cost reduction, however, extends its payoff time considerably (NASH, 2006).

Siregar (2004) studied ejectors and liquid ring vacuum pump in one of his studies. The study was about optimization of electric power production process for the Sibayak geothermal field, Indonesia. The NCG fraction was 3.07% (by weight of steam). The liquid ring vacuum pump power consumption was calculated as 803 kW for a single-flash GPP with the capacity of 20 MW. Similar studies had been conducted by Swandaru in 2006 for Patuha geothermal field in Indonesia. In the field NCG concentration is 1.77 % (by weight of steam). As NCG removal system 3-stage NCG removal system exists at first two stages with SJE and the last stage is LRVPp. In the study, the steam consumption of SJEs and power consumption of LRVP were determined.

The complex and unique nature of GPPs reveals to use design and simulation software. The majority of existing commercial software are developed for reservoir and

geothermal field modeling (Milicich et al., 2010; Tanaka and Itoi, 2010; Holzbecher and Sauter 2010), borehole heat exchangers and heat pumps (Kim et al., 2010; Cisarova et al., 2010), geochemical modeling of geothermal fluids (Hasse et al., 2006, Putten and Colonna, 2007), direct use applications (HeatMap, 2010) and GPPs (Blomster et al., 1975; GETEM, 2010; Aspen-HYSYS, 2010). The oldest known GPP software is GEOCOST, which consists of deterministic and static cost models to simulate the production of electricity from geothermal energy (Blomster et al., 1975). The GEOCOST includes only steam jet ejectors as NCG removal system, not applicable to high NCG fields. GETEM, static model, determines the performance of flashed-steam GPPs and it includes steam jet ejectors, LRVPs and hybrid NCG removal systems. The compressors and reboilers are not included in GETEM software (GETEM, 2010). ASPEN-HYSYS, which is a static and dynamic modeling tool for conceptual design, optimization, business planning, asset management and performance monitoring of energy systems by offering a comprehensive thermodynamics foundation of physical properties. GPPs can be modeled by the software but it does not include a specific module for NCG removal systems (Aspen-HYSYS, 2010). Since there is a substantial lack of design and simulation software of GPPs including NCG gas removal options, the Thesis aims to develop a model to provide a guide or reference which could quickly and easily be used to determine the GPP gas removal system which maximizes the power output at minimum cost. The model includes mass, energy and exergy balances, and economical analysis under steady-state, steady-flow conditions.

Energy and exergy balances of geothermal power plants have been conducted by many researchers. The studies mostly are focused on determination of exergetic efficiency of the plants and simulation of dead state properties. The authors considered that NCG content is zero through the cycle or NCGs are taken into consideration only at the gas extraction system not the entire cycle (DiPippo and Marcille, 1984; DiPippo, 1992, 1994, 2004; Cadenas, 1999; Cerci, 2003; Siregar, 2004; Kwambai, 2005; Aqui et al., 2005; Dagdas et al., 2005; Ozturk et al., 2006; Kanoglu et al., 2007). The Thesis differs from the previous studies by considering NCG fraction through the entire cycle during mass, energy and exergy balances.

The developed model allows the designer to simulate the disturbed parameters to forecast and validate the performance of flashed steam GPPs under various working conditions, which is useful for system design. Furthermore, the model can support new plant designs at the earlier phases to avoid possibly costly late modifications caused by

conceptual design errors. The simulation models can also help personnel involved with the plant at various levels to become familiarized with its behavior before the first plant start-up, and considerably shorten the commissioning time.

CHAPTER 4

MODELING

The thermodynamic and economical models of flashed-steam GPPs (single and double-flash) have been developed with an emphasis on NCG removal systems, in order to obtain the maximum power output at lowest production cost. Four different gas removal options which are two-stage SJES, two-stage HS (steam jet ejector and liquid ring vacuum pump), two-stage CS and RS are evaluated based on mass, energy and exergy balances, and economical analysis under varies geothermal fluid, power plant, environmental and economical parameters. The model is validated by Kizildere GPP data.

In this chapter, the thermodynamic and economical equations for single-flash GPP model given in detail are subjected to double-flash GPP model.

4.1. Thermodynamic Model

4.1.1. Mass, Energy and Exergy Balance Equations

Energy is defined as motion or the ability to cause motion and is always conserved in a process. The First Law of Thermodynamics states that *energy can neither be created nor destroyed*. Energy is available in many different forms and may be converted between these forms. On the other hand, exergy is defined as work or the ability to cause work and is always *conserved in a reversible process*, but is *always consumed in an irreversible process.* The Second Law of Thermodynamics states that *conversions of energy are possible only if the total entropy increases*. While energy is a measure of *quantity*, exergy is a measure of *quantity and quality*.

An exergy balance is a mathematical tool for evaluation of exergy flows through a system (Figure 4.1). Most cases of thermodynamic imperfection cannot be detected by mass and energy balances. A careful evaluation of processes using exergy balance enables the identification of the source of inefficiencies and waste, which leads to

improved designs and resultant savings. Exergy balance is a tool for identifying the types, locations and magnitudes of thermal losses using conservation of mass and energy principle together with the Second Law of Thermodynamics. Identifying and quantifying these losses allows for the evaluation and improvement of the designs of thermodynamic systems (Rosen, 2002; Kwambai, 2005).

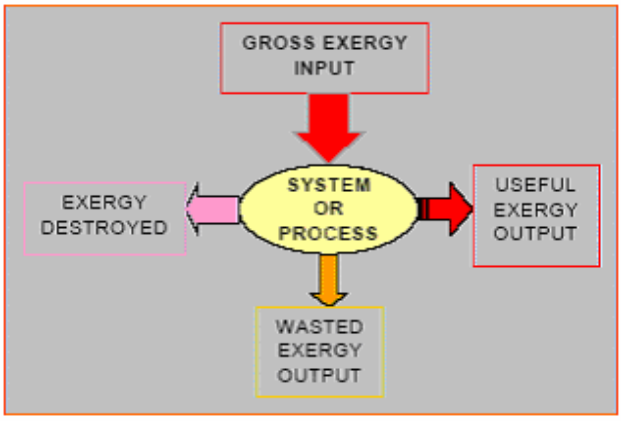

Figure 4.1. Illustration of exergy flow through a system.
(Source: Kwambai, 2005)

The main equations of mass, energy and exergy balance used in the static (steady-state, steady-flow) model are summarized in Table 4.1.

Table 4.1. Main equations of the model.

	Equation	Equation Number
Mass	$\dot{m} = \dot{m}_l + \dot{m}_s + \dot{m}_{NCG}$	(4.1)
	$x = (\dot{m}_s + \dot{m}_{NCG})/\dot{m}$	(4.2)
	$f = \dot{m}_{NCG}/(\dot{m}_s + \dot{m}_{NCG})$	(4.3)
	$\sum(\dot{m})_{in} = \sum(\dot{m})_{out}$	(4.4)
	$\dot{m}_l = (1-x)\times\dot{m}$	(4.5)
	$\dot{m}_s = x\times(1-f)\times\dot{m}$	(4.6)
	$\dot{m}_{NCG} = x\times f\times\dot{m}$	(4.7)

(cont. on next page)

Table 4.1. (cont.)

Energy	$\dot{m} \times h = \dot{m}_l \times h_l + \dot{m}_s \times h_s + \dot{m}_{NCG} \times h_{NCG}$	(4.8)
	$\sum (\dot{m} \times h)_{in} = \sum (\dot{m} \times h)_{out}$	(4.9)
Exergy	$\dot{E}x_{in} = \dot{E}x_{out} + \dot{E}x_{destroyed}$	(4.10)
	$\dot{E}x_{out} = \dot{E}x_{desired} + \dot{E}x_{waste}$	(4.11)
	$\dot{E}x_{destroyed} = T_0 \times s$	(4.12)
	$\dot{E}x = \dot{E}x_f + \dot{E}x_s + \dot{E}x_{CO_2}$	(4.13)
	$\dot{E}x = \dot{m} \times [(h - h_0) - T_0 \times (s - s_0)]$	(4.14)

The most commonly used measure of the performance of a system in terms of exergy is the exergetic efficiency which is a measure of the performance of a system relative to the maximum theoretical performance of the same system. *Exergetic efficiency* is defined as the ratio of the sum of desired exergy outputs to the sum of the necessary exergy inputs and given by Eq. 4.15.

$$\eta_{Ex} = \frac{\dot{E}x_{desired}}{\dot{E}x_{in}} \tag{4.15}$$

Figure 4.2 shows the schematic diagram of representative single-flash GPP model. The plant mainly consists of production wells, wellhead/main separator(s), turbine, condenser, NCG removal system, cooling tower and auxiliary equipment such as pumps and fans.

Geothermal fluid which is a mixture of liquid, water vapor and NCGs at the wellhead is separated into the steam and liquid phases at the separator. Steam phase is directed to the turbine contains water vapor and NCGs. After passing the turbine; steam, condensate and NCGs flow to the condenser where NCGs are accumulated and extracted by a gas removal system. The rest is pumped to the cooling tower which helps the temperature of the fluid drops down to the cooling water temperature to be re-used in the condenser. Liquid phase is driven by circulation pumps and air is drawn into the cooling tower by fans.

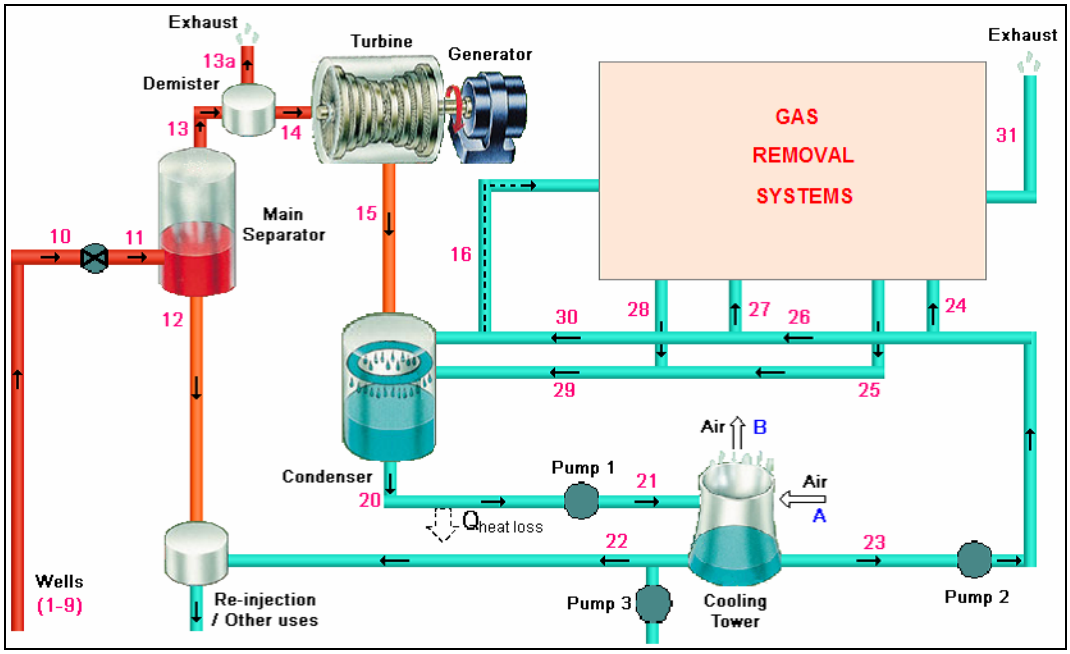

Figure 4.2. Schematic diagram of representative single-flash GPP.

Overall mass, energy and exergy balance for steady-state conditions with reference to Figure 4.2, can be expressed as below (Kwambai, 2005). The subscript numbers refer to state locations on Figure 4.2.

$$\dot{m}_{10} + \dot{m}_{air_A} = \dot{m}_{12} + \dot{m}_{13a} + \dot{m}_{22} + \dot{m}_{31} + \dot{m}_{air_B} \tag{4.16}$$

$$\dot{W}_{net} = \dot{W}_{gen} - \sum \dot{W}_{aux} \tag{4.17}$$

$$\dot{W}_{aux} = \sum \dot{W}_{grs} + \dot{W}_{motor,pump} + \dot{W}_{motor,fan} + \dot{W}_{other} \tag{4.18}$$

$$\dot{E}x_{10} + \dot{E}x_{air,A} = \dot{E}x_{12} + \dot{E}x_{13a} + \dot{E}x_{22} + \dot{E}x_{heatloss,pipe} + \dot{E}x_{31} + \dot{E}x_{air,B} + \dot{W}_{net} + \sum I_{GPP} \tag{4.19}$$

where

$\dot{E}x_{heatloss,pipe}$: Exergy loss through pipe between condenser exit and cooling tower inlet,

$\sum I_{GPP}$: Total destroyed exergies.

The overall exergetic efficiency of the plant is expressed as:

$$\eta_{overall} = \frac{\dot{W}_{net}}{\dot{E}x_{10}} \tag{4.20}$$

The GPP is simplified into sub-systems, each with distinct mass, energy and exergy inflows and outflows and approximated into steady-state flow. In the following part, mass, energy and exergy balance equations of all plant components, which are separator, demister, turbine-generator, condenser, cooling tower, NCG removal system and auxiliary equipment such as fans and pumps, are introduced.

4.1.1.1. Separator

The geothermal fluid is separated into vapor and liquid in a steam separator (Figure 4.3 and 4.4). As it is illustrated in Figure 4.3, the sequence of processes begins with geothermal fluid under pressure at state 10 (see also Figure 4.2) close to the saturation curve.

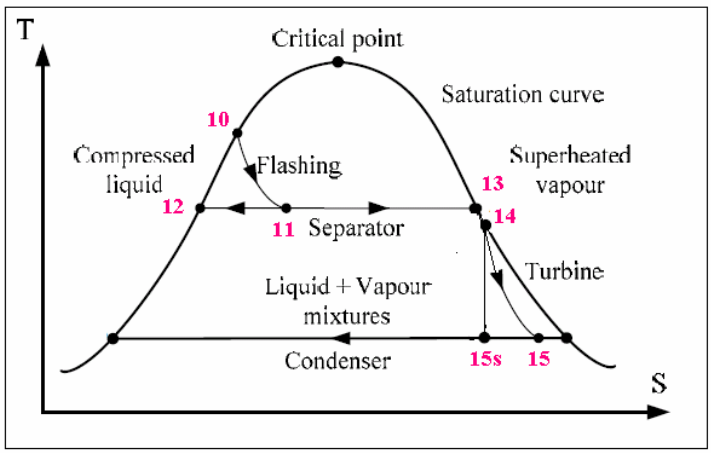

Figure 4.3. T-s diagram for a single-flash plant.
(Source: DiPippo, 2005)

The flashing process is modeled as one at constant enthalpy, an isenthalpic process, because it occurs steadily, spontaneously, essentially adiabatically, and with no

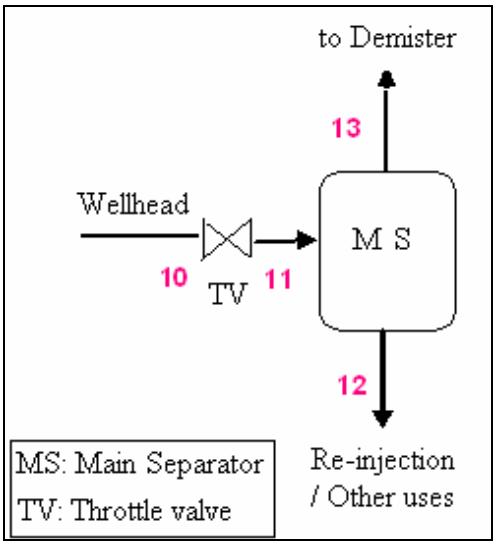

Figure 4.4. Main separator flow process.

work involvement. Any change in the kinetic or potential energy of the fluid as it undergoes the flash, is also neglected. Thus it can be written as:

$$h_{11} = h_{10} \tag{4.21}$$

The separation process is an isobaric process, once the flash has taken place.

$$P_{11} = P_{12} = P_{13} = P_{sep} \tag{4.22}$$

The quality of dryness fraction, x of the mixture that forms after the flash, state 11, can be found from:

$$x_{11} = \frac{h_{11} - h_{12}}{h_{13} - h_{12}} \tag{4.23}$$

The mass flowrate of steam that flows to the turbine coming from the separator is given by:

$$\dot{m}_{13} = x_{11}\dot{m}_{11} \tag{4.24}$$

Then, the mass flowrate of the brine from the separator is written as:

$$\dot{m}_{12} = (1 - x_{11}) \times \dot{m}_{11} \tag{4.25}$$

Exergy loss and exergetic efficiency:

$$I_{sep} = \dot{E}x_{10} - \dot{E}x_{12} + \dot{E}x_{13} \tag{4.26}$$

$$\eta_{Ex\,sep} = \frac{\dot{E}x_{13}}{\dot{E}x_{10}} \tag{4.27}$$

4.1.1.2. Demister

A demister, shown in Figure 4.5, is employed prior to the turbine to remove the condensate from the steam and make sure dry steam is introduced to the turbine. The pressure drop through the demister is taken as 10 kPa and the flashed mass flowrate is considered as 1% of the steam flowrate (Swandaru, 2006).

$$\dot{m}_{13a} = 0.01 \times \dot{m}_{13} \tag{4.28}$$

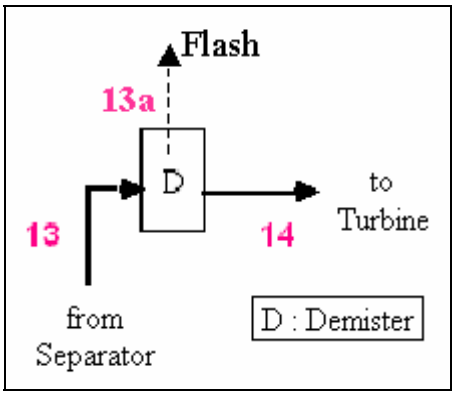

Figure 4.5. Flow diagram of demister.

Exergy loss and exergetic efficiency:

$$I_{dem} = \dot{E}x_{13} - \dot{E}x_{14} - \dot{E}x_{13a} \tag{4.29}$$

$$\eta_{Ex,dem} = \frac{\dot{E}x_{14}}{\dot{E}x_{13}} \tag{4.30}$$

4.1.1.3. Steam Turbine and Generator

Turbine expansion process is illustrated in Figure 4.6. For a turbine under steady operation, the inlet state of the working fluid and the exhaust pressure are fixed. Therefore, the ideal process for an adiabatic turbine is an isentropic process between the inlet state and the exhaust pressure (Figure 4.7).

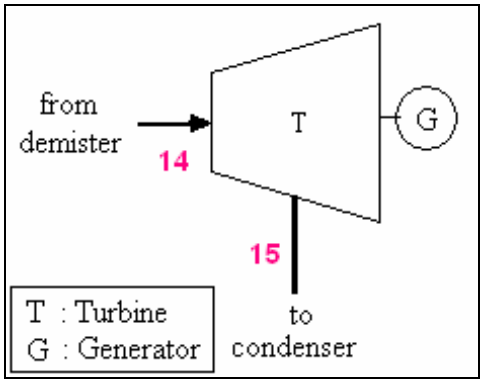

Figure 4.6. Turbine expansion flow process.

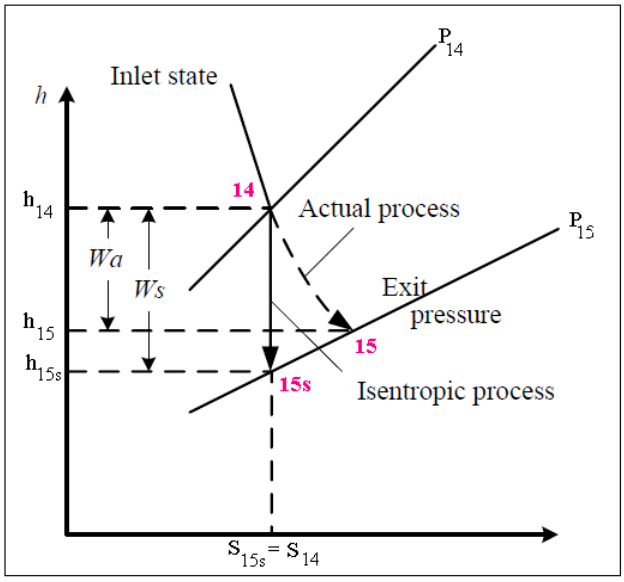

Figure 4.7. h-s diagram for the actual process and isentropic of an adiabatic turbine

Turbine power is given by the following equation:

$$\dot{W}_{tur} = \dot{m}_{14} \times (h_{14} - h_{15}) \tag{4.31}$$

The turbine isentropic efficiency (η_{tur}) is given by:

$$\eta_{tur} = \frac{\text{Actual turbine work}}{\text{Isentropic turbine work}} = \frac{\dot{W}_{tur}}{\dot{W}_{tur,is}} \tag{4.32}$$

Usually the changes in kinetic and potential energies, associated with a fluid stream flowing through a turbine, are small relative to the change in enthalpy and can be neglected. Then the work output of an adiabatic turbine simply becomes the change in enthalpy, and the equation becomes (Swandaru, 2006);

$$\eta_{tur} = \frac{h_{14} - h_{15}}{h_{14} - h_{15,is}} \tag{4.33}$$

Steam turbine efficiencies are calculated by a modified Baumann rule (DiPippo, 1982);

$$\eta_{tur} = 0.85 \times (1 - 1.2 \times (1 - x_{15,is})) \tag{4.34}$$

To determine the steam turbine efficiency, it is necessary to calculate the isentropic quality ($x_{15,is}$) at the turbine exit.

$$x_{15,is} = \frac{s_{15,is} - s_{l,15}}{s_{15} - s_{l,15}} \tag{4.35}$$

The actual turbine power is calculated using the actual enthalpy of the geothermal fluid at state 15 by the help of Eq. 4.33. Thus, the turbine power is calculated by Eq. 4.31. The turbine-generator power is defined by the following equation:

$$\dot{W}_{gen} = \dot{W}_{tur} \times \eta_{gen} \tag{4.36}$$

Exergy loss and exergetic efficiency:

$$I_{tur-gen} = \dot{E}x_{14} - \dot{E}x_{15} - \dot{W}_{tur} \tag{4.37}$$

$$\eta_{Ex_{tur-gen}} = \frac{\dot{W}_{tur}}{\dot{E}x_{14} - \dot{E}x_{15}} \tag{4.38}$$

4.1.1.4. Condenser

The primary purpose of the condenser is to condense the exhaust steam leaving the turbine. The circulating water system supplies cooling water to the turbine condensers and thus acts as the vehicle by which heat is rejected from the steam cycle to the environment. Its performance is vital to the efficiency of the power plant itself because a condenser operating at the lowest temperature possible results in maximum turbine work and cycle efficiency and in minimum heat rejection.

The typical condensate temperature attained in practice is 45-50°C, corresponding to a condenser pressure of 9.6-12.5 kPa-abs (El-Wakil, 1984; Moghaddam, 2006).

Figure 4.8 presents the temperature distribution in the condenser. The circulating-water inlet temperature should be sufficiently lower than the steam-saturation temperature to result in reasonable values of ΔT_0. It is usually recommended that ΔT_i should be between about 11 and 17°C and that ΔT_0, should not be less than 2.8°C. The enthalpy drop and turbine work per unit pressure drop is much greater at the low-pressure end than the high-pressure end of a turbine (El-Wakil, 1984).

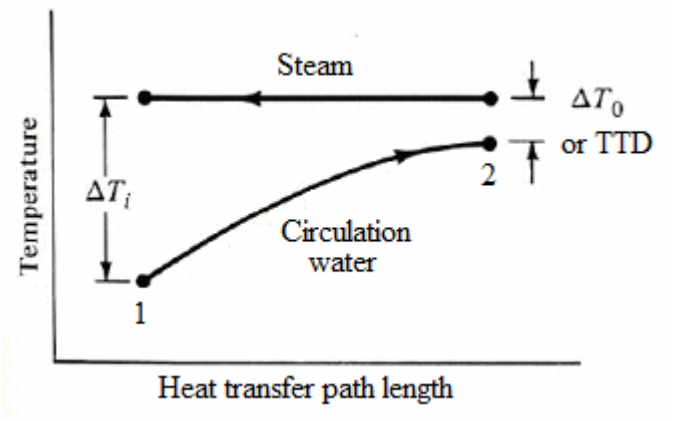

Figure 4.8. Condenser temperature distribution.
(Source: Siregar, 2004)

There exist two types of condensers, which are direct contact and surface condensers. The most common type used in GPPs is direct-contact condensers (Siregar, 2004). The flow diagram of a direct-contact condenser is shown in Figure 4.9. Steam leaving the turbine (15) is exhausted into the condenser where it is mixed with a spray of cold water from the cooling tower (30) and gas coolers of the NCG removal system (29). The steam condenses on the water droplets and the condensate drains through a barometric leg (20) into a seal pit tank to overcome atmospheric pressure. NCGs and small amount of steam are sucked from the condenser (16) by NCG removal system.

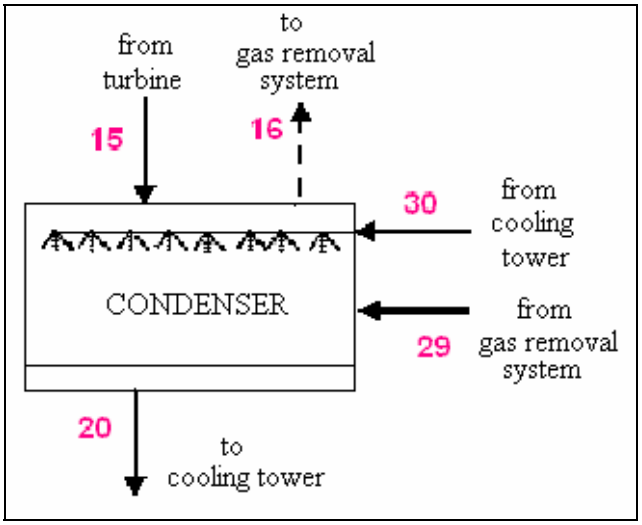

Figure 4.9. Condenser flow diagram.

The condenser heat load can be calculated using the following equation:

$$\dot{Q}_{con} = \dot{m}_{15} \times h_{15} - \dot{m}_{16} \times h_{16} - \left[\dot{m}_{l,15} + (\dot{m}_{s,15} - \dot{m}_{s,16})\right] \times h_{20} \tag{4.39}$$

The cooling water mass flowrate is calculated as:

$$\dot{m}_{30} = (\dot{Q}_{con} - \dot{m}_{29} \times (h_{20} - h_{29})) / (h_{20} - h_{30}) \tag{4.40}$$

Exergy loss and exergetic efficiency:

$$I_{con} = \dot{E}x_{15} + \dot{E}x_{29} + \dot{E}x_{30} - \dot{E}x_{16} - \dot{E}x_{20} \tag{4.41}$$

$$\eta_{Ex,con} = \frac{\dot{E}x_{16} + \dot{E}x_{20}}{\dot{E}x_{15} + \dot{E}x_{29} + \dot{E}x_{30}} \tag{4.42}$$

4.1.1.5. Cooling Tower

Power plants generate large quantities of waste heat that is often discarded through cooling water in nearby lakes or rivers. In some cases, however, the cooling water supply is limited or thermal pollution is a serious concern. In such cases the waste heat must be rejected to the atmosphere, with cooling water re-circulating and serving as a transport medium for heat transport between the source and the sink (the atmosphere). One way of achieving this is through the use of cooling tower.

A cooling tower is an evaporative heat transfer device in which atmospheric air cools warm water, with direct contact between the water and the air, by evaporating part of the water (Siregar, 2004).

The mass and energy balances between hot water and cold air entered, cold water and hot air exiting the cooling tower are shown in Figure 4.10.

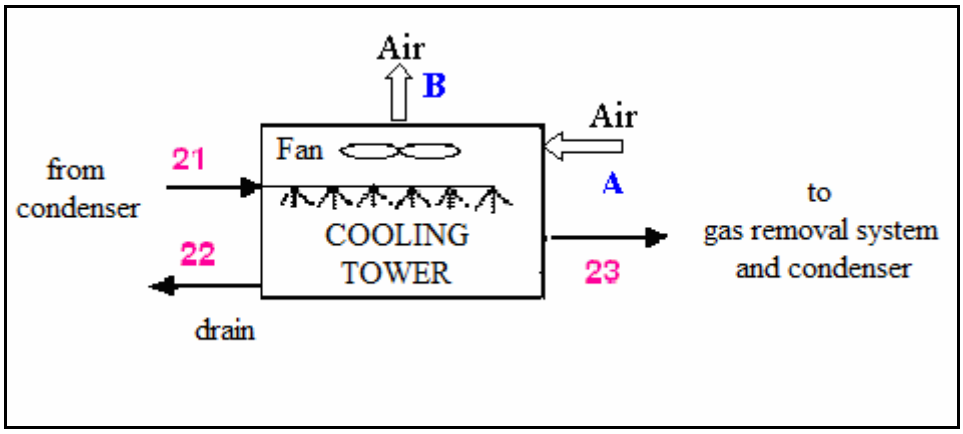

Figure 4.10. Cooling tower flow diagram.

The circulating condensate leaves (20) the condenser is pumped by a circulating water pump (Pump1) to the top of the cooling towers (21). Water reaches the top of the cooling towers with 3°C temperature drop. As the water droplets fall down and break up into fine droplets, a stream of air (A) flows across the water droplets thus creating cooling by evaporation and convection-conduction mechanisms. The stream of air is created by suction of air fans ($\dot{W}_{fan}$) located at the top of the cooling towers. The water droplets eventually fall into the cold pond from where it is transferred into the condenser inlet pipeline (23). Some water goes to the gas cooler of the NCG removal system and the rest into the condenser. Warm moist air leaves the cooling tower (B) driven out by air fans ($\dot{W}_{fan}$). Some condensate is lost to the air. Changes in potential and kinetic energies and heat transfer are all negligible. No mechanical work is done. The dry air goes through the tower unchanged. The water vapor in the air gains mass due to the evaporated water. Thus, based on a unit mass of dry air, and with the subscripts A and B referring to air inlet and exit, and the subscripts 21 and 23 to circulating water inlet and exit, respectively (the air leaving the system at B is often saturated):

Following psychometric practice, the equations are written for a unit mass of dry air (El-Wakil, 1984).

$$h_{a_A} + \omega_A \div h_{s_A} + W_{21} \times h_{l_{21}} = h_{a_B} + \omega_B \times h_{s_B} + W_{23} \times h_{l_{23}} \tag{4.43}$$

$$\omega_B - \omega_A = W_{21} - W_{23} \tag{4.44}$$

From the cooling water calculation in the condenser section, it is known that the volume flowrate of hot cooling water entering the cooling tower is $\dot{m}_{cw}$ (m^3/s). Thus, dry air mass flowrate can be found from:

$$\dot{m}_a = \dot{m}_{cw} / W_{21} \tag{4.45}$$

Exergy loss and exergetic efficiency:

$$I_{ct} = \dot{E}x_{21} + \dot{E}x_{air,A} + \dot{W}_{fan} - \dot{E}x_{22} - \dot{E}x_{23} - \dot{E}x_{air,B} \tag{4.46}$$

$$\eta_{Ex,ct} = \frac{\dot{E}x_{21} + \dot{E}x_{air,A} - I_{ct} - \dot{E}x_{22} - \dot{E}x_{exhaust}}{\dot{E}x_{21} + \dot{E}x_{air,A}} \tag{4.47}$$

4.1.1.6. NCG Removal Systems

CS, SJES, HS and RS is modeled as NCG removal systems.

4.1.1.6.1. Compressor System

A two-stage CS flow diagram is shown in Figure 4.11.

Compression is ideally an isentropic process. To determine the actual enthalpy at compressor exit is quite complex since the geothermal steam is a mixture of water vapor and CO_2. Therefore, the isentropic enthalpies of water vapor and CO_2 are calculated separately. Then, the isentropic enthalpy of the mixture is calculated using the mass flowrate of water vapor and CO_2 and their isentropic enthalpies.

$$h_{17,is} = \frac{\dot{m}_{s,17} \times h_{s,17,is} + \dot{m}_{NCG,17} \times h_{NCG,17,is}}{\dot{m}_{17}} \tag{4.48}$$

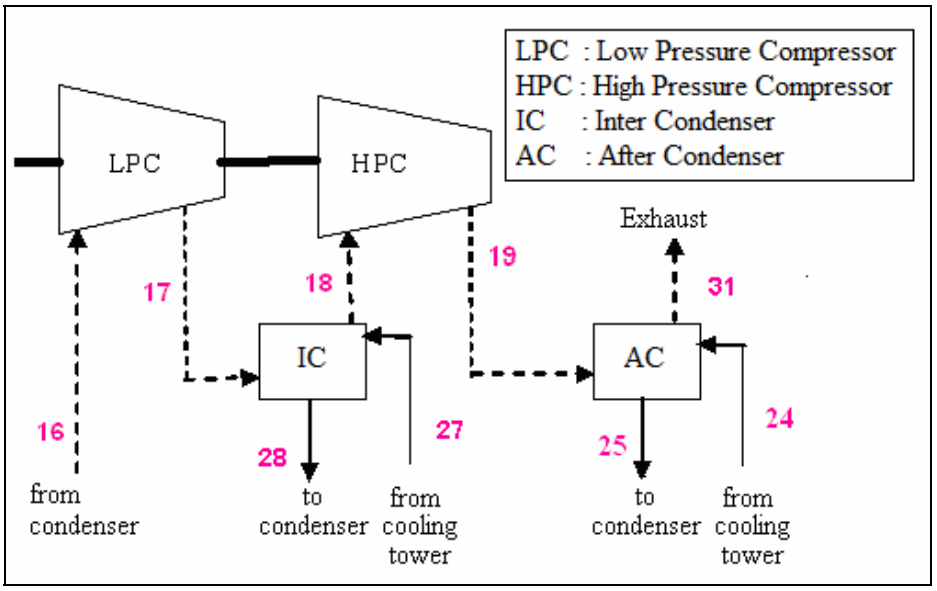

Figure 4.11. Two-stage CS flow diagram

The actual enthalpy at the compressor exit is calculated using Eq. 4.49.

$$\eta_{comp} = \frac{h_{17,is} - h_{16}}{h_{17} - h_{16}} \tag{4.49}$$

Exergy loss and exergetic efficiency:

$$\begin{aligned} I_{LPC} &= \dot{E}x_{16} - \dot{E}x_{17} + \dot{W}_{LPC} \\ I_{HPC} &= \dot{E}x_{18} - \dot{E}x_{19} + \dot{W}_{HPC} \end{aligned} \tag{4.50}$$

$$\begin{aligned} \eta_{Ex,LPC} &= \frac{\dot{E}x_{17} - \dot{E}x_{16}}{\dot{W}_{LPC}} \\ \eta_{Ex,HPC} &= \frac{\dot{E}x_{19} - \dot{E}x_{18}}{\dot{W}_{HPC}} \end{aligned} \tag{4.51}$$

4.1.1.6.2. Steam Jet Ejector System

Two-stage SJES flow diagram is shown in Figure 4.12.

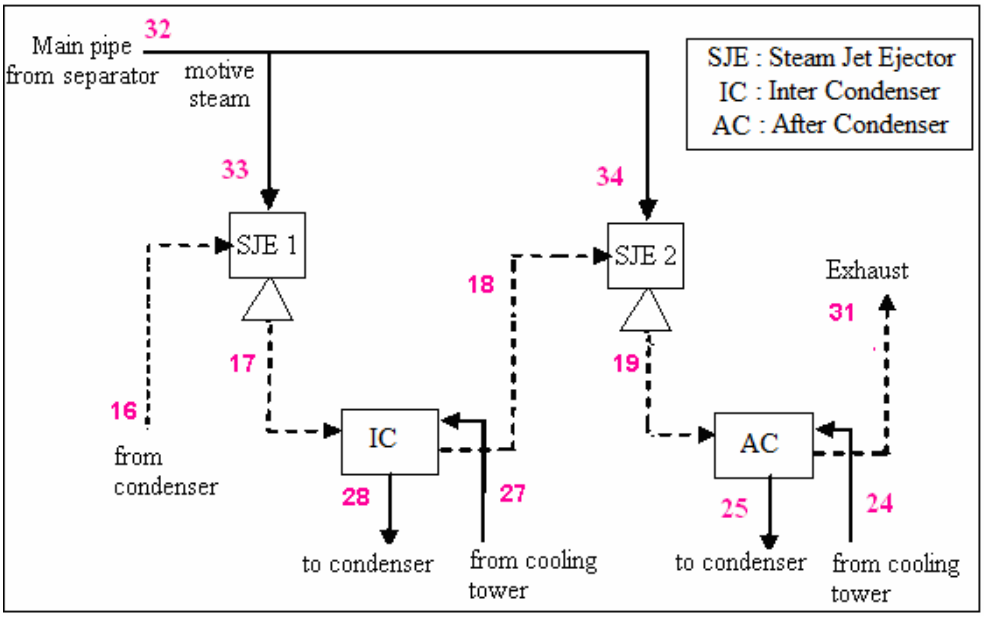

Figure 4.12. Two-stage SJES flow diagram.

The suction and discharge pressure of each stage is determined by the following calculations (Geothermal Institute, 1996b). Each stage uses equal pressure ratios based on system suction and discharge pressure of 90% condenser pressure and 105 kPa. The following formula decides the suction and discharge pressures for each stage through equal ratios:

$$\frac{P_{17}}{P_{16}} = \frac{P_{19}}{P_{18}} \tag{4.52}$$

SJEs are feed by the motive steam, which leaves the separator. Between the stages the gas coolers are used. *Dalton's laws of partial pressure* and *ideal gas equations* are used to calculate necessary motive steam flowrate at point 33 and 34 (Hall, 1996).

Calculate the entrainment ratio using the equation which was determined from the entrainment ratio curve (Figure 4.13).

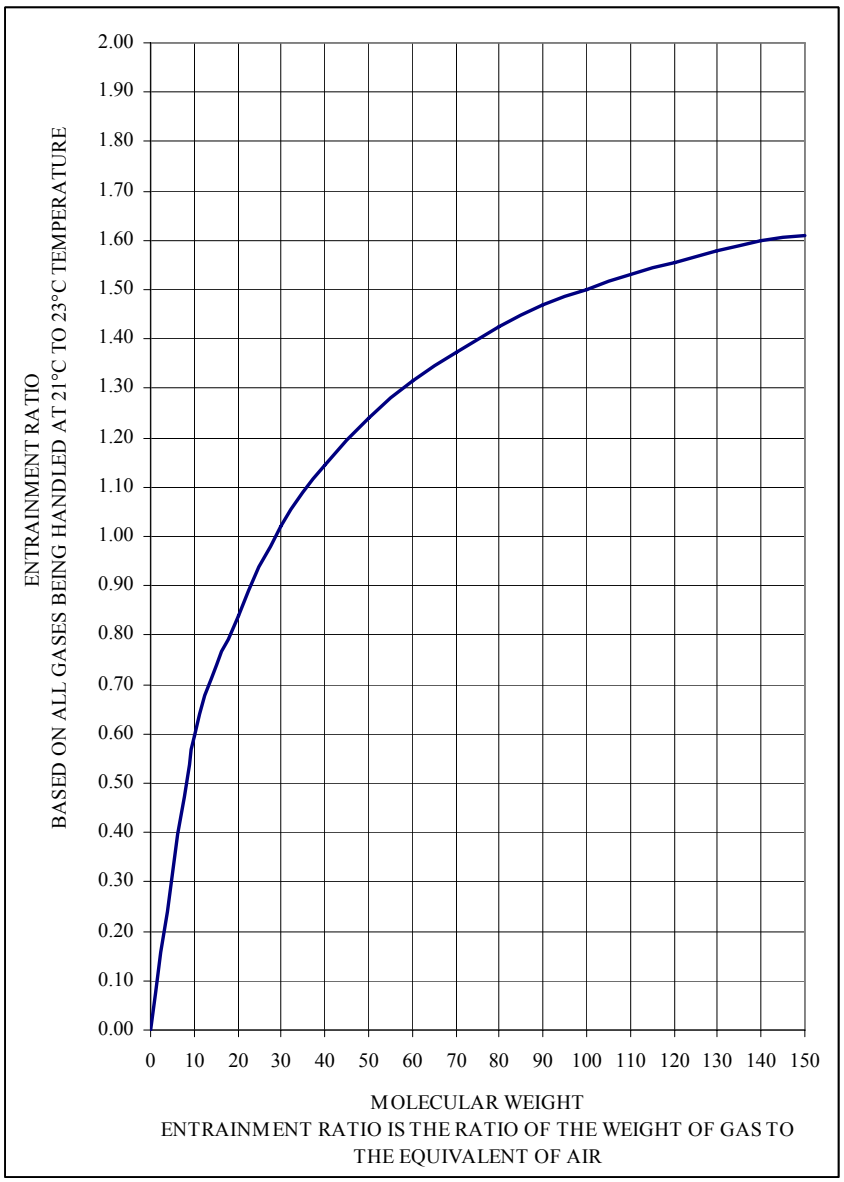

Figure 4.13. Entrainment ratio curve.
(Source: Geothermal Institute, 1996b)

The entrainment ratio for NCG can be determined by the equation:

$$E_{NCG} = \left[\left(5.73 \times 10^{-4} + 18.36\right) + \frac{\left(2.01 \times (M_{NCG}^{0.86})\right)}{\left(18.36 + (M_{NCG}^{0.86})\right)} \right] \tag{4.53}$$

The entrainment ratio for steam can be determined by the equation:

$$E_s = \left[\left(5.73\times10^{-4} + 18.36\right) + \frac{\left(2.01\times(M_{H_2O}^{0.86})\right)}{\left(18.36 + (M_{H_2O}^{0.86})\right)} \right] \tag{4.54}$$

Calculate total air equivalent (*TAE*):

$$TAE = \left[\frac{\dot{m}_{NCG}}{E_{NCG}} + \frac{\dot{m}_s}{E_s} \right] \tag{4.55}$$

The compression ratio is defined as the ratio of discharge to suction as expressed in Eq. 4.51. The expansion ratio for the first and second stages is defined as the ratio of motive steam pressure to suction pressure:

$$\begin{aligned} Er_1 &= \frac{P_{33}}{P_{16}} \\ Er_2 &= \frac{P_{34}}{P_{18}} \end{aligned} \tag{4.56}$$

The air steam ratio (AS) can be found by a curve (Figure A.1) that has been transformed into a small program in EES called procedure ratio_1. Inputs required for this program are the expansion ratio and the compression ratio.

Finally, the motive steam mass flowrate for both stages can be found from:

$$\dot{m}_{33} = \frac{TAE_1}{AS_1} \tag{4.57}$$

$$\dot{m}_{34} = \frac{TAE_2}{AS_2} \tag{4.58}$$

Exergy loss and exergetic efficiency:

$$\begin{aligned} I_{sje1} &= \dot{E}x_{16} + \dot{E}x_{33} - \dot{E}x_{17} \\ I_{sje2} &= \dot{E}x_{18} + \dot{E}x_{34} - \dot{E}x_{19} \end{aligned} \tag{4.59}$$

$$\eta_{Ex,sje1} = \frac{\dot{E}x_{16} + \dot{E}x_{33} - I_{sje1}}{\dot{E}x_{16} + \dot{E}x_{33}}$$
$$\eta_{Ex,sje2} = \frac{\dot{E}x_{18} + \dot{E}x_{34} - I_{sje2}}{\dot{E}x_{18} + \dot{E}x_{34}} \quad (4.60)$$

4.1.1.6.3. Hybrid System

The flow diagram of HS which is a combination of SJE and LRVP is demonstrated in Figure 4.14.

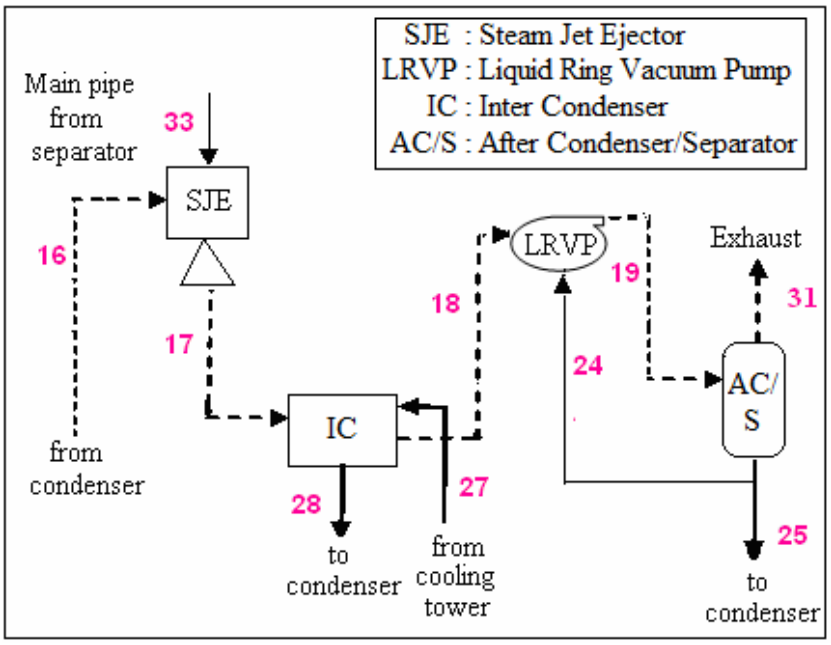

Figure 4.14. The flow diagram of HS.

The power of the LRVP is calculated by the following equation (Siregar, 2004):

$$\dot{W}_{LRVP} = \left[\frac{\gamma}{\gamma - 1}\right] \frac{\dot{m}_{NCG} \times Ru \times T_{NCG}}{\eta_{LRVP} \times M_{NCG}} \left[\left(\frac{P_{19}}{P_{18}}\right)^{\left(1-\frac{1}{\gamma}\right)} - 1\right] \quad (4.61)$$

Exergy loss and exergetic efficiency:

$$I_{LRVP} = \dot{E}x_{18} - \dot{E}x_{19} + \dot{W}_{LRVP} \tag{4.62}$$

$$\eta_{Ex,LRVP} = \frac{\dot{E}x_{19} - \dot{E}x_{18}}{\dot{W}_{LRVP}} \tag{4.63}$$

4.1.1.6.4. Reboiler System

RSs offer the only technology available for removing NCGs from geothermal steam upstream of the turbine. In the Thesis, a vertical tube evaporator reboiler is used (Figure 4.15).

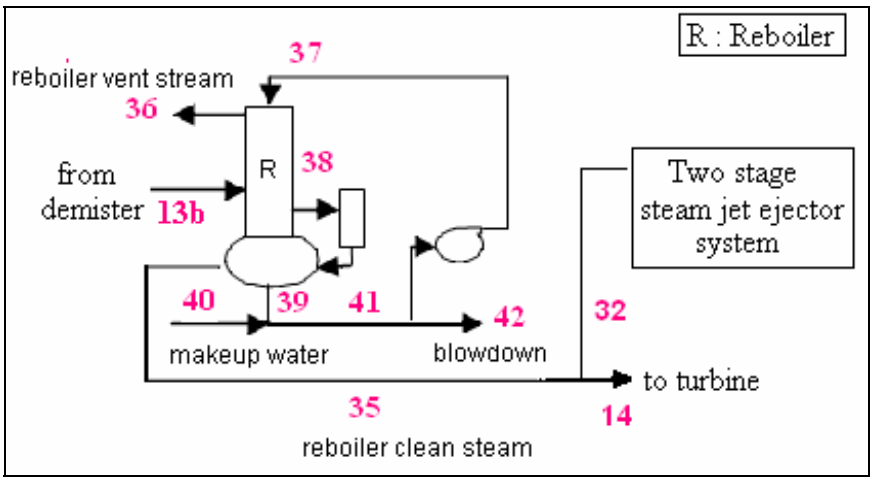

Figure 4.15. RS flow diagram.

The rejection of NCGs to vent stream and steam/NCG weight ratio in vent gas are taken as 98% and 50%-50%, respectively. Blowndown is taken as 1% (Eq. 4.66). RS requires at least 330 kPa pressure drop between the separator and turbine inlet according to a study for KGPP (Coury, et al., 1996; Vorum and Fritzler, 2000; Gunerhan, 1996).

$$\dot{m}_{NCG,36} = 0.98 \times \dot{m}_{NCG,13b} \tag{4.64}$$

$$\dot{m}_{s,36} = \dot{m}_{NCG,36} \tag{4.65}$$

$$\dot{m}_{s,42} = (\dot{m}_{s,13b} - \dot{m}_{s,36}) \times 0.01 \tag{4.66}$$

Exergy loss and exergetic efficiency:

$$I_{reboiler} = \dot{E}x_{13b} - \dot{E}x_{35} - \dot{E}x_{36} \tag{4.67}$$

$$\eta_{Ex,reboiler} = \frac{\dot{E}x_{35}}{\dot{E}x_{13b}} \tag{4.68}$$

4.1.1.6.5. Inter and After Condensers

In a multi-stage system, inter and after condensers are typically used between the stages. By condensing the vapor prior to the next stage, the vapor load is reduced. This allows smaller NCG removal systems to be used, and reduces steam consumption. After condenser can also be added to condense vapor from the final stage. Adding an after condenser will not affect overall system performance, but may ease disposal of vapor and acts as a noise suppressor. (Birgenheier et al., 1993; Swandaru, 2006).

- **Inter condenser**

Flow diagram of inter condenser (IC) is shown in Figure 4.16.

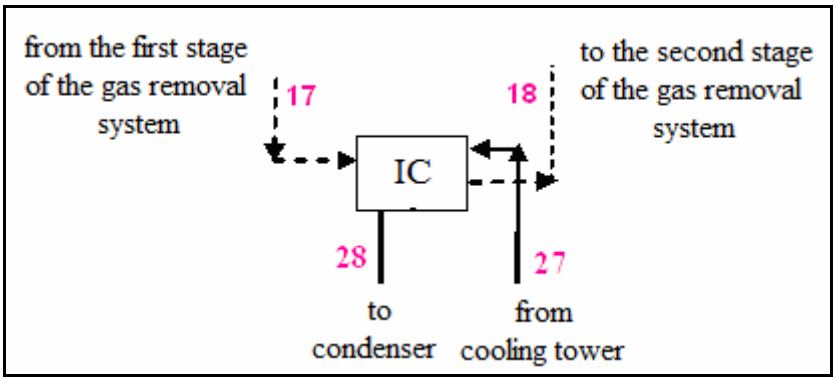

Figure 4.16. The inter condenser flow diagram.

Inter condenser heat load:

$$\dot{Q}_{ic} = \dot{m}_{s,17} \times h_{s,17} + \dot{m}_{NCG,17} \times h_{NCG,17} - \dot{m}_{s,18} \times h_{s,18} - \dot{m}_{NCG,18} \times h_{NCG,18} - \left[(\dot{m}_{s,17} - \dot{m}_{s,18})\right] \times h_{28} \tag{4.69}$$

The cooling water mass flowrate:

$$\dot{m}_{cw,1} = \frac{\dot{Q}_{ic}}{(h_{28} - h_{27})} \tag{4.70}$$

Exergy loss and exergetic efficiency:

$$I_{ic} = \dot{E}x_{17} + \dot{E}x_{27} - \dot{E}x_{18} - \dot{E}x_{28} \tag{4.71}$$

$$\eta_{Ex,ic} = \frac{\dot{E}x_{17} + \dot{E}x_{27} - I_{ic}}{\dot{E}x_{17} + \dot{E}x_{27}} \tag{4.72}$$

- **After condenser**

In Figure 4.17 flow diagram of after condenser (AC) is presented.

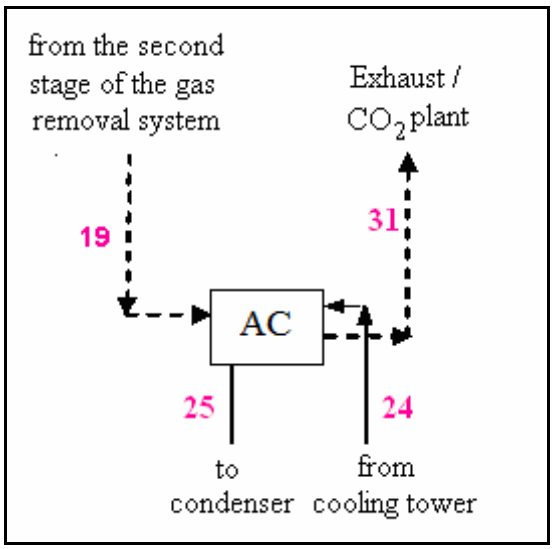

Figure 4.17. The after condenser flow diagram.

Similarly with inter condenser calculations, heat load:

$$\dot{Q}_{ac} = \dot{m}_{s,19} \times h_{s,19} + \dot{m}_{NCG,19} \times h_{NCG,19} - \dot{m}_{NCG,31} \times h_{NCG,31} - \dot{m}_{s,19} \times h_{25} \tag{4.73}$$

and cooling water mass flowrate:

$$\dot{m}_{cw,2} = \frac{\dot{Q}_{ac}}{(h_{25} - h_{24})} \tag{4.74}$$

Exergy loss and exergetic efficiency:

$$I_{ac} = \dot{E}x_{19} + \dot{E}x_{24} - \dot{E}x_{31} - \dot{E}x_{25} \tag{4.75}$$

$$\eta_{Ex,ac} = \frac{\dot{E}x_{19} + \dot{E}x_{24} - I_{ac}}{\dot{E}x_{19} + \dot{E}x_{24}} \tag{4.76}$$

4.1.1.7. Water Circulation Pumps and Cooling Tower Fans

In a power plant, pumps play an important part in cooling process. The representative single-flash GPP employs mainly three water circulation pumps are considered as shown in Figure 4.18.

- Pump1: from the condenser exit to the cooling tower inlet,
- Pump2: from the cooling tower exit to the condenser inlet,
- Pump3: for makeup water to the cooling tower inlet.

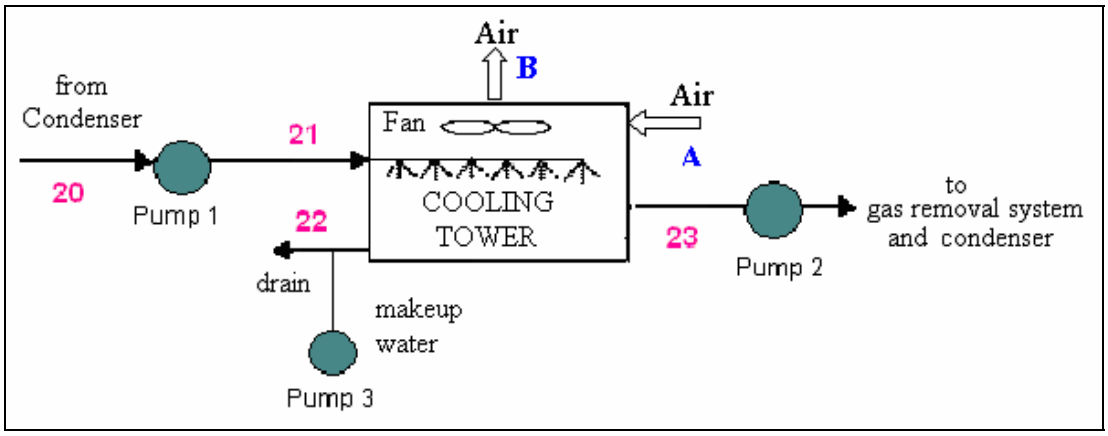

Figure 4.18. Water circulation pumps in the GPP.

Make-up water must be added to the cycle to replace the water loss due to evaporation and air draft. To minimize the water carried away by the air, drift eliminators are installed in the wet cooling tower above the spray section (Cengel and Boles, 2006). The makeup water flowrate is calculated by

$$\dot{m}_{makeup} = 1.22 \times Evaporation\ loss \tag{4.77}$$

The evaporation loss rate is 1-1.5% of the total circulating water flowrate. Blowdown is normally 20% of evaporation loss but sometimes the value is similar to evaporation loss, depending upon the content of chemicals, content of various minerals, and the size of the plant. The drift loss is perhaps 0.03% of the total circulating water flowrate (Siregar, 2004).

$$\begin{aligned} Evaporation\ loss &= \dot{m}_a \times (\omega_2 - \omega_1) \\ Drift\ and\ blowdown\ loses &: 0.22 \times Evaporation\ loss \end{aligned} \tag{4.78}$$

The following equation is used to calculate the power of water circulation pumps $\dot{W}_{pump}$, in watt:

$$\dot{W}_{pump} = \frac{\dot{V}_l \times \Delta P}{\eta_{pump}} \tag{4.79}$$

$$\dot{W}_{motor,pump} = \frac{\dot{W}_{pump}}{\eta_{motor,pump}} \tag{4.80}$$

Exergy loss and exergetic efficiency:

$$I_{pump} = \dot{E}x_{in} - \dot{E}x_{out} + \dot{W}_{pump} \tag{4.81}$$

$$\eta_{Ex,pump} = \frac{\dot{E}x_{in} - \dot{E}x_{out}}{\dot{W}_{pump}} \tag{4.82}$$

The air circulation in the cooling tower is provided by fans and the power of the fan is determined in similar way with water circulation pumps by using Eqs. 4.79-82.

4.2. Economical Model

GPPs, like most types of power plants, promote economic growth. One of the unique external benefits of geothermal power, unlike many traditional types of power, is sustainable development. GPPs provide long-term, stable, well-paying jobs (typically in rural areas), and supply income to local, state, and federal economies through decades of reliable, secure, domestic, renewable energy production (Kagel, 2006).

The prime objective of every project is to be profitable. Profits are related to the difference between the price obtained for power and the cost of producing of a geothermal project. The financial structure, conditions and related costs are important factors influencing the levelized cost of energy and profitability of the project. Therefore, in the Thesis, flashed-steam GPPs are evaluated depending on NPV, IRR and SPT methods. Besides, cost of electricity production of the plant for four different NCG removal system options are determined to compare the NCG removal systems to each other.

4.2.1. Geothermal Power Production Cost

Power plant design is a complex activity that aims to minimize both construction and O&M costs in a long-term perspective. It thus consists of defining the optimal size of power plant equipment and choosing the best suited technologies and construction materials to deal with site and resource particularities.

Geothermal power production cost is composed of two major cost components:

- Initial capital investment cost
- Operation and maintenance (O&M) costs.

4.2.1.1. Initial Capital Investment Cost

Initial capital investment cost of GPPs is very site and resource specific. The major cost components of the initial investment cost are:

- Exploration,
- Confirmation,
- Drilling,
- Permitting,
- Steam Gathering System,
- Power Plant Design&Construction,
- Transmission.

The wide range of the exploration costs is resulted of the nature and size of exploration activities. Current projects tend to be smaller, focus on more difficult areas than past projects and may use more advanced and thus more expensive exploration technologies (GEA, 2005).

The confirmation cost mainly consists of reservoir design, engineering and the drilling of some injection capacity to dispose of fluids from production well tests. This corresponds roughly to one-fourth of the total drilling costs. Resulting confirmation costs may however vary widely according to the resource characteristics and drilling success rate (GEA, 2005).

Drilling cost is highly dependent upon rock permeability, resource temperature and pressure, well productivity, number of wells, depth and diameter of wells and operating time of the drilling rig (GEA, 2005).

Permitting cost includes exploration and site development permits together. Permitting cost is unique depending on the geothermal region and located city and country (GEA, 2005). In Turkey the unit range of the tender cost for permitting was 565-2030 USD/kW in 2008 (Sener and Uluca, 2009).

The steam gathering cost includes the cost of the network of pipes connecting the power plant with all production and injection wells. The cost for these facilities varies widely depending on the distance from the production and injection wells to the power plant, the flowing pressure and chemistry of the produced fluids (GEA, 2005).

Power plant design and construction cost are unique in terms of site (accessibility and topography, local weather conditions, water availability and land type) and resource characteristics (temperature, chemistry etc.) and these characteristics effect on the power conversion technology (steam vs. binary) and power system cost (GEA, 2005).

Transmission cost includes the cost of building a new transmission line to connect the power plant to the grid. Because, valuable geothermal resources are not always located in areas furnished with transmission facilities. Transmission lines are quite expensive and their cost may be a hurdle to a project's competitiveness (GEA, 2005).

The capital investment cost components and ranges of GPPs are summarized in Table 4.2.

Table 4.2. Capital investment cost components and unit cost range.
(Source: GEA, 2005)

Capital Investment Cost Component		Cost Range (USD/kWe)
Exploration		14-263
Confirmation		150
Drilling		600-1200
Permitting		565-2030*
Steam Gathering System		30-400
Power Plant Design&Construction	Binary	1100-2700
	Flash	1062-2400
Transmission		13-236

*Values specific for Turkey (since 2008). (Source: Sener and Uluca, 2009)

Typical cost breakdown of geothermal power projects is summarized in Figure 4.19.

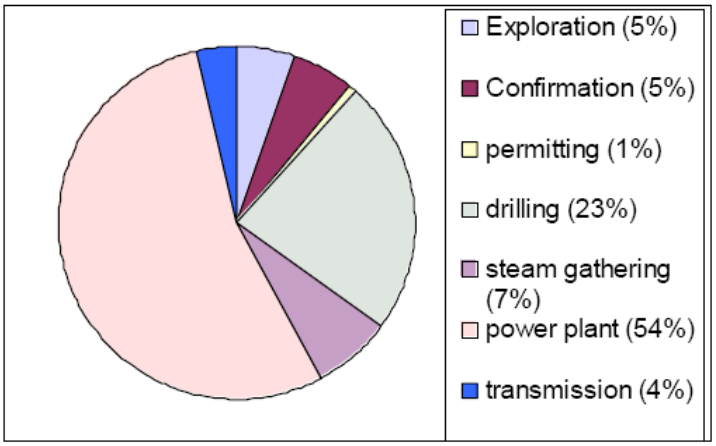

Figure 4.19. Typical cost breakdown of geothermal power projects.
(Source: GEA, 2005)

4.2.1.2. Operation and Maintenance Cost

Each power plant has specific O&M cost that depends on the quality and design of the power plant, the characteristics of the geothermal resource, the environmental regulations and requirements applicable to the site, and the structure and efficiency of the company. Major parameters affecting O&M cost are related to the plant requirement,

- the amount of chemicals and other consumables used during operation,
- the extent of make-up drilling requirements, and
- the cost of the equipment that has to be replaced throughout the years.

According to the available data presented by GEA (2005), O&M cost changes in a range of 10 to 45 USD/MWh and average costs are listed in Table 4.3 On the other hand, in the study of Vorum and Fritzler (2000), O&M costs were taken as 5% of the initial capital investment cost.

Table 4.3. Average O&M cost.
(Source: GEA, 2005)

O&M Cost Components	Average Cost (USD/MWh)
Operation cost	7
Power plant maintenance	9
Steam field maintenance & make-up drilling costs	8
TOTAL	24

4.2.1.3. Factors Affecting Geothermal Power Production Cost

The resource temperature, depth, chemistry, permeability and capacity factor are the major factors affecting the cost of the geothermal power production. The site accessibility and topography, local weather conditions, land type and ownership are additional parameters affecting the cost and time required to bring the power plant online.

The resource temperature will determine the power conversion technology (steam vs. binary) as well as the overall efficiency of the power system. Cost estimates and temperature data is shown in Figure 4.20 (Brugman, 1996).

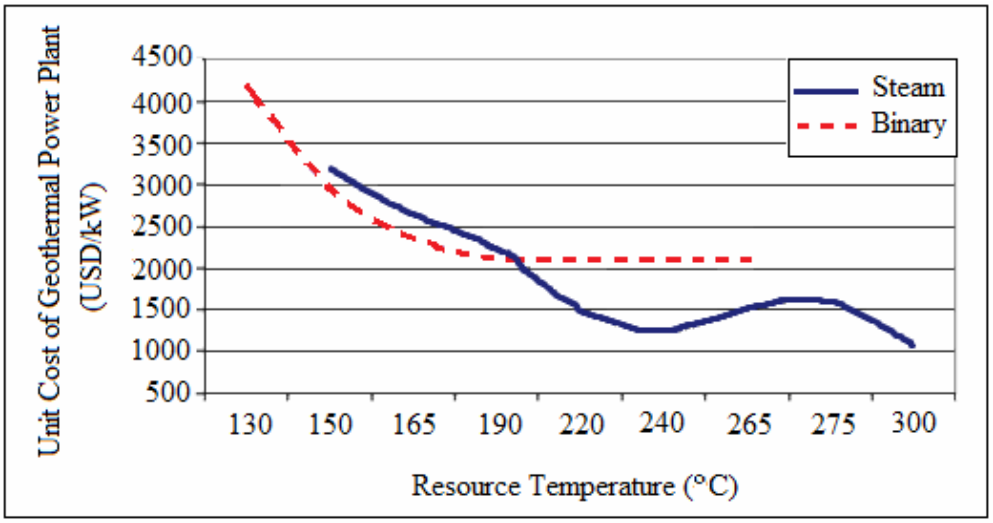

Figure 4.20. Unit cost of GPP vs. resource temperature.
(Source: Brugman, 1996)

The chemical characteristic of geothermal fluid may require additional equipment that can deal with specific problems or may influence the size of some power plant components. Current detailed cost estimates and variability ranges for these impacts are unfortunately not available. Brugman (1996) provides cost estimates for different projects with various resource characteristics and locations. Cost information for equipment needed to dealing with NCG disposal and H2S abatement is displayed in Table 4.4. (GEA, 2005).

Table 4.4. Additional cost information of the power plant according to chemistry of the resource. (Source: Brugman, 1996)

	Average Unit Cost (USD/kW)	Unit Cost Range (USD/ kW)
NCG Removal	9	3-85
H_2S Abatement	33	0-75

The capacity factor (CF) of GPPs corresponds to the ratio between the amount of energy actually delivered to the grid and the potential energy that it could have delivered during the period of time considered. GPPs typically have a CF around 90%, which is higher than most other power production technology. The capacity factor will determine the quantity of electricity produced and thus the amount of kWh on which all power production costs (i.e. Capital Investment Costs and O&M costs) will be spread out (GEA, 2005).

4.2.2. Economic Evaluation Methods and General Equations

The purpose of an economic analysis is to determine differences between outflows and inflows of the project. In accordance with the result of an economic analysis, the project manager can compare different investments and their cash flow profiles. If the total amount of net incomes is greater than total net outcomes for a considered investment, the project will be accepted. At the end of this evaluation, a project manager decides either this project is applicable or not and selects the appropriate project among the alternatives (Erdogmus, 2003; EIEI, 1997).

There are several economical parameters, such as economic project life, salvage or amortization cost, cash flows, discount or interest rate, which have major effects on the investment decision.

An economic analysis and finance scheduling for renewable energy investments should be based on long-term consideration. If the duration extends, the degree of uncertainty of cash flows will be increased. Physical life of an investment is the duration in which all of the facilities are realized. Economic project life of the GPPs is taken as 20-25 years (Vorum and Fritzler, 2000; Lund and et al., 1998; Triyono, 2001; GEA, 2005; Kanoglu and Cengel, 1999).

Salvage or amortization cost is the market value of an asset at the end of its life. This concept includes both the cost of an investment at the end of the economic and physical lives. Therefore, to determine the accurate salvage or amortization cost is important in proposed investments.

Most economic analysis involves conversion of estimated or given cash flows to some point or points in time. The difference between cash inflows and cash outflows for the project life is defined as cash flows. Cash flow diagrams are used to visualize cash flows. Individual cash flows are represented as vertical arrows along a horizontal time scale, which covers the life of a project. Upward-pointing arrows generally used to indicate net inflows whereas downward-pointing arrows used to show net outflows. A sample cash flow diagram is drawn in Figure 4.21 (GEA, 2005; Erdogmus, 2003).

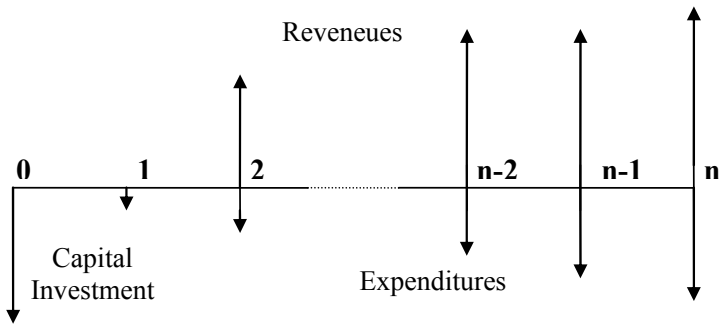

Figure 4.21. A sample cash flow diagram.

Discount rate has vital role in economical analysis. Higher discount rates enable investor to select the project that gives higher cash flows in the earliest years of the investments while smaller discount rates enable investor to select the project which has high net cash flow.

There exist various economical evaluation methods for the financial viability analysis of investments, which are based on the some input values: revenues, disbursements, and capital investment costs. These methods are:

- Net present value method
- Net future value method
- Internal rate of return method
- Payback time period method
- Benefit/ Cost ratio method
- Net Benefit/Cost ratio method

In the Thesis, NPV, IRR and SPT methods are used. Addition of these methods, cost of electricity production is calculated.

Cost of electricity production can be defined as cost of per kWh electricity production and it includes initial capital investment and O&M costs. Therefore, cost of electricity production is one of the parameters which gives an idea about project profitability. Besides the profitability, electricity sales price range can be determined by the help of the cost of the electricity production.

The general equations in the economical analysis are listed in Table 4.5.

Table 4.5. General equations of economical analysis.

	Equation	Equation No
Tax cost	$Tax_n = TI_n * TR$	(4.83)
Taxable income	$TI_n = \mathrm{Re}v - OM_{\mathrm{cost}} - AC_n$	(4.84)
Book value*	$BV_n = 0.9BV_{n-1}$	(4.85)
Amortization cost	$AC_n = BV_{n-1} - BV_n$	(4.86)

*The first BV is the capital investment cost of the system.

4.2.2.1. Net Present Value Method

NPV method takes the time value of money into the consideration. NPV criterion of an investment is defined as the difference of present value of benefits and

costs in the project exploitation period. Calculations are based on a specific rate of discount that should be determined before. Mathematical expression of NPV criterion is given by Eq. 4.87.

$$NPV = \sum_{n=k+1}^{t} \frac{B_n}{(1+i)^n} - \sum_{n=0}^{k} \frac{C_n}{(1+i)^n} \tag{4.87}$$

If the NPV is calculated for one project and the result is greater than zero, the project or investment is attractive and could be accepted. When the evaluation is realized among alternative projects, the project, which has the greatest NPV, should be recommended for acceptance. Selecting of the most profitable project is not the main objective in this method. If the discount rate and benefits in the future are well estimated, these methods are easily applied on projects. Determination of a discount rate is important in the present value calculations. Different discount rates give various results. Higher discount rates enable investor to select the project that gives higher cash flows in the earliest years of the investments while smaller discount rates enable investor to select the project which has high net cash flow. On the other hand, discount rates are accepted as constant throughout the economic life of the project in the present value calculations. As a matter of fact, it is variable with regard to changing market economies. Usage of different discount rates for different years is quite difficult. NPV method does not reflect the real output of investment project. If this method is used for more than one project, which have different size, selecting of the most appropriate project is not always correct. Therefore, IRR method is more realistic than NPV method.

4.2.2.2. Internal Rate of Return Method

IRR method is also called as discounted cash flow return, profitability index, or simply rate of return method. The IRR measures the performance of an investment as a rate of return unlike NPV which express it as an amount of return. It expresses the real return on any investment. Therefore IRR is related with the calculation of expected profit for the prospective investment. Profit in simple terms is what is left after all the income has been received and all the costs or expenditures have been settled. The IRR

or break-even interest rate is a hypothetical discount rate that equates the sum of the present values of all cash inflows to the sum of the present values of all cash outflows. IRR use same cash flows used in NPV method. However discount rate is an unknown parameter in this method. A minimum standard of desirability, which is determined by an investor, is compared against the calculated value of discount rate that sets the NPV equal to zero. If the calculated rate is higher or equal to the market interest rate, it is profitable to undertake prospective project. IRRs should be ranked from the highest IRR down for the selection of project among alternative projects. On the other hand, it gives an idea to investor to choose the correct time for borrowing money for the project and payable the maximum interest rate. Investments are classified by counting the number of sign changes in its net cash flow sequence. A change from either "+" to "-" or "-"to "+" is counted as one sign change (Figure 4.22). Simple investment is defined as one in which the initial cash flows are negative and there is only one sign change in the net cash flow (Erdogmus, 2003).

Cash flows change during the phases of a project. Generally, the net cash flows are negative in the construction period of projects. They become positive in the following years. If the future net cash flows changes perpetually or project's net benefits switch sign more than once over time, there may be no or multiple IRRs associated with the project. The NPVs of project exhibits different behaviors in these cases. In these circumstances, NPV method should be preferred.

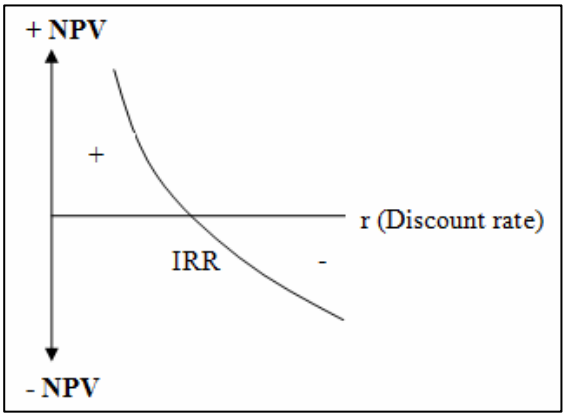

Figure 4.22. NPV profile for a simple investment.

Mathematical expression for IRR is given by Eq. 4.88.

$$NPV = \sum_{n=k+1}^{t} \frac{B_n}{(1+IRR)^n} - \sum_{n=0}^{k} \frac{C_n}{(1+IRR)^n} = 0 \tag{4.88}$$

4.2.2.3. Simple Payback Time Method

The SPT, the most commonly used and simple method for assessing the economic desirability of an investment, is defined as the length of time required to recover the initial cost of an investment from the net cash flow produced by that investment for an interest rate of zero. In other words, SPT is calculated by dividing the investment cost to the net revenue of the system.

The given detailed equations of thermodynamics and economical models for single-flash GPP in this chapter are also valid for double-flash GPP model which only the results are presented in Chapter 6.

CHAPTER 5

METHODOLOGY

The code is developed using Engineering Equation Solver (EES) software for flashed-steam GPPs with the ability of mass, energy, exergy balances and economical analysis by focusing various NCG removal systems. General flow diagram of the model, which consists of two modules as single-flash and double-flash GPPs, is given in Figure 5.1. The main components of flashed-steam GPPs are wellhead, separator, demister, turbine and generator, condenser, cooling tower, circulation pumps and cooling tower fans. NCG removal systems, which are focused in this Thesis, are CS, SJES, HS and RS. The NCG removal systems are modeled for given design parameters and assumptions using mass and energy, exergy balance equations and economical analysis. Then, simulation is conducted for geothermal field (NCG fraction, separator pressure), power plant (condenser pressure and turbine inlet temperature), environmental (wet bulb temperature) and economical (interest rate, tax rate, O&M cost ratio, electricity sales price) parameters.

5.1. Assumptions and Input Parameters

Assumptions are classified into four groups: geothermal field, power plant, environmental and economical parameters.

5.1.1. Geothermal Field Properties

1. Geothermal fluid is a saturated vapor-liquid mixture at the wellhead.
2. The presence of NCGs is treated as only CO_2 since it constitutes over 80% of the NCGs in most liquid dominated geothermal fields (Michaeliedes, 1982).
3. Geothermal fluid properties at each state are determined by considering the geothermal fluid is a mixture of liquid, water vapor and NCGs stream.

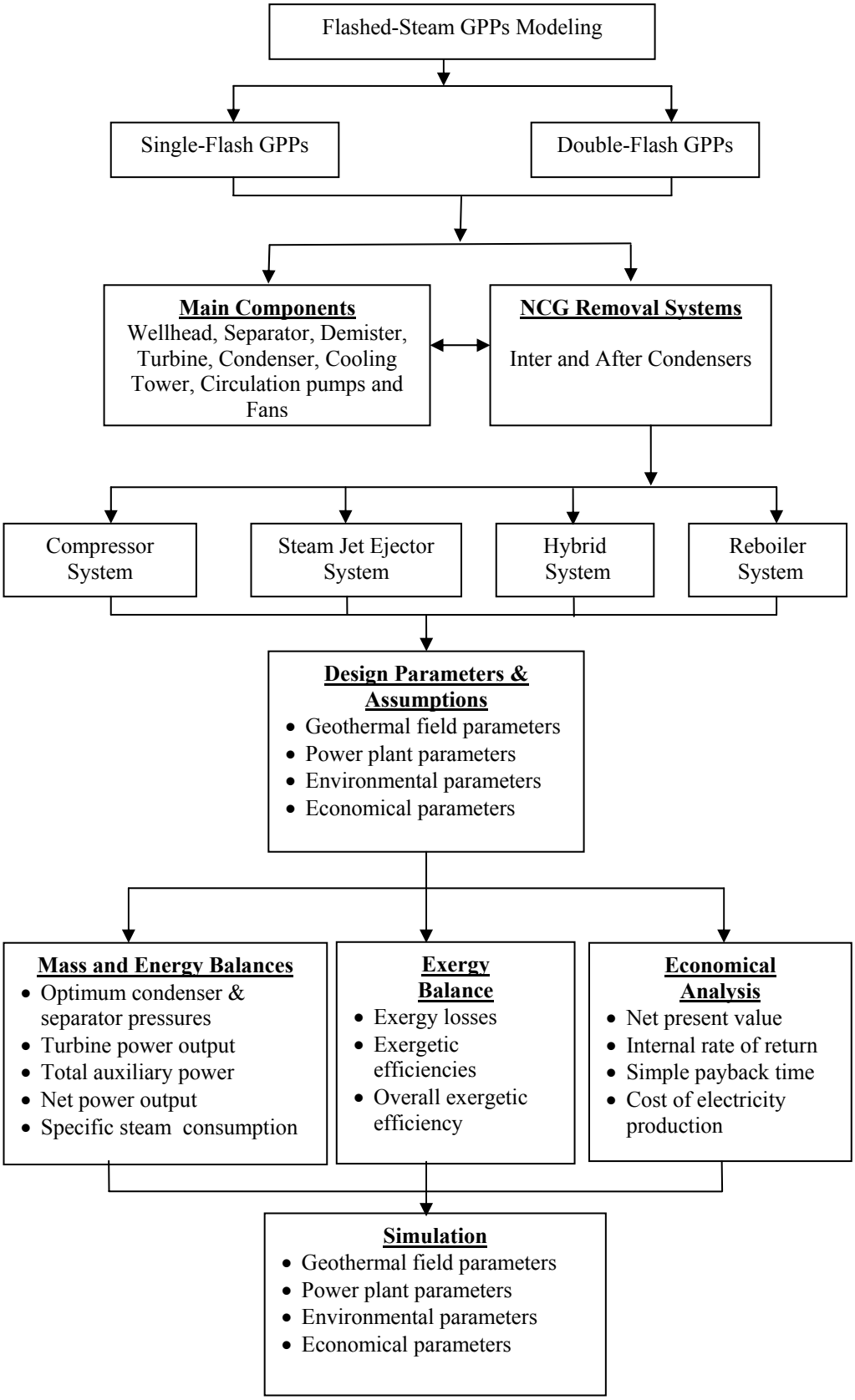

Figure 5.1. Flow diagram of the model.

5.1.2. Plant Properties

1. Geothermal fluid properties at each state are determined by considering the geothermal fluid is a mixture of liquid, water vapor and NCG stream.
2. For all processes of the power plant, CO_2 is considered not to dissolve in the water.
3. Turbine efficiency is calculated according to Baumann Rule (DiPippo, 1982) and the calculation of isentropic quality considers the existence of NCGs.
4. The temperature difference between cooling water entering the cooling tower and hot air leaving the cooling tower is 6°C (Siregar, 2004; Swandaru, 2006).
5. The temperature drop of the condenser exit to the cooling tower entrance is 3°C (Swandaru, 2006).
6. The temperature of CO_2 gas is assumed same as to the wet bulb temperature of cooling water (Swandaru, 2006).
7. NCG removal systems are considered as two-stage.
8. Each stage is assumed to use equal pressure ratios based on system suction and discharge pressure of 90% condenser pressure and 105 kPa.
9. The pressure drop throughout the inter and after condensers is assumed as 1 kPa.

5.1.3. Environmental Properties

1. Meteorological data of the location.
2. Wet bulb temperature is determined from outdoor temperature, pressure and humidity.

5.1.4. Economical Properties

1. Economic life span is 20 years.
2. Amortization life is considered same as economic life span.
3. Amortization coefficient is taken as 0.1 by dividing 200% to the amortization year of 20.
4. Annual O&M cost is assumed constant during the economic life of the plant.

5. Taxable income consists of revenue, O&M cost and amortization cost.
6. The amortization cost value at the end of the plant's economic life of the plant is taken as salvage cost.
7. Inflation is not taken into account.
8. Capital investment is considered at the first year of the construction.
9. Revenue, O&M cost, amortization cost and tax are issued one year later of the capital investment.

Input parameters of the model are summarized in Table 5.1.

Table 5.1. Input parameters of the model.

Input Parameters			
Geothermal field	Flowrate (kg/s)	Wells	
	Pressure (kPa)	Wells	
		Wellhead	
		Separator	CS
			SJES
			HS
			RS
	Temperature (°C)	Wells	
	NCG fraction (%)	At main separator exit	
Power plant	Pressure (kPa)	Condenser	
		Pressure drop between main separator exit and turbine inlet	
		Pressure drop throughout the reboiler	
		Pressure drop of fans/circulation pumps	
		NCG removal system final stage discharge pressure	
	Temperature (°C)	Water at cooling tower exit	
	Efficiency (%)	Generator	
		Compressor	
		LRVP	
		Fans/Circulation pumps	
		Fans/Circulation pumps motor	
Environmental	Pressure (kPa)	Dead state	
	Temperature (°C)	Dead state	
	Relative humidity (%)	Dead state	

(cont. on next page)

Table 5.1. (cont.)

Economical	Cost (USD)	Unit cost of GPP	
		Electricity sales price per kWh	
		NCG removal system cost	CS
			SJES
			HS
			RS
	O&M cost ratio (%)	Ratio of total investment cost of GPP	
	Interest rate (%)		
	Tax rate (%)		
	Capacity factor (%)		
	Installed capacity (MW)		

5.2. Computational Model

A code is written to model flashed steam GPPs in EES software. EES is a powerful tool for solving engineering problems and is useful in solving thermodynamic and heat transfer problems since it offers several built-in libraries comprising of thermodynamic and thermophysical properties. There are two major differences between EES and existing numerical equation-solving programs. First, EES automatically identifies and groups equations that must be solved simultaneously. Second, EES provides many built-in mathematical and thermophysical property functions useful for engineering calculations. Hence there is no need to look these values up in tables. The EES allows the user to write his/her own equations, draw sketches on diagram windows and conduct simulation on diagram window with any input parameter. Both single and double flash GPPs are modeled but only single flash model is introduced in this section since the same equations and principles apply to double-flash model

The sketch of the single-flash model is drawn and located on main diagram window of EES (Figure 5.2). Figure 5.2 is depicted that, the model gives an opportunity to change the design parameters since most of the design parameters are taken as inputs in the model. The model consists of three modules namely

- Mass & energy balances
- Exergy balance
- Economical analysis

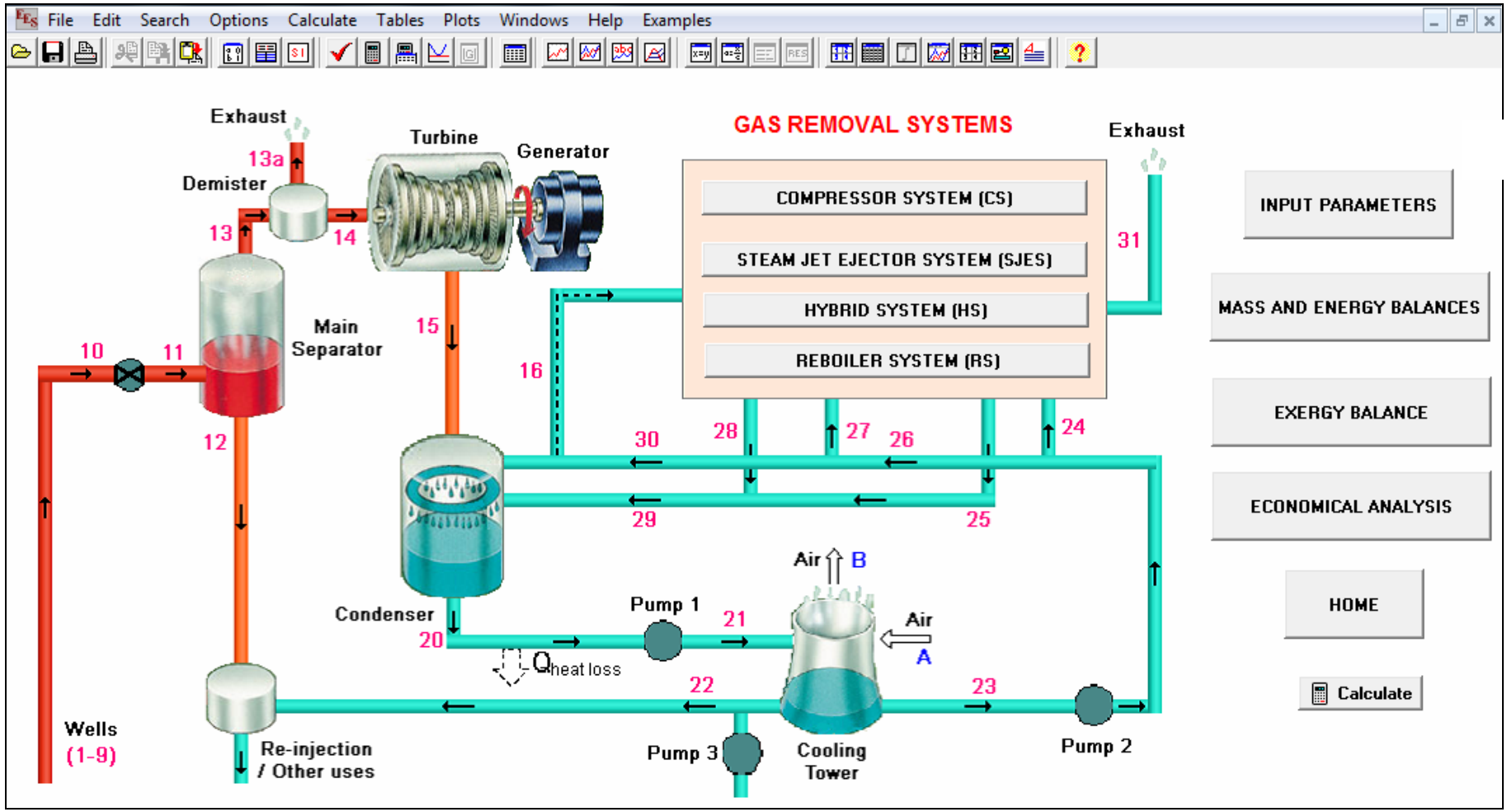

Figure 5.2. Diagram window view of the single-flash GPP model.

5.2.1.1. Mass and Energy Balances Module

The module is the combination of several sub-modules and mainly computes the net power output and total auxiliary power of the plant. The sub-modules are

- Separator-demister module (Section 4.1.1.1 and 4.1.1.2),
- Turbine-generator module (Section 4.1.1.3)
- Condenser module (Section 4.1.1.4)
- Cooling tower module (Section 4.1.1.5)
- NCG removal system module, contains equations for four different NCG removal system (Section 4.1.1.6)
- Auxiliary power module (Section 4.1.1.7)

The flow diagram of mass and energy balance module is demonstrated in Figure 5.3. The figure exhibits the input and output parameters of each sub-module. The sub-models work simultaneously using output parameters of each sub-module as input parameters of the others. The main output of the module is net power output, total auxiliary power of the plant and specific steam consumption of the plant.

First step of the module is to determine the optimum separator and condenser pressures which give the maximum net power output and minimum total auxiliary power.

NCG removal system sub-module contains equations for four different NCG removal systems. Using the optimum separator and condenser pressures, the module runs for NCG removal systems to calculate net power output and total auxiliary power of the plant.

Mass flowrate, temperature and pressure at each state of the plant are determined in this module.

Results screen view of mass and energy balance module is shown Figure 5.4.

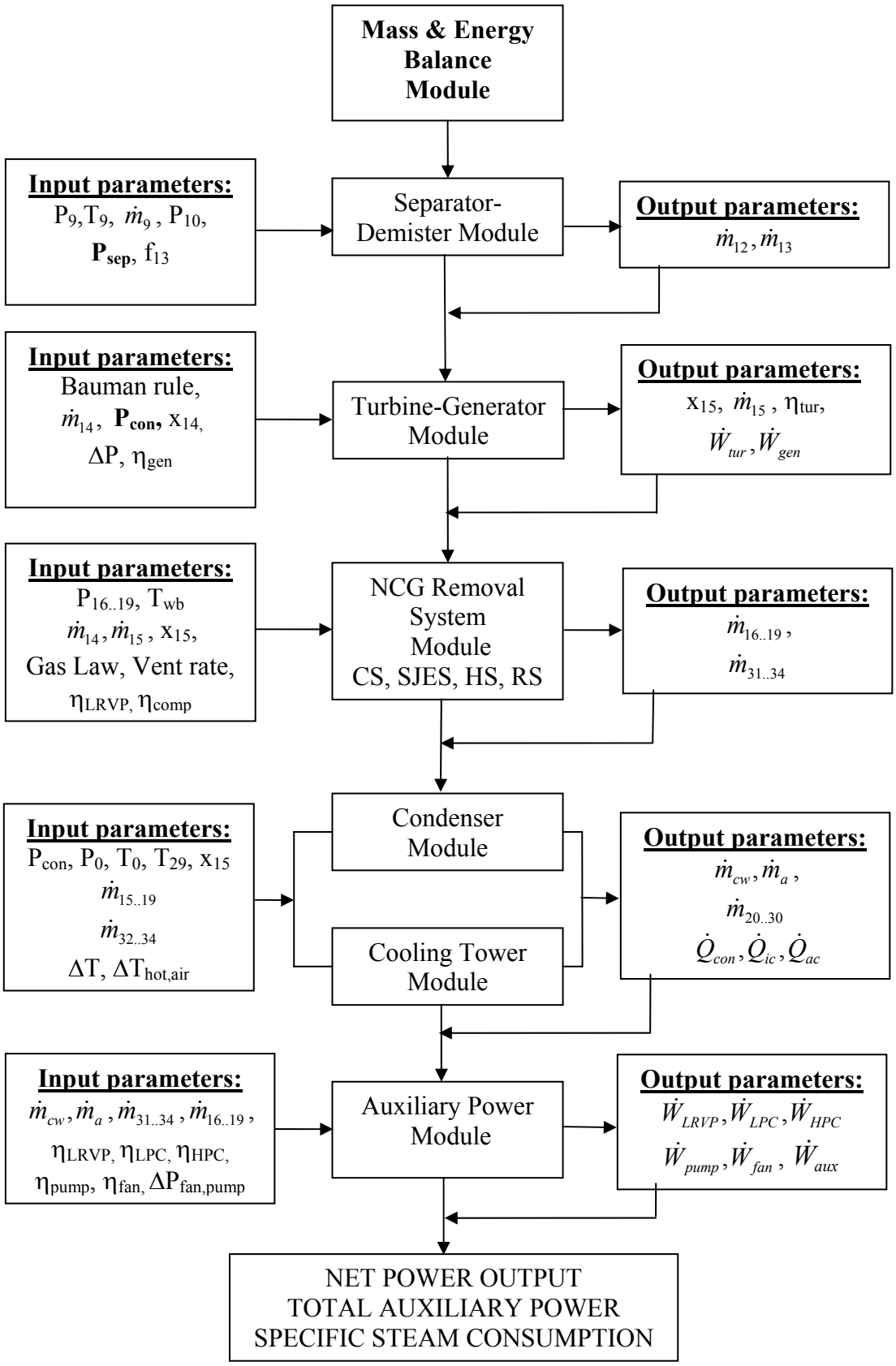

Figure 5.3. Flow diagram of mass and energy balance module.

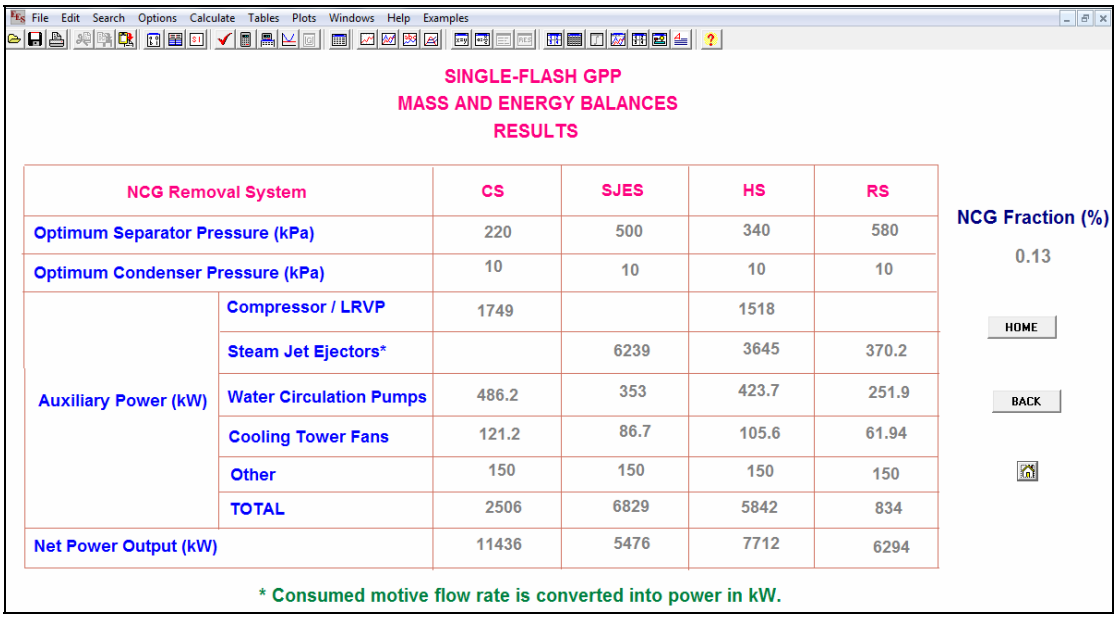

Figure 5.4. Results screen view of mass and energy balance module.

5.2.1.2. Exergy Balance Module

The flow diagram of exergy balance module is shown in Figure 5.5. As it is demonstrated in Figure 5.5, exergy balance module mainly consists of two sub-modules namely exergy losses and exergetic efficiencies. The input parameters of the module are;

- Environmental parameter:
  - dead-state temperature and
  - dead-state pressure
- The outputs of mass and energy balance
  - flowrate, temperature and pressure output at each state of the plant
  - turbine power output,
  - generator power output,
  - net power output,
  - auxiliary power of NCG removal systems, pumps and fans ($\dot{W}_{LRVP}, \dot{W}_{LPC}, \dot{W}_{HPC}, \dot{W}_{pump}, \dot{W}_{fan}$)

The thermodynamical definitions and equations of exergy balance are given in Chapter 4 in detail. Module first calculates exergy of each state by Eq. 4.10-4.14

considering input parameters explained above. Then exergy losses and exergetic efficiencies of each component of the plant is computed. The module results with the determination of overall exergetic efficiency of the plant by Eq. 4.20.

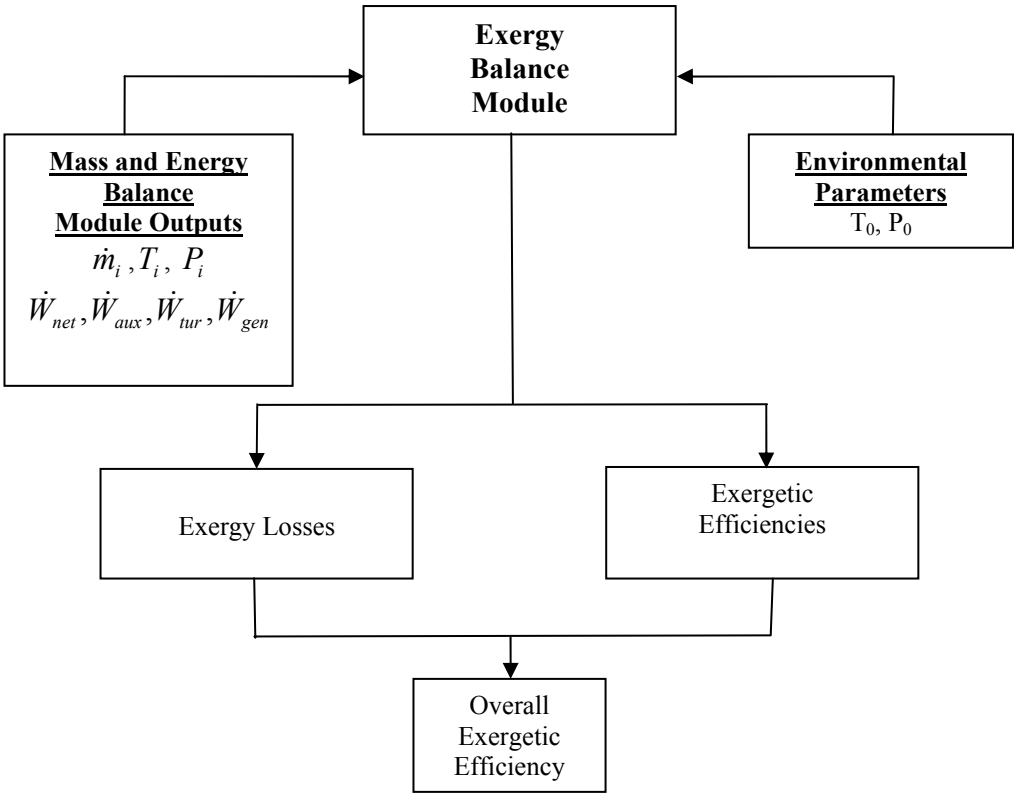

Figure 5.5. Flow diagram of exergy balance module.

Similar to mass and energy balance module, exergy balance includes four different NCG removal system options. Exergy losses and exergetic efficiencies of the plant for each NCG removal system option are computed by the module. Results screen view of exergy losses and exergetic efficiencies sub-modules are illustrated in Figure 5.6 and Figure 5.7.

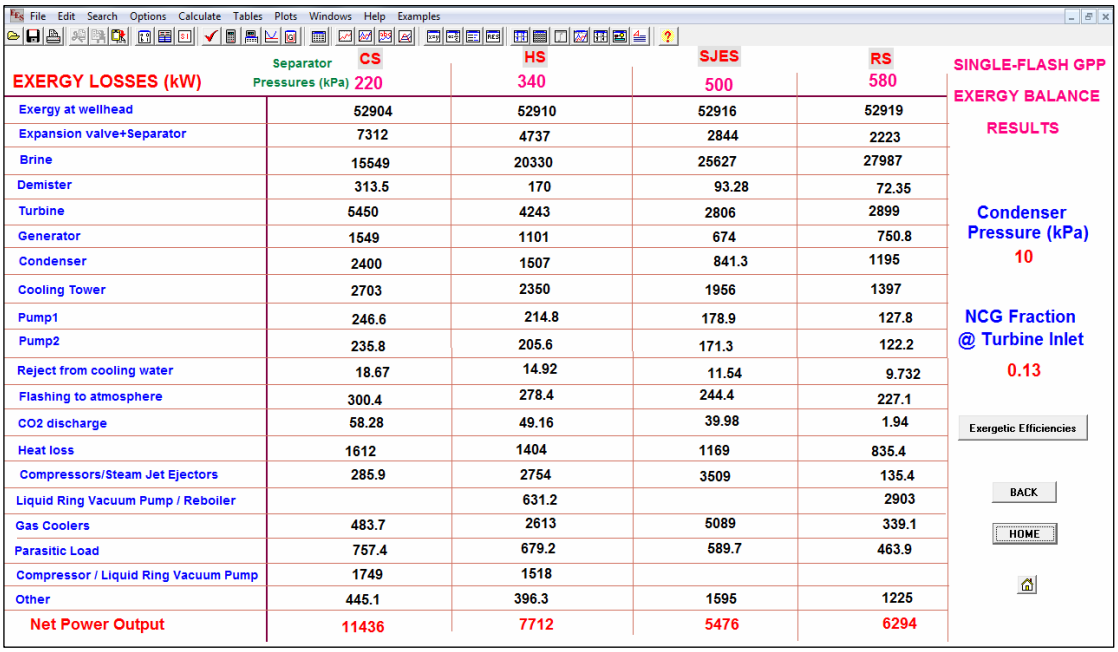

EXERGY LOSSES (kW)	Separator Pressures (kPa) CS 220	HS 340	SJES 500	RS 580
Exergy at wellhead	52904	52910	52916	52919
Expansion valve+Separator	7312	4737	2844	2223
Brine	15549	20330	25627	27987
Demister	313.5	170	93.28	72.35
Turbine	5450	4243	2806	2899
Generator	1549	1101	674	750.8
Condenser	2400	1507	841.3	1195
Cooling Tower	2703	2350	1956	1397
Pump1	246.6	214.8	178.9	127.8
Pump2	235.8	205.6	171.3	122.2
Reject from cooling water	18.67	14.92	11.54	9.732
Flashing to atmosphere	300.4	278.4	244.4	227.1
CO2 discharge	58.28	49.16	39.98	1.94
Heat loss	1612	1404	1169	835.4
Compressors/Steam Jet Ejectors	285.9	2754	3509	135.4
Liquid Ring Vacuum Pump / Reboiler		631.2		2903
Gas Coolers	483.7	2613	5089	339.1
Parasitic Load	757.4	679.2	589.7	463.9
Compressor / Liquid Ring Vacuum Pump	1749	1518		
Other	445.1	396.3	1595	1225
Net Power Output	11436	7712	5476	6294

Figure 5.6. Results screen view of exergy losses sub-module of the model.

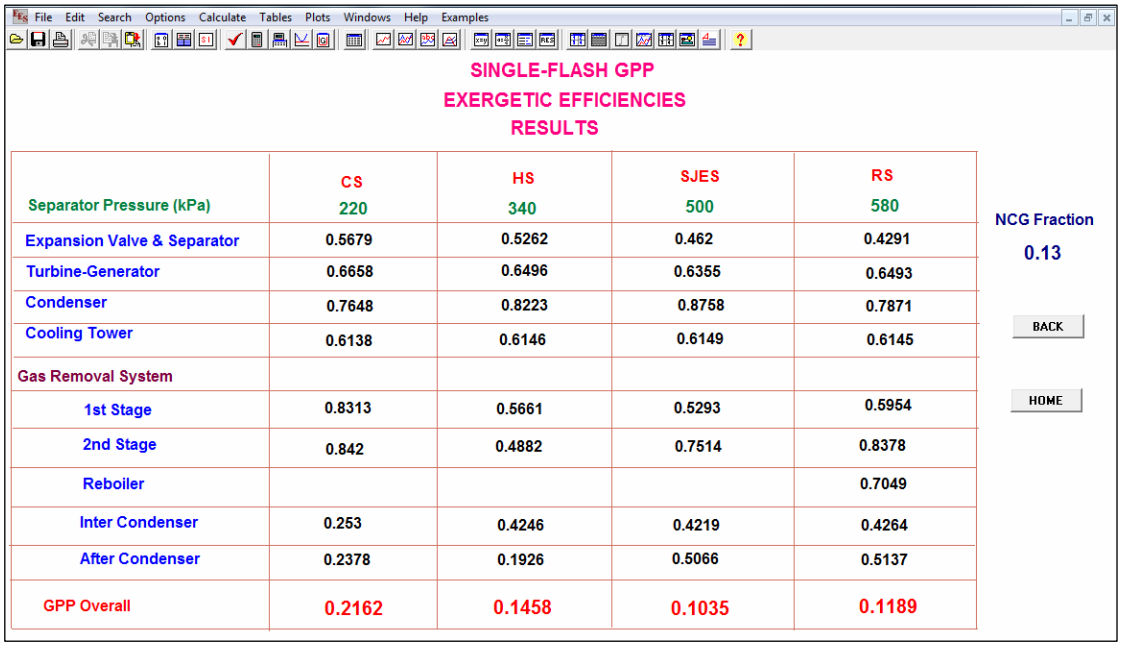

SINGLE-FLASH GPP
EXERGETIC EFFICIENCIES
RESULTS

Separator Pressure (kPa)	CS 220	HS 340	SJES 500	RS 580
Expansion Valve & Separator	0.5679	0.5262	0.462	0.4291
Turbine-Generator	0.6658	0.6496	0.6355	0.6493
Condenser	0.7648	0.8223	0.8758	0.7871
Cooling Tower	0.6138	0.6146	0.6149	0.6145
Gas Removal System				
1st Stage	0.8313	0.5661	0.5293	0.5954
2nd Stage	0.842	0.4882	0.7514	0.8378
Reboiler				0.7049
Inter Condenser	0.253	0.4246	0.4219	0.4264
After Condenser	0.2378	0.1926	0.5066	0.5137
GPP Overall	0.2162	0.1458	0.1035	0.1189

Figure 5.7. Results screen view of exergetic efficiencies sub-module of the model.

5.2.1.3. Economical Analysis Module

The module uses mass and energy balance module outputs and economical parameters such as interest and tax rates, NCG removal system and GPP costs,

electricity sales price, O&M cost ratio and amortization cost coefficient as inputs. Total investment cost, annual electricity production and annual net revenue are computed in the first step of the module. Furthermore, NPV, IRR, SPT and cost of electricity production calculations follow the cash flow determination. The flow diagram and the results screen view of the module are shown in Figure 5.8 and 5.9, respectively.

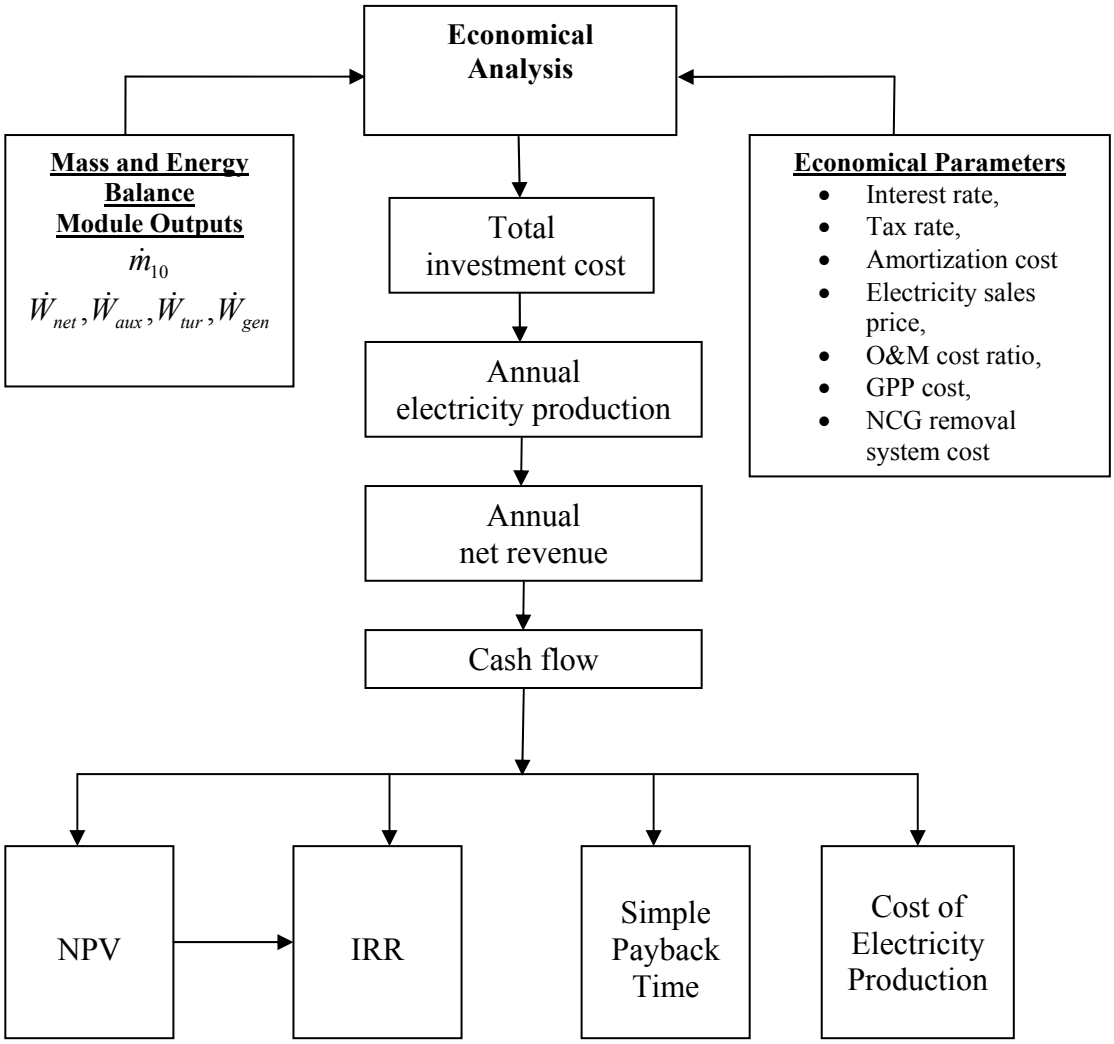

Figure 5.8. Flow diagram of economical analysis module.

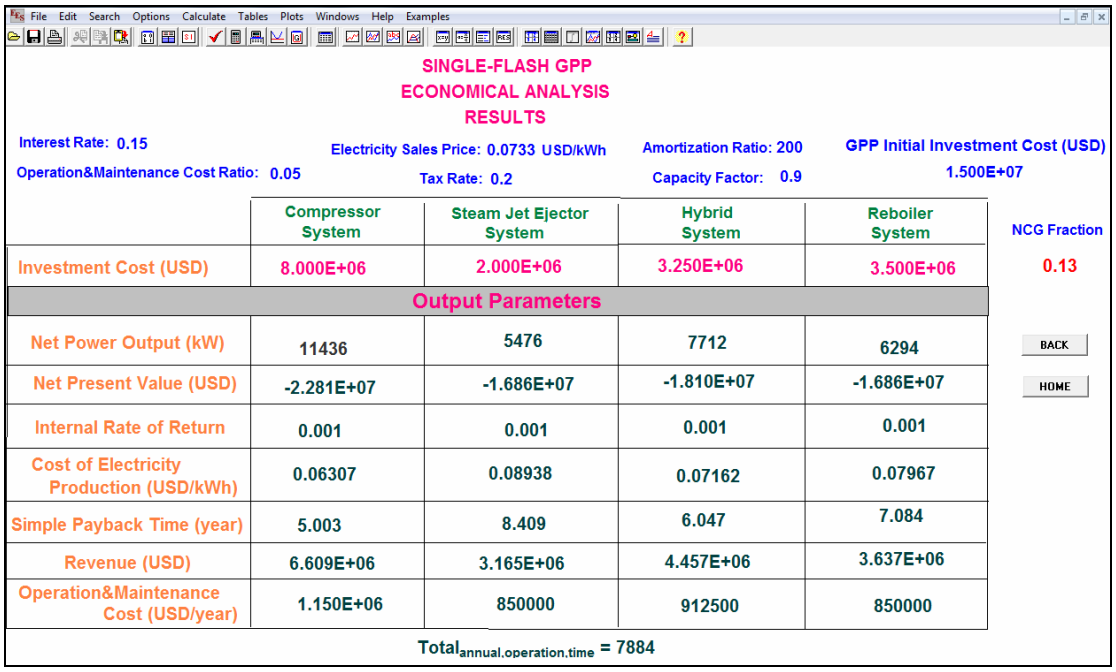

Figure 5.9. Result screen view of economical analysis module.

5.2.1.4. Simulation

The model is simulated to evaluate the effect of the input parameters which are listed in Table 5.1 on the model results. The parameters and the flow diagram of simulation are presented in Figure 5.10.

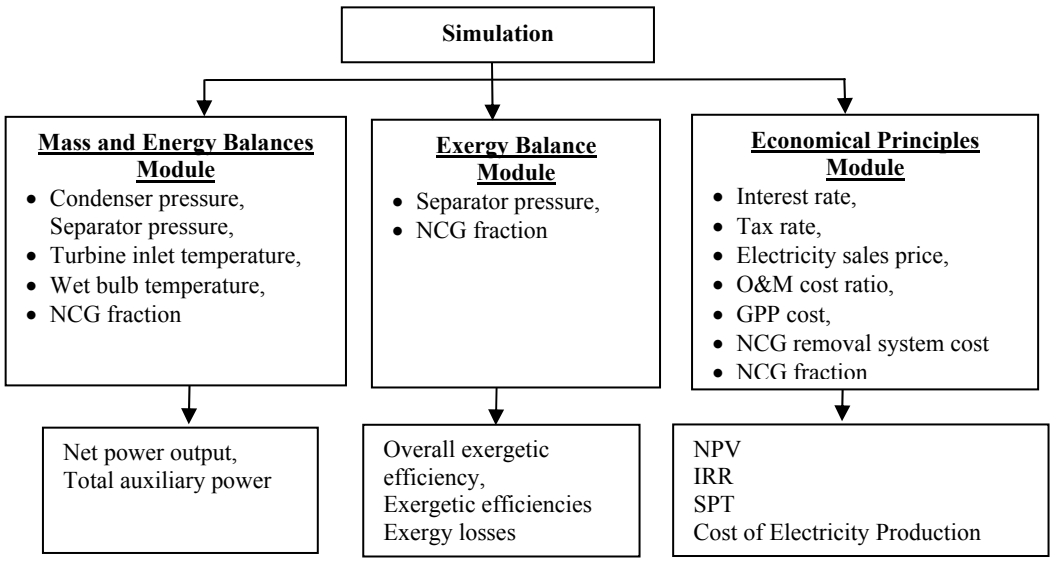

Figure 5.10. Flow diagram of simulation module.

CHAPTER 6

RESULTS

The results are classified in two categories as single-flash and double-flash GPPs. The annual average of the Kizildere GPP operational data are taken as input parameters of the model.

6.1. Single-Flash GPPs

6.1.1. Mass and Energy Balances

The objective of a detailed mass and energy balance of a single-flash GPP is to compute the net power output, total auxiliary power and specific steam consumption of the plant for various NCG removal system alternatives.

Kizildere GPP operational data and main assumptions are listed in Table 6.1. The main results of the mass and energy balance of the plant are presented in Table 6.2.

Table 6.1. Input parameters of the model.

	Parameters		Values
Geothermal field	Flowrate (kg/s)	Wells	281.6
	Pressure (kPa)	Wells	1,800
		Wellhead	1,330
		Separator	460
	Temperature (°C)	Wells	204.7
	NCG fraction (%)	At main separator exit	13
Power plant	Pressure (kPa)	Condenser	10
		Pressure drop between main separator exit and turbine inlet	10
		Pressure drop throughout the reboiler	320
		Pressure drop of fans/circulation pumps	0.1

(cont. on next page)

Table 6.1. (cont.)

Power plant	Pressure (kPa)	NCG removal system final stage discharge pressure	105
	Temperature (°C)	Water at cooling tower exit	29
	Efficiency (%)	Generator	90
		Compressor	75
		LRVP	40
		Fans/Circulation pumps	70
		Fans/Circulation pumps motor	85
Environmental	Pressure (kPa)	Dead state	95
	Temperature (°C)	Dead state	16
	Relative humidity (%)	Dead state	65

Table 6.2. Main results of the mass and energy balance of the plant with Kizildere operational data.

NCG Removal System		**CS**	**SJES**	**HS**	**RS**
Separator Pressure (kPa)		460	460	460	460
Condenser Pressure (kPa)		10	10	10	10
Auxiliary Power (kW)	Compressor /LRVP	1262		1299	
	Steam Jet Ejector *		6666	3038	180
	Water Circulation Pumps	346	372.4	360.3	192
	Cooling Tower Fans	86.3	91.5	89.8	47.2
	Other	150	150	150	150
	TOTAL	**1844**	**7279**	**4936**	**569.2**
Net Power Output (kW)		**10235**	**5466**	**7447**	**5667**

6.1.1.1. Validation of the Model

The model is validated only with the annual average electricity production capacity (net power output) of Kizildere GPP, which uses compressors as NCG removal system, since the recorded data of the plant components are limited. Figure 6.1 indicates that the average net power output of Kizildere GPP in 1984-2004 is 9505 kW (DPT, 2001; Gokcen, 2004). By using actual annual operational data of Kizildere GPP, listed

in Table 6.1, net power output of CS is computed by the model as 10235 kW (Table 6.2), which is within 7.7% in recorded data.

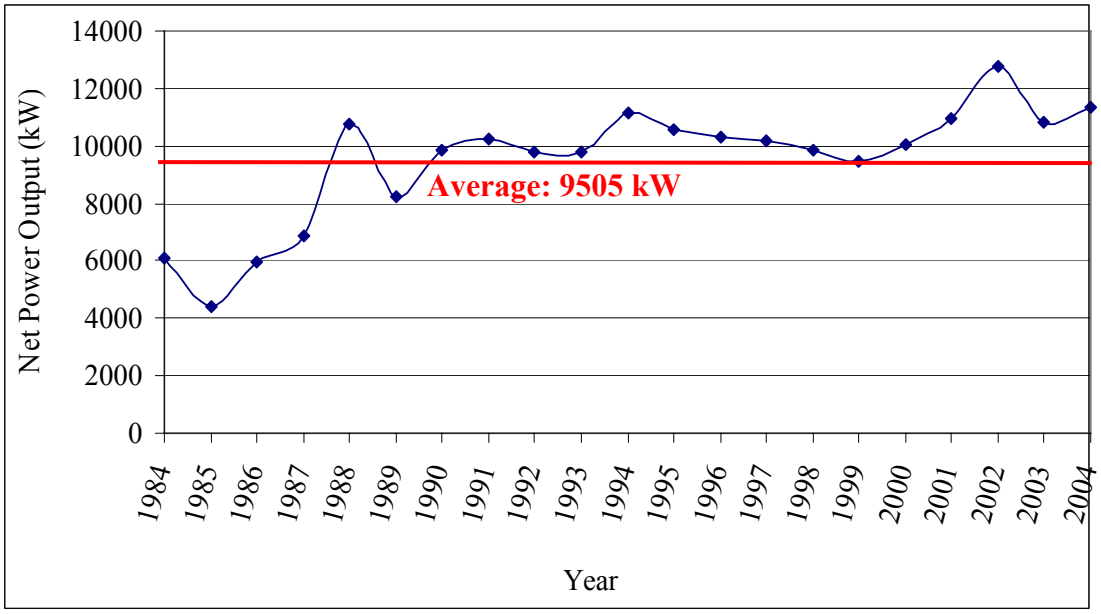

Figure 6.1. Annual average net power output of Kizildere GPP.
(Source: DPT, 2001; Gokcen, 2004)

6.1.1.2. Simulation Results

Effects of NCG fracftion, wet bulb temperature, separator and condenser pressures, and turbine inlet temperature are evaluated on net power output and auxiliary power of the plant by simulation. The simulation range for each parameter is given in Table 6.3. Base case uses the data, which are given in Table 6.1.

Table 6.3. Simulation range for the parameters of mass and energy balances.

Parameter	Base Case	Simulation Range	Number of Simulation
Separator Pressure (kPa)	460	100,120,…,1000	46
Condenser Pressure (kPa)	10	8,9,10	3
NCG Fraction (%)	13	0,1,2,…,25	26
Wet Bulb Temperature (^{o}C)	12.2	5,10,….,25	5
Turbine Inlet Temperature (^{o}C)	147.9	130-260	14

6.1.1.2.1. Condenser and Separator Pressures

The temperature regime in the condenser is one of the limiting factors for determining of condenser pressure. As it is given in section 4.1.1.4., the difference between saturated temperature and cooling water inlet temperature (ΔT_i) should be between about 11 and 17°C. Condenser pressure range is taken as 4-20 kPa to check the ΔT_i, and the results are illustrated in Figure 6.2. The Figure indicates that recommended temperature range falls into 8-10 kPa condenser pressure range. Therefore, the range for condenser pressure is taken as 8-10 kPa for simulation.

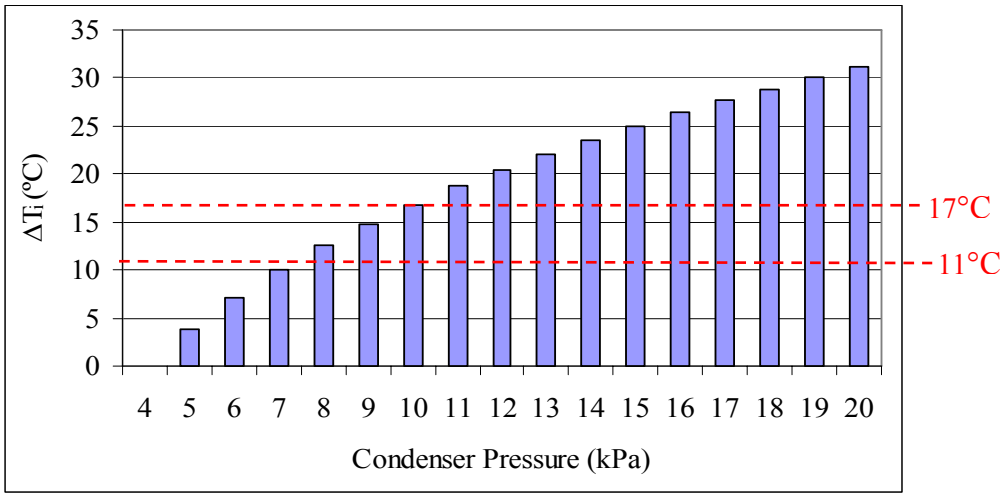

Figure 6.2. Condenser pressure vs. ΔT_i.

Net power output of the plant is calculated for condenser and separator pressures of 8-10 kPa and 100-1000 kPa, respectively to evaluate the effects of condenser and separator pressures on thermodynamic performance of the plant. The net power output versus separator pressures are shown in Figure 6.3 at 13% NCG fraction. It is seen that from Figure 6.3 increasing separator pressure increases the net power output upto a peak value, which corresponds to optimum separator pressure. Further increase in separator pressure shows a dramatic decrease in net power production caused by a consequent decrease in steam flowrate. Optimum separator pressures obtained from the Figure 6.3 is 220 kPa for CS, 500 kPa for SJES, 340 kPa for HS and 580 kPa for RS at 13% NCG fraction.

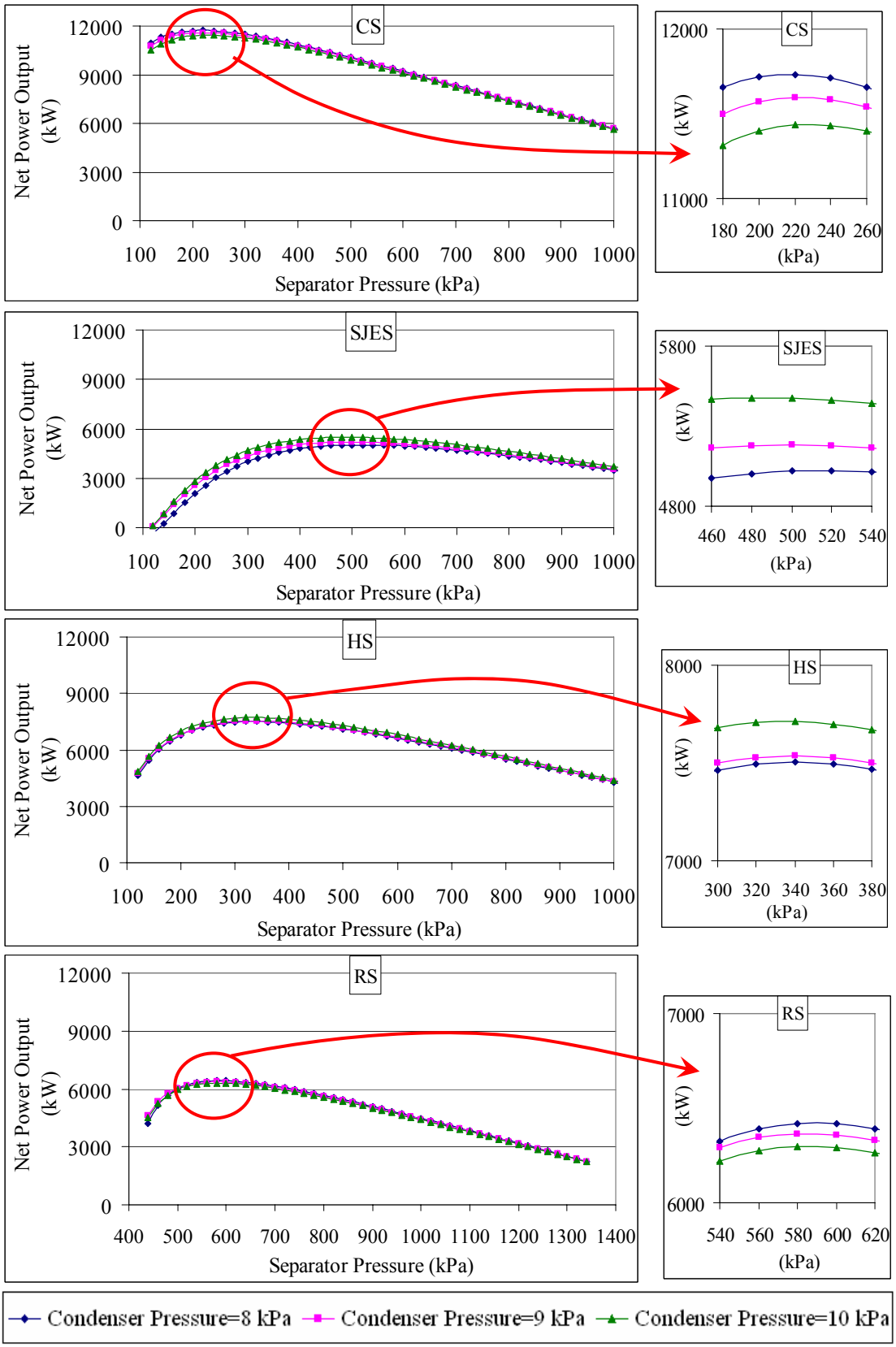

Figure 6.3. Net power output of the plant for various separator and condenser pressures.

To be able to compare thermodynamic performance of the plant with operational and optimum separator pressures, net power output and auxiliary power of the plant are calculated at optimum separator pressure for each NCG removal system and the results, which are summarized in Table 6.4, show that the net power outputs are increased as 0.2-11.7% by using optimum separator pressures.

Table 6.4. Main results of mass and energy balances of the plant at optimum separator pressures.

NCG Removal System		**CS**	**SJES**	**HS**	**RS**
Optimum Separator Pressure (kPa)		220	500	340	580
Condenser Pressure (kPa)		10	10	10	10
Auxiliary Power (kW)	Compressor /LRVP	1749		1518	
	Steam Jet Ejector *		6239	3645	370
	Water Circulation Pumps	486	353	424	252
	Cooling Tower Fans	121	87	106	62
	Other	150	150	150	150
	TOTAL	**2506**	**6829**	**5843**	**834**
Net Power Output (kW)		**11436**	**5476**	**7712**	**6294**

* Consumed motive flow rate is converted into power in kW.

Effect of condenser pressure on net power output and auxiliary power are evaluated for a range of 8-10 kPa (Figure 6.4). Figure 6.4 exhibits that increase in condenser pressure causes an increment in net power output for SJES and HS while a decrement encountered for CS and RS. On the other hand, increasing condenser pressure decreases auxiliary power requirement accompanies which reduces O&M costs. As an example; changing the condenser pressure from 8 kPa to 10 kPa results 2.5% (296 kW) decrement in net power output of CS, the decrement in auxiliary power is 14% (406 kW). Because of higher auxiliary power allows for larger equipment and cost, 10 kPa condenser pressure can be selected as optimum condenser pressure with the lowest auxiliary power.

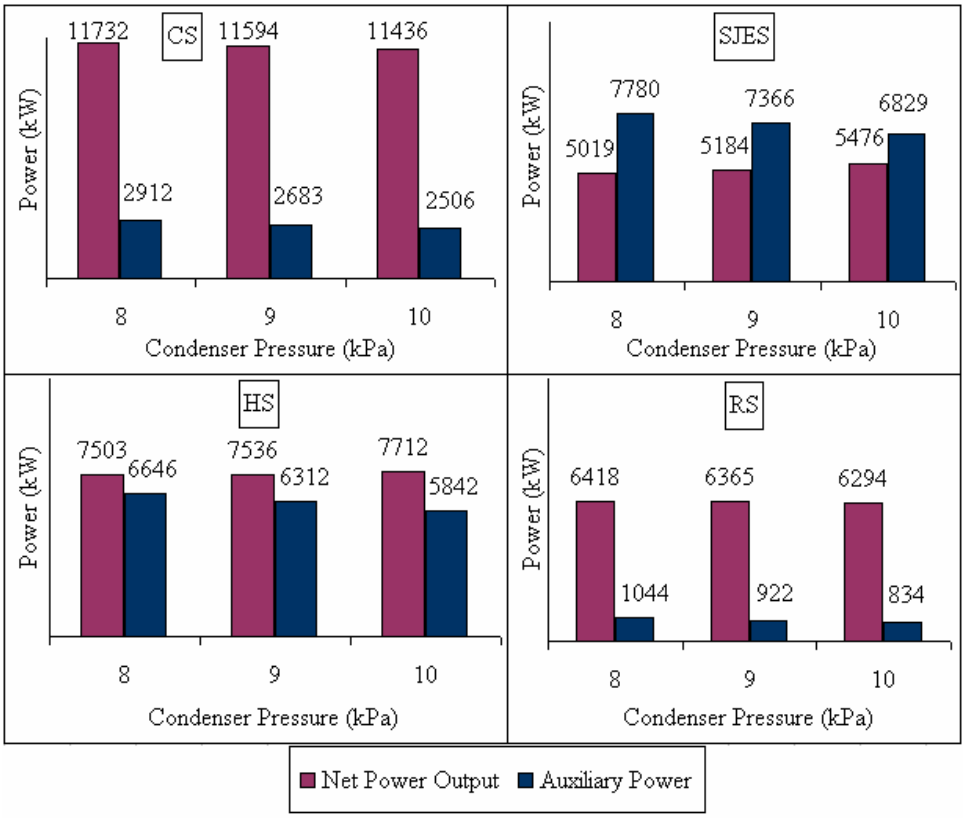

Figure 6.4. Net power output and total auxiliary power of the plant for various condenser pressures for optimum separator pressures.

6.1.1.2.2. NCG Fraction

The effect of NCG fraction on the turbine power output, auxiliary power and net power output at the conditions, given in Table 6.1, for a 0-25% range of NCG fraction are plotted in Figure 6.5. The Figure indicates that, auxiliary power increases and net power output decreases with increasing NCG fraction. The plant which is employed with compressors generates highest net power output at each NCG fraction. Increment in NCG fraction (1%) causes a net power output loss of 0.4% for CS, 2.2% for HS, 2.5% for RS and 2.7% for SJES. Especially, SJES has a dramatical decrease on net power output by NCG fraction. On the other hand, it is interesting to see, the turbine power output of CS increases with increasing NCG fraction. The reason for that is increment in steam quality at the separator by considering NCG in the steam. Therefore, separator pressure has vital importance for maximizing the net power output. In Figure 6.6., separator pressure versus net power output of the plant for various NCG fractions (0-25% by weight of steam) is demonstrated at 10 kPa condenser pressure.

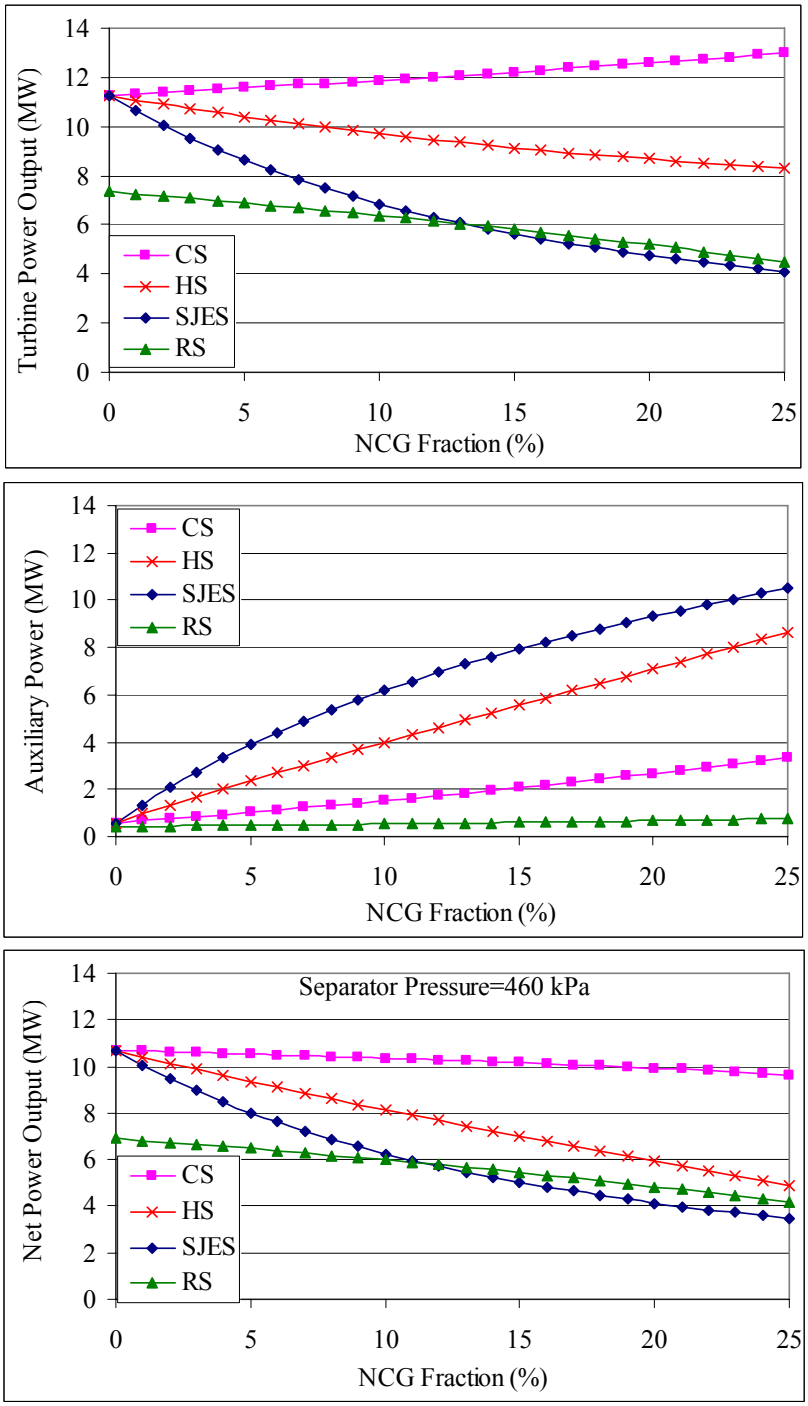

Figure 6.5. Turbine power output, net power output and auxiliary power of the plant vs. NCG fraction.

The Figure 6.6 indicates that each option exhibits the same behavior for zero NCG fraction except RS. Because RS requires at least 330 kPa pressure drop between the separator and turbine inlet, while the other NCG removal systems require 10 kPa.

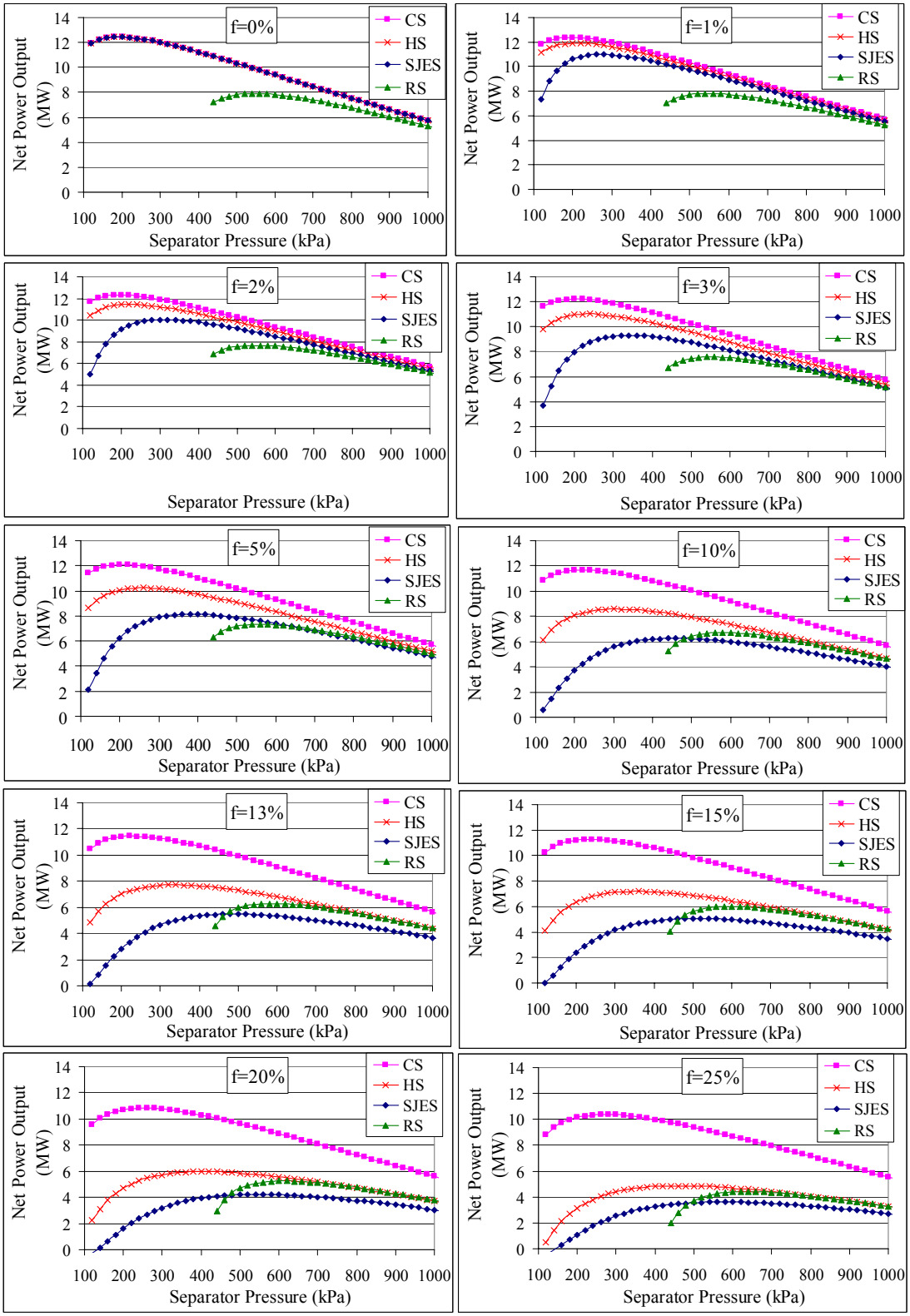

Figure 6.6. Separator pressure vs net power output of the plant for various NCG fractions.

Figure 6.6 shows that, optimum separator pressures, which maximize the net power output, are changed by NCG fraction.

Figure 6.7 gives a better insight of the optimum separator pressures depending on NCG fraction. Increasing NCG fraction increases optimum separator pressures for each NCG removal system.

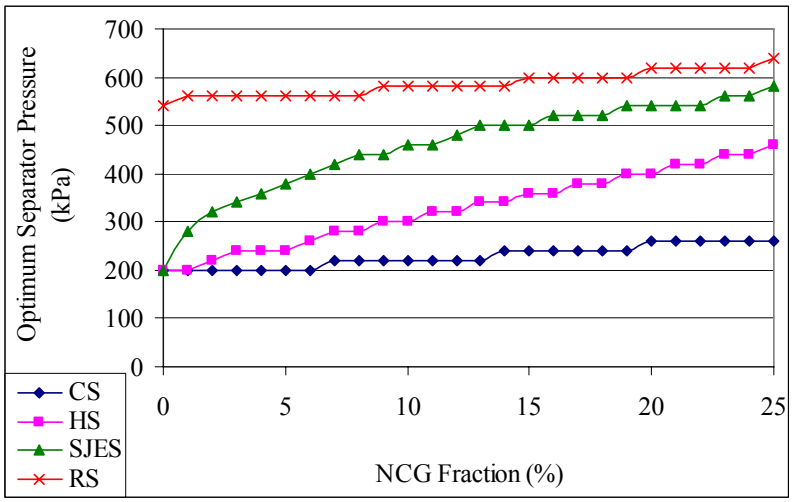

Figure 6.7. Optimum separator pressures vs. NCG fraction.

Specific steam consumption, the ratio of steam flowrate at separator exit to net power output of the plant, is one of the criteria for the comparison of the NCG removal systems and it is shown in Figure 6.8 for various NCG fractions (0-25% weight).

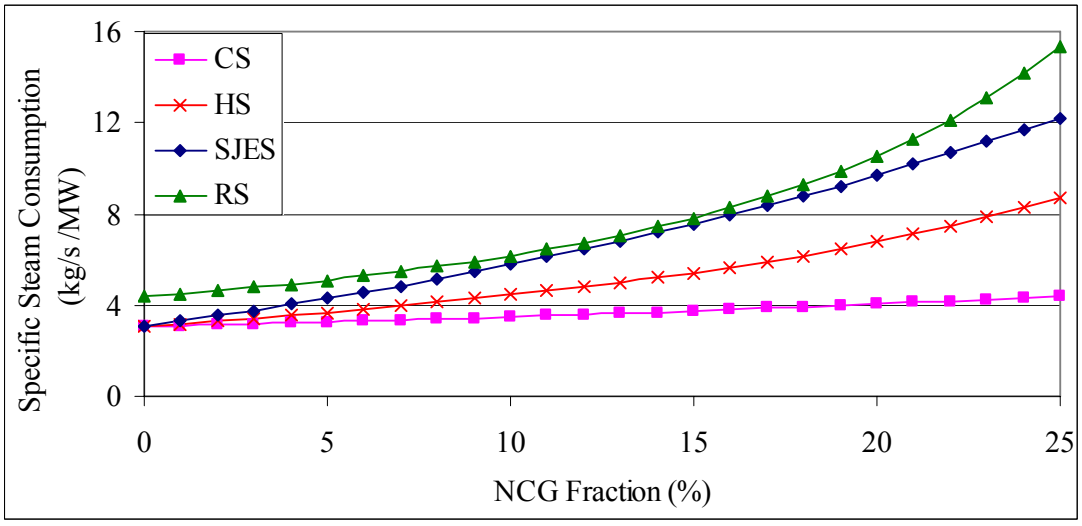

Figure 6.8. Specific steam consumption for various NCG fractions.

RS has the highest and CS has the lowest specific steam consumption among NCG removal systems. Specific steam consumption is increased as approximately 1.73% for CS, 7.38% for HS, 10.07% for RS and 11.94% for SJES by 1% increment in NCG fraction and it is observed that, while specific steam consumption of CS does not change very much by increasing NCG fraction, specific steam consumption of SJES changes dramatically.

6.1.1.2.3. Turbine Inlet Temperature

The effect of turbine inlet temperature is analyzed on net power output of the plant. Figure 6.9 is drawn by taking the turbine inlet temperature in the range of 130-260^{o}C at optimum separator and condenser pressures with 13% NCG fraction and 12.2^{o}C wet bulb temperature.

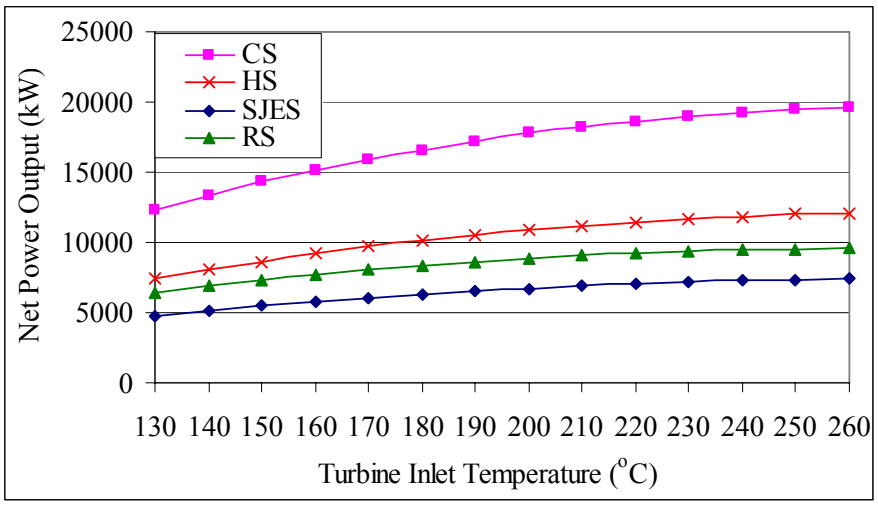

Figure 6.9. Turbine inlet temperature vs. net power output of the plant at optimum separator and condenser pressures.

As it can be observed from Figure 6.9, the net power output increases with increasing turbine inlet temperature. As an example, by 10°C increasing in turbine inlet temperature of CS, the net power output of the turbine increases 2.6%. Because, superheated steam enters the turbine with increasing the turbine inlet temperature. Therefore, the turbine efficiency increases. That means, if a pre-heater can be used before entrance the turbine, the net power output increases. As a pre-heater a heat exchanger can be used by feeding the steam at compressor exit.

6.1.1.2.4. Wet Bulb Temperature

Wet bulb temperature is important parameter to determine the motive steam flowrate for the NCG removal system. In Figure 6.10 and Table 6.5, wet bulb temperature vs. net power output and auxiliary power of the plant at optimum condenser and separator pressures are shown.

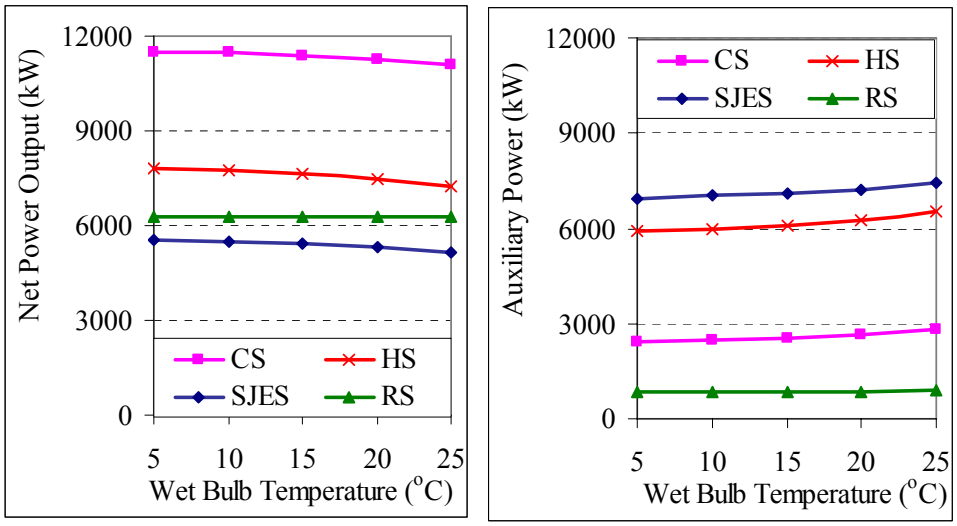

Figure 6.10. Net power output and auxiliary power of the each system vs. wet bulb temperature.

Table 6.5. Wet bulb temperature vs net power output and auxiliary power of the plant.

Wet Bulb Temperature (°C)		5	10	15	20	25
CS	Net Power Output (kW)	11514	11464	11391	11280	11104
	Auxiliary Power (kW)	2428	2478	2551	2662	2838
SJES	Net Power Output (kW)	5561	5507	5430	5316	5144
	Auxiliary Power (kW)	6955	7015	7101	7228	7419
HS	Net Power Output (kW)	7819	7748	7643	7485	7236
	Auxiliary Power (kW)	5897	5977	6093	6269	6545
RS	Net Power Output (kW)	6302	6297	6289	6276	6257
	Auxiliary Power (kW)	824	831	840	853	875

As it can be observed from Figure 6.10, the net power output of the plant decreases with increasing wet bulb temperature. Because by increasing the wet bulb temperature, increases the motive steam flowrate, since the auxiliary power increases. The results of Table 6.5 is depicted that net power output is decreased as 0.18% for CS, 0.37% for SJES and HS and 0.04% for RS, while auxiliary power is increased as 0.84% for CS, 0.33% for SJES, 0.55% for HS and 0.31% for RS by 1^{o}C increment in wet bulb temperature.

6.1.2. Exergy Balance

Exergy balance is carried out to determine the overall second law of efficiency (exergetic efficiency) for the power plant, identify the locations and processes where exergy is wasted, lost or destroyed and suggest steps that can be taken to reduce exergy losses and wastes. General assumptions of mass and energy balances are vital for exergy balances. The dead state for the geothermal fluid can be chosen to be the state of environment at which the temperature and the atmospheric pressure are 16°C and 95 kPa, respectively. These values are obtained from the local meteorological data (TTMD, 2000),

In the exergy balance condenser pressure is taken as 10 kPa, which is determined as optimum condenser pressure for each NCG removal system option. The operational turbine inlet pressure of Kizildere GPP (450 kPa) is taken as comparison pressure, because of each NCG removal system option has different optimum separator pressure. 13% NCG fraction, average value of Kizildere GPP, is considered in exergy analyses.

6.1.2.1. Compressor System

The representative model of CS is shown in Figure 6.11.

The energy and exergy rates of the geothermal fluid and the CO_2 gas are calculated starting from the reservoir through the major states of the geothermal fluid, including the NCG removal system, and the results are tabulated in Table 6.6 and Figure 6.12 for 460 kPa separator, 10 kPa condenser pressures with 13% NCG fraction. The locations of states are shown on the plant schematic in Figure 6.11.

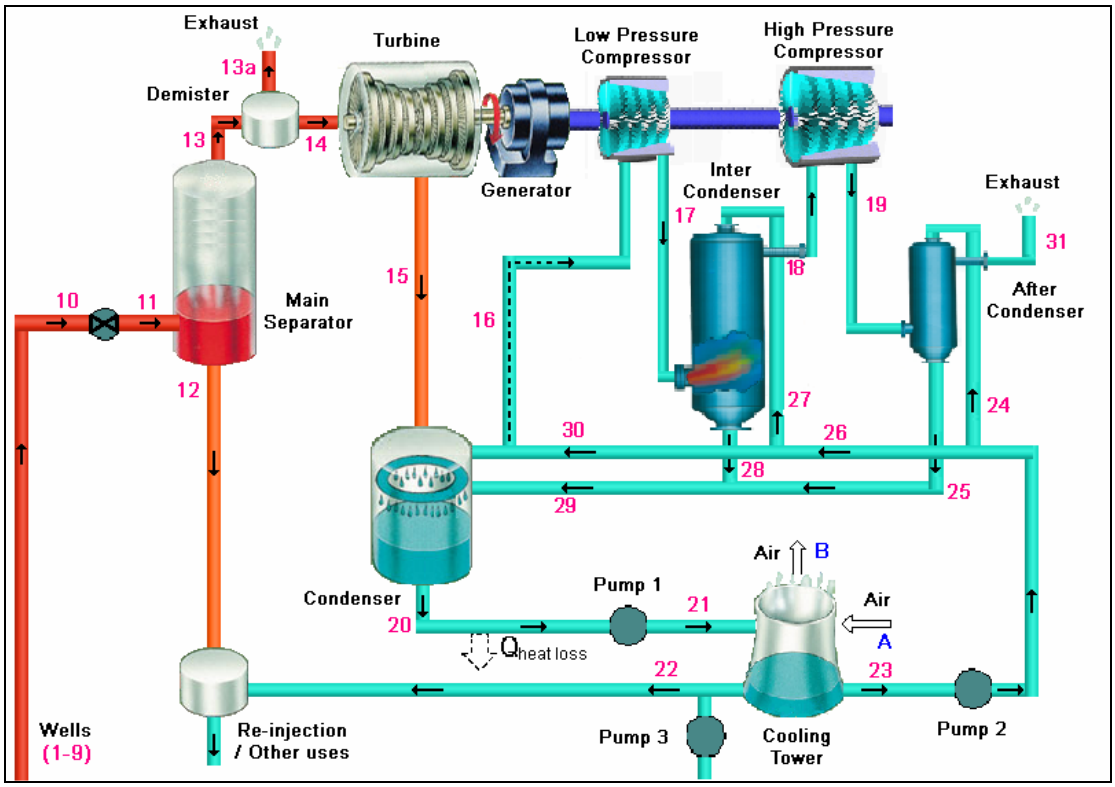

Figure 6.11. The representative model of CS.

Table 6.6. Property values at major locations of CS.

State No	T (°C)	P (kPa)	m (kg/s)	m_f (kg/s)	m_g (kg/s)	m_{CO2} (kg/s)	Enthalpy (kJ/kg)	Specific exergy (kJ/kg)	Energy rate (kW)	Exergy rate (kW)
9	204.7	1800	281.6	276.8	0	4.8	861.3	188.9	242542	53194
10	192.7	1330	281.6	269.1	7.6	4.8	861.3	187.9	242542	52915
11	148.7	460	281.6	244.4	32.4	4.8	861.3	176.5	242542	49702
12	148.7	460	244.4	244.4	0	0	626.8	99.8	153190	24384
13	148.7	460	37.2	0	32.4	4.8	2402	680.4	89354	25311
14	147.9	450	36.8	0	32	4.8	2401	677.5	88405	24946
15	45.8	10	36.8	3.3	28.8	4.8	2037	163.8	75002	6031
16	43.7	9	5.2	0	0.4	4.8	198.4	-103.0	1023	-531
17	170.6	31.2	5.2	0	0.4	4.8	324	1.4	1670	7
18	69.3	30.3	4.9	0	0.1	4.8	89.2	-49.8	436	-243
19	200	105	4.9	0	0.1	4.8	215.1	56.1	1051	274

(cont. on next page)

Table 6.6. (cont.)

20	45.8	10	1026	1026	0	0	191.7	5.9	196684	6078
21	42.8	95	1026	1026	0	0	179.2	4.8	183859	4930
22	29	95	12.6	12.6	0	0	121.5	1.1	1526	14
23	29	95	994.1	994.1	0	0	121.5	1.1	120783	1090
24	29	95	10.3	10.3	0	0	121.5	1.1	1256	11
25	45.8	10	10.4	10.4	0	0	191.7	5.9	1999	62
26	29	95	983.8	983.8	0	0	121.5	1.1	119532	1078
27	29	95	16.8	16.8	0	0	121.5	1.1	2046	18
28	45.8	10	17.1	17.1	0	0	191.7	5.9	3280	101
29	45.8	10	27.5	27.5	0	0	191.7	5.9	5279	163
30	29	95	967	967	0	0	121.5	1.1	117491	1060
31	98.2	95	4.8	0	0	4.8	63.9	8.8	306	42

In Table 6.6, point 9 represents average reservoir conditions of the production wells. Point 10 is the wellhead properties of the geothermal fluid. It can be seen that some exergy values have a negative sign in Table 6.6. This means that the work input to the stream is required to bring it to the dead state.

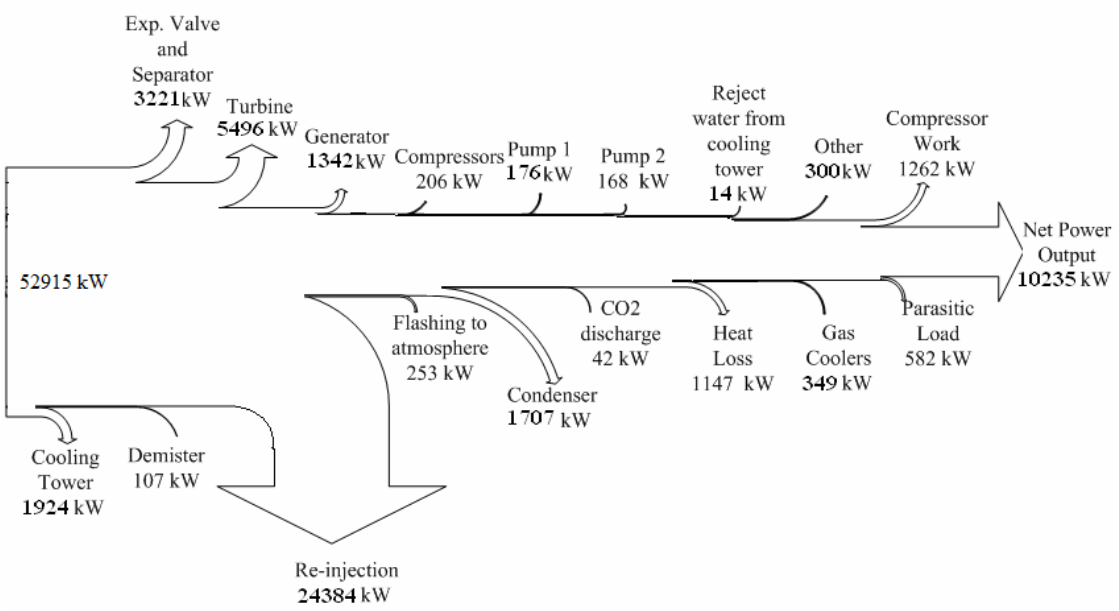

Figure 6.12. Exergy flow chart for CS.

Overall exergy balance of the system is shown in Figure 6.13.

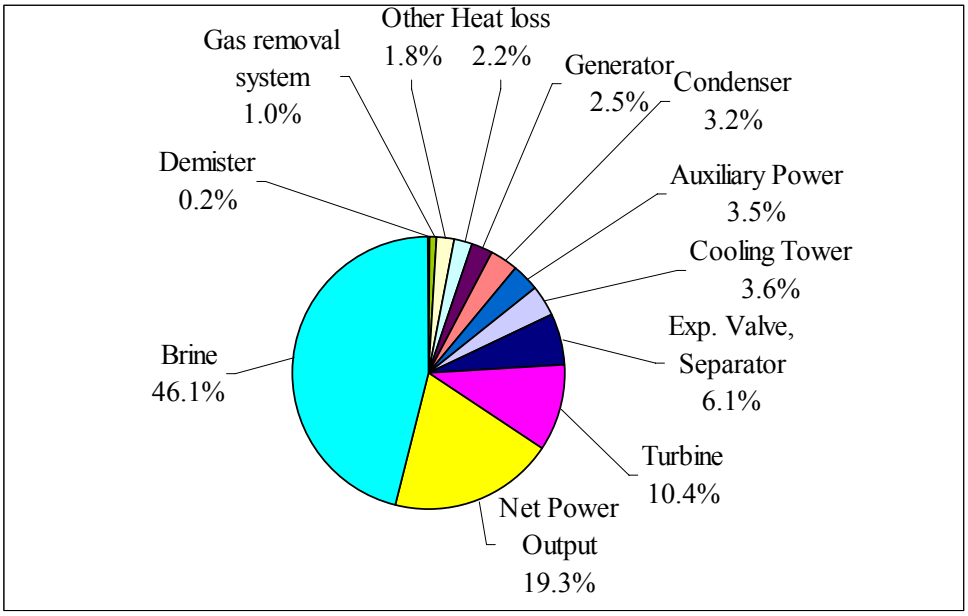

Figure 6.13. Overall exergy balance of CS.

Production wells provide a total exergy of 52915 kW at the wellhead. Major exergy destructions occur due to the separation of steam from geothermal fluid, the discharge of the geothermal fluid from the separator, turbine, and generator, cooling tower, condenser and NCG removal system.

A total exergy of 3221 kW is destroyed during the separation process itself as the geothermal fluid is flashed into steam and brine in the separators, and this loss corresponds to 6.1% of the total exergy input. The remaining brine stream at relatively low temperature and pressure after passing through the silencer is re-injected or sent to the other applications. A total exergy of 24384 kW, which amounts 46.1% of the total exergy input is brine. The demister is located between the separator and turbine. There is 10 kPa pressure drop from separator to turbine. Therefore, the exergy loss of the demister is around 107 kW and 1% of the steam is flashed from demister with 253 kW exergy waste. The exergy loss of the turbine is 5496 kW, which amount 10.4% of the total exergy input. The exergy further destroyed in the generator during the conversion of the mechanical shaft work to the electrical energy. This accounts for 2.5% of the total exergy destruction. Cooling tower and condenser are the other vital components with 1924 and 1707 kW exergy destruction, respectively. The pipe between the condenser

exit and cooling tower inlet is assumed to have 3°C temperature drop. Therefore, the exergy destruction with heat loss is calculated as 1147 kW. The exergy loss is 206 kW for the compressor and 349 kW for gas coolers in NCG removal system. The total exergy loss of the NCG removal system is 556 kW, which is 1% of the total exergy input. A further usage of exergy output is consumed by internal devices such as auxiliaries, pumps, fans and control systems. This parasitic load is calculated as 582 kW and compressor work is 1262 kW. This completes all the exergy losses in the plant, and thus the total exergy destruction becomes 42680 kW, which is 80.7% of the total exergy input. The remaining 10235 kW leaves the plant as the net power output.

The optimum separator pressure is determined as 220 kPa for CS for 10 kPa condenser pressure at 13% NCG fraction. Exergy balance is conducted for optimum separator pressure (Table 6.7) and the results show that, the exergy destruction of the plant components are increased by comparing with the results of the exergy balance for 460 kPa operational separator pressure. The exergy loss of the brine is decreased around 16.7% with optimum separator pressure, which results an increase on overall exergetic efficiency of the plant from 19.3% to 21.6%.

Table 6.7. Exergy losses of CS at optimum and operational separator pressures.

Separator pressure		**460 kPa**		**220 kPa**	
		Exergy loss		**Exergy loss**	
		(kW)	**(%)**	**(kW)**	**(%)**
Exergy at wellhead		**52915**		**52904**	
Exergy losses of main equipments		**38524**	**72.8**	**35758**	**67.6**
	Expansion valve+Separator	3221	6.1	7312	13.8
	Brine	24384	46.1	15549	29.4
	Demister	107	0.2	314	0.6
	Turbine	5496	10.4	5450	10.3
	Generator	1342	2.5	1549	2.9
	Condenser	1707	3.2	2400	4.5
	Cooling tower	1924	3.6	2703	5.1
	Pump1	176	0.3	247	0.5
	Pump2	168	0.3	236	0.4

(cont. on next page)

Table 6. 7. (cont.)

Reject to atmosphere or river		**309**	**0.6**	**377**	**0.7**
	Reject from cooling water	14	0.0	19	0.0
	Flashing to atmosphere	253	0.5	300	0.6
	CO_2 discharge	42	0.1	58	0.1
Heat loss		**1147**	**2.2**	**1612**	**3.0**
	Pipe (from condenser to cooling tower)	1147	2.2	1612	3.0
Other		**300**	**0.6**	**444**	**0.9**
NCG removal system		**556**	**1.0**	**770**	**1.4**
	Compressors	206	0.4	286	0.5
	Inter and after condenser	349	0.7	484	0.9
Auxiliary power		**1844**	**3.5**	**2506**	**4.7**
	Parasitic load (pumps, fan etc.)	582	1.1	757	1.4
	Compressor work	1262	2.4	1749	3.3
Net power output		**10235**	**19.3**	**11486**	**21.6**

In Table 6.8, exergetic efficiencies of main components of CS at optimum separator pressure (220 kPa) and operational separator pressure (460 kPa) are given.

Table 6.8. Exergetic efficiencies of main components of CS at optimum and operational separator pressures.

Separator pressure		**460 kPa**	**220 kPa**
Equipment		Exergetic efficiency (%)	Exergetic efficiency (%)
Expansion valve + Separator		47.8	56.8
Turbine-generator		63.9	66.6
Condenser		76.5	76.5
Cooling tower		61.4	61.4
NCG removal system			
	Compressor 1	83.1	83.1
	Compressor 2	84.2	84.2
	Inter condenser	25.3	25.3
	After condenser	23.8	23.8
GPP overall		19.3	21.6

Table 6.8 is depicted that changing the separator pressure effects mainly on exergetic efficiency of the separation process and the exergetic efficiency of the separation is increased approximately 9% by using optimum separator pressure.

6.1.2.2. Steam Jet Ejector System

The flow diagram of SJES is demonstrated in Figure 6.14. Property values at major locations of SJES are summarized in Table 6.9 at 460 kPa separator pressure and 13% NCG fraction. Exergy distribution throughout the plant is calculated using Table 6.9 and shown in Figure 6.15.

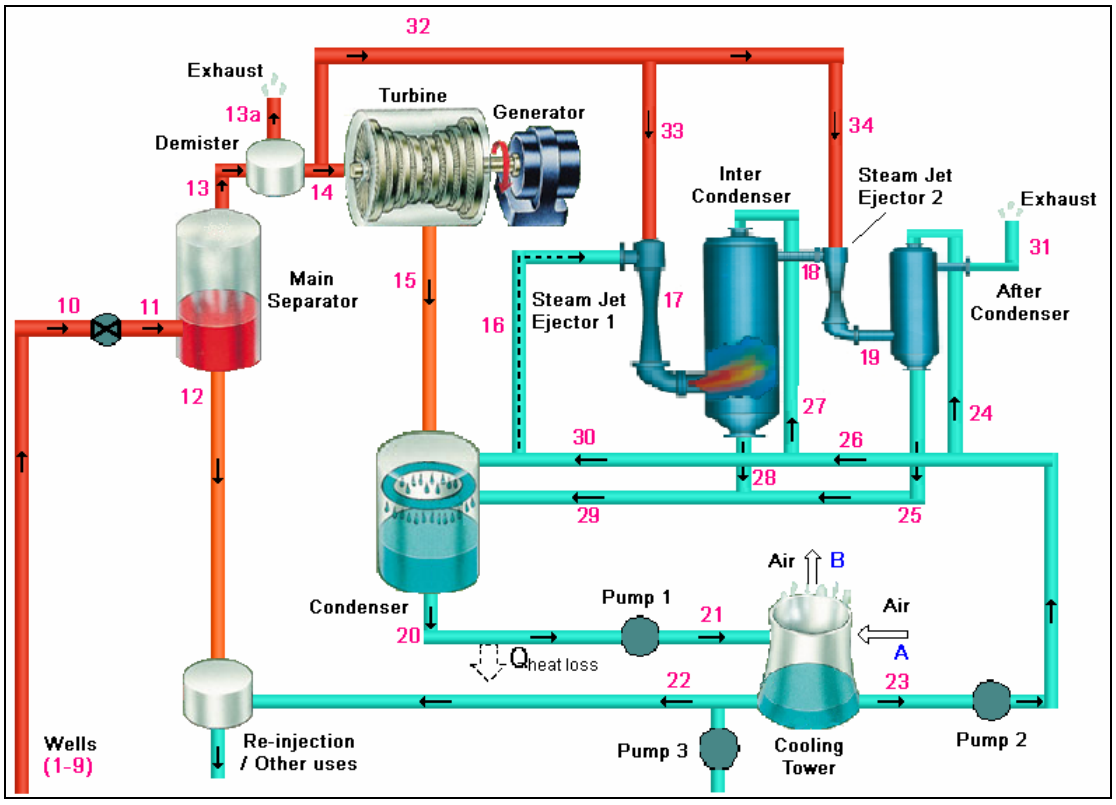

Figure 6.14. The representative model of SJES.

Table 6.9. Property values at major locations of SJES.

State No	T (°C)	P (kPa)	m (kg/s)	m_f (kg/s)	m_g (kg/s)	m_{CO2} (kg/s)	Enthalpy (kJ/kg)	Specific exergy (kJ/kg)	Energy rate (kW)	Exergy rate (kW)
9	204.7	1800	281.6	276.8	0	4.836	861.3	188.9	242542	53194
10	192.7	1330	281.6	269.1	7.626	4.836	861.3	187.9	242542	52915
11	148.7	460	281.6	244.4	32.36	4.836	861.3	176.5	242542	49702
12	148.7	460	244.4	244.4	0	0	626.8	99.77	153190	24384
13	148.7	460	37.2	0	32.36	4.836	2402	680.4	89354	25311
14	147.9	450	18.54	0	16.13	2.41	2401	677.5	44515	12561
15	45.79	10	18.54	1.653	14.47	2.41	2037	163.8	37766	3037
16	43.74	9	2.594	0	0.1846	2.41	198.4	-103	515	-267
17	113.8	31.24	8.017	0	4.902	3.115	1688	228.1	13533	1829
18	69.28	30.25	3.177	0	0.0628	3.115	89.24	-49.81	284	-158
19	127.6	105	16.04	0	11.26	4.787	1943	406	31166	6512
20	45.79	10	1103	1103	0	0	191.7	5.924	211445	6534
21	42.79	95	1103	1103	0	0	179.2	4.805	197658	5300
22	29	95	11.03	11.03	0	0	121.5	1.096	1340	12
23	29	95	1071	1071	0	0	121.5	1.096	130127	1174
24	29	95	408.9	408.9	0	0	121.5	1.096	49681	448
25	45.79	10	420.1	420.1	0	0	191.7	5.924	80533	2489
26	29	95	662.2	662.2	0	0	121.5	1.096	80457	726
27	29	95	175.5	175.5	0	0	121.5	1.096	21323	192
28	45.79	10	180.3	180.3	0	0	191.7	5.924	34564	1068
29	45.79	10	600.4	600.4	0	0	191.7	5.924	115097	3557
30	29	95	486.7	486.7	0	0	121.5	1.096	59134	533
31	98.18	95	4.787	0	0	4.787	63.86	8.787	306	42
32			18.29	0	15.91	2.378	2401	677.5	43914	12391
33	147.9	450	5.423	0	4.718	0.705	2401	677.5	13021	3674
34	147.9	450	12.87	0	11.19	1.673	2401	677.5	30901	8719

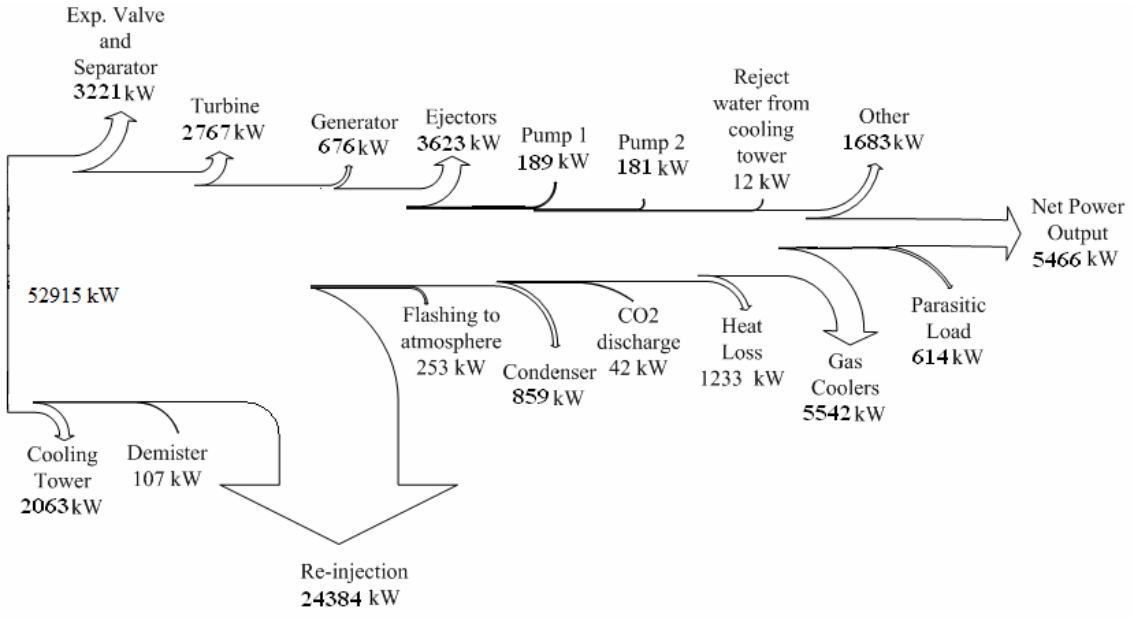

Figure 6.15. Exergy flow chart for SJES.

In detail overall exergy balance of the plant is shown in Figure 6.16.

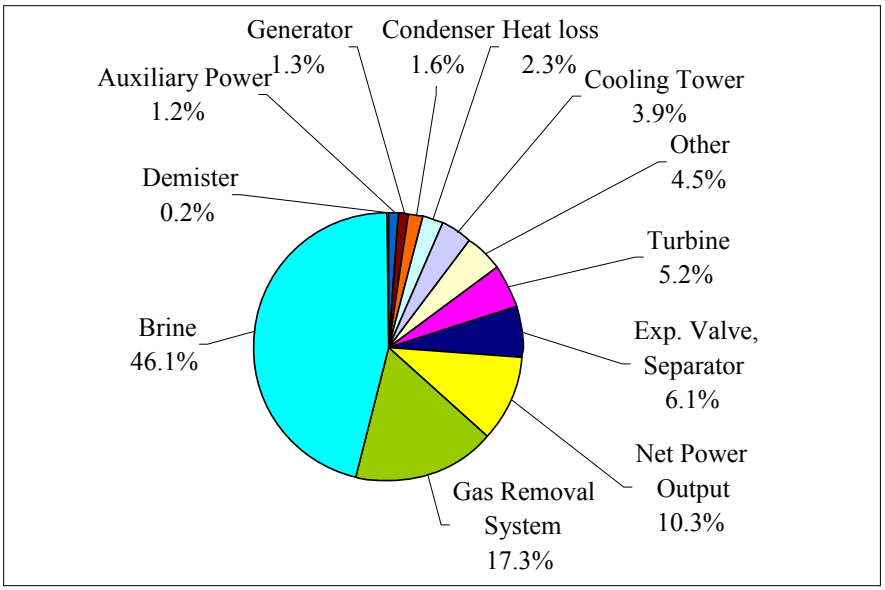

Figure 6.16. Overall exergy balance of SJES.

Figure 6.15 and 6.16 represent that after exergy destruction of the brine the second largest exergy destruction of the plant occurs at NCG removal system by 17.3% of total exergy input. Total exergy destruction of the NCG removal system is 9165 kW

total exergy loss with 3623 kW from steam jet ejectors and 5542 from gas coolers. The other major exergy loss occurs throughout the separation process with 3221 kW and 6.1% of total exergy input. The exergy further destroyed in the turbine and generator couple with total of 3443 kW, which amounts 6.5 % of the total exergy input of 52915 kW. Cooling tower and condenser has 2063 kW and 859 kW exergy destructions, respectively. The exergy destruction is calculated as 614 kW for the internal usage. The total exergy destruction of the plant becomes 47449 kW, which is 89.7% of the total exergy input. The remaining 5466 kW leaves the plant as the net power output.

The results of the exergy analyses for 460 kPa operational and 500 kPa optimum separator pressure are given in Table 6.10. It is clearly seen from the Table, the results are not changed much because of the separator pressures are close to each other.

Table 6.10. Exergy losses of SJES at optimum and operational separator pressures.

Separator pressure		**460 kPa**		**500 kPa**	
		Exergy loss		**Exergy loss**	
		(kW)	**(%)**	**(kW)**	**(%)**
Exergy at wellhead		**52915**		**52916**	
Exergy losses of main equipments		**34447**	**65.1**	**35191**	**66.5**
	Expansion valve+Separator	3221	6.1	2844	5.4
	Brine	24384	46.1	25627	48.4
	Demister	107	0.2	93	0.2
	Turbine	2767	5.2	2806	5.3
	Generator	676	1.3	674	1.3
	Condenser	859	1.6	841	1.6
	Cooling tower	2063	3.9	1956	3.7
	Pump1	189	0.4	179	0.3
	Pump2	181	0.3	171	0.3
Reject to atmosphere or river		**307**	**0.6**	**296**	**0.6**
	Reject from cooling water	12	0.0	12	0.0
	Flashing to atmosphere	253	0.5	244	0.5
	CO_2 discharge	42	0.1	40	0.1

(cont. on next page)

Table 6.10. (cont.)

Heat loss		**1233**	**2.3**	**1169**	**2.2**
	Pipe (from condenser to cooling tower)	1233	2.3	1169	2.2
Other		**1683**	**3.2**	**1596**	**3.0**
NCG removal system		**9165**	**17.3**	**8598**	**16.2**
	SJEs	3623	6.8	3509	6.6
	Inter and after condensers	5542	10.5	5089	9.6
Auxiliary power		**614**	**1.2**	**590**	**1.1**
	Parasitic load (pumps, fan etc.)	614	1.2	590	1.1
			0.0		0.0
Net power output		**5466**	**10.3**	**5476**	**10.3**

Exergetic efficiencies of the main components of SJES are given in Table 6.11. The table indicates that while the overall exergetic efficiency of the plant with CS is 19.3, it is reduced to 10.3% with SJES.

Table 6.11. Exergetic efficiencies of main components of SJES at optimum and operational separator pressures.

Separator pressure		**460 kPa**	**500 kPa**
Equipment		Exergetic efficiency (%)	Exergetic efficiency (%)
Expansion valve+Seperator		47.8	46
Turbine-generator		63.9	63.6
Condenser		87.9	87.6
Cooling tower		61.5	61.5
NCG removal system			
	SJE 1	53.7	52.9
	SJE 2	76.1	75.1
	Inter condenser	42.3	42.2
	After condenser	50.8	50.7
GPP overall		10.3	10.4

6.1.2.3. Hybrid System

The flow diagram of HS is shown in Figure 6.17.

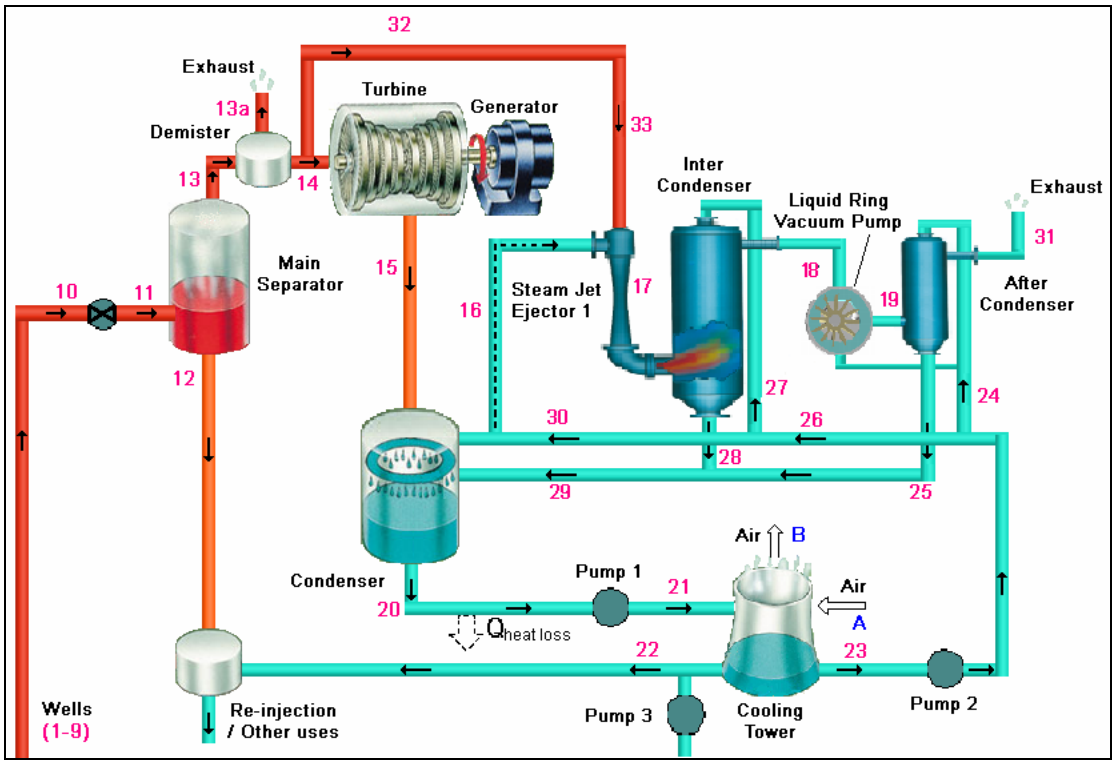

Figure 6.17. The representative model of HS.

Exergy balance is conducted to the plant at 460 kPa separator pressure and 13% NCG fraction and the results are given in Table 6.12.

Table 6.12. Property values at major locations of HS.

State No	T (°C)	P (kPa)	m (kg/s)	m_f (kg/s)	m_g (kg/s)	m_{CO2} (kg/s)	Enthalpy (kJ/kg)	Specific exergy (kJ/kg)	Energy rate (kW)	Exergy rate (kW)
9	204.7	1800	281.6	276.8	0	4.836	861.3	188.9	242542	53194
10	192.7	1330	281.6	269.1	7.626	4.836	861.3	187.9	242542	52913
11	148.7	460	281.6	244.4	32.36	4.836	861.3	176.5	242542	49702
12	148.7	460	244.4	244.4	0	0	626.8	99.77	153190	24384

(cont. on next page)

Table 6.12. (cont.)

13	148.7	460	37.2	0	32.36	4.836	2402	680.4	89354	25311
14	147.9	450	28.49	0	24.79	3.704	2401	677.5	68404	19302
15	45.79	10	28.49	2.54	22.25	3.704	2037	163.8	58034	4667
16	43.74	9	3.987	0	0.2838	3.704	198.4	-103	791	-411
17	113.8	31.24	12.32	0	7.535	4.787	1688	228.1	20796	2810
18	69.28	30.25	4.884	0	0.097	4.787	89.24	-49.81	436	-243
19	304.8	105	4.884	0	0.097	4.787	325.2	105.5	1588	515
20	45.79	10	1068	1068	0	0	191.7	5.924	204736	6327
21	42.79	95	1068	1068	0	0	179.2	4.805	191386	5132
22	29	95	11.77	11.77	0	0	121.5	1.096	1430	13
23	29	95	1036	1036	0	0	121.5	1.096	125874	1135
24	29	95	17.99	17.99	0	0	121.5	1.096	2186	20
25	45.79	10	18.09	18.09	0	0	191.7	5.924	3468	107
26	29	95	1018	1018	0	0	121.5	1.096	123687	1116
27	29	95	269.7	269.7	0	0	121.5	1.096	32769	296
28	45.79	10	277.2	277.2	0	0	191.7	5.924	53139	1642
29	45.79	10	295.3	295.3	0	0	191.7	5.924	56609	1749
30	29	95	748.1	748.1	0	0	121.5	1.096	90894	820
31	98.18	95	4.787	0	0	4.787	63.86	8.787	306	42
32	147.9	450	8.335	0	7.251	1.084	2401	677.5	20012	5647
33	147.9	450	8.335	0	7.251	1.084	2401	677.5	20012	5647

Exergy flow chart (Figure 6.18) is drawn by calculating exergy destruction throughout the plant and overall exergy balance of HS is shown in Figure 6.19 in detail. Exergy destruction of the NCG removal system is the second largest exergy losses of the plant with 5059 kW, which amounts of 9.6% of total exergy input of 52915 kW. The other major exergy destructions are 8% of turbine, 6.1% of separation process, 3.8% of cooling tower, 3.6% of parasitic load and 2.5% of condenser.

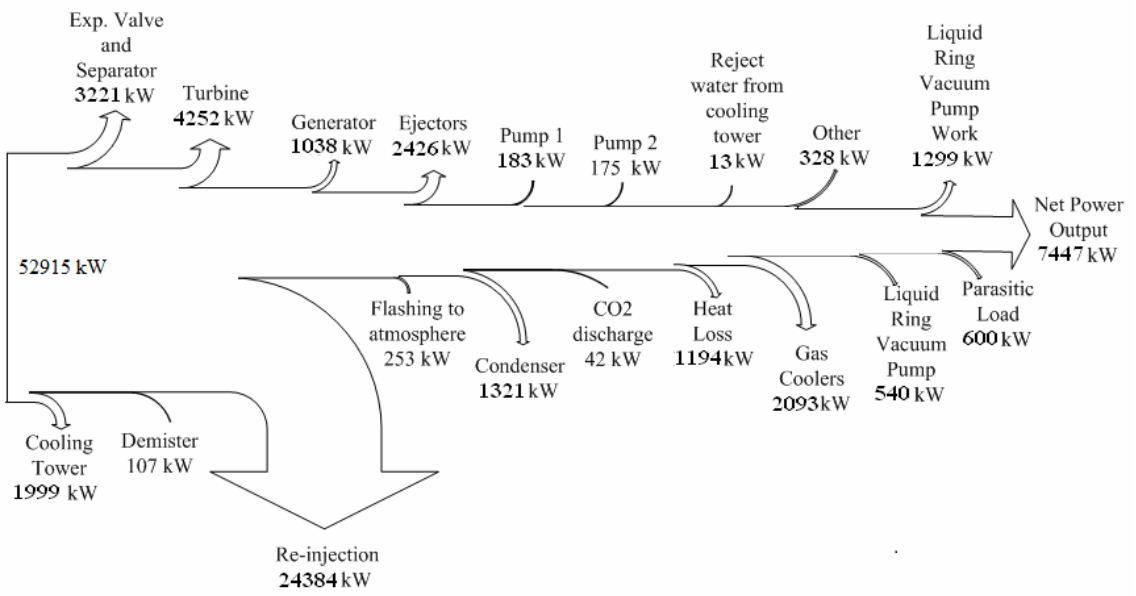

Figure 6.18. Exergy flow chart for HS.

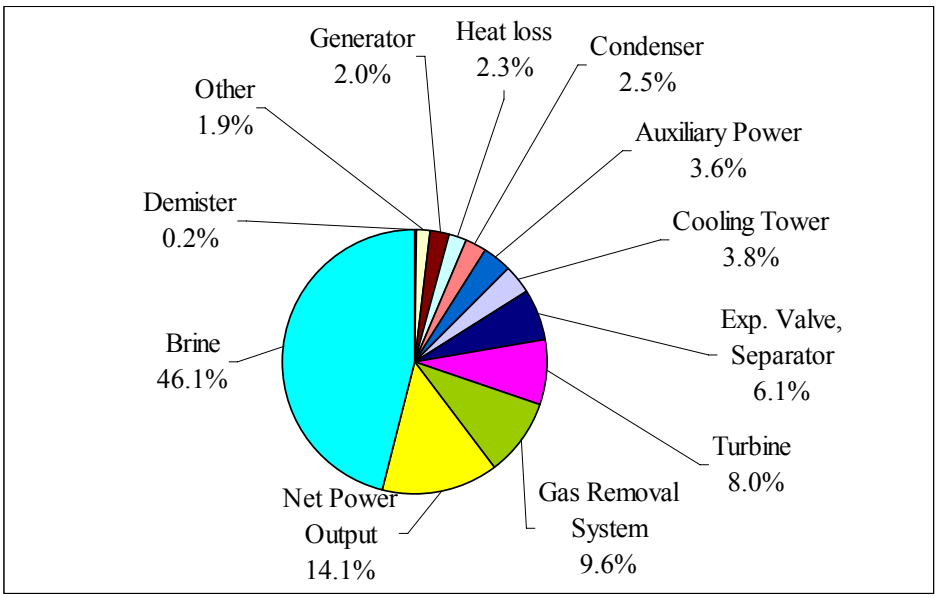

Figure 6.19. Overall exergy balance of HS.

Optimum separator pressure for 13% NCG fraction is determined as 340 kPa for HS. Exergy losses of HS for optimum separator pressure and operational separator pressure are given in Table 6.13. The exergy loss of the brine is decreased around 8% and overall exergetic efficiency increases to 14.6% from 14.1% with using optimum separator pressure.

Table 6.13. Exergy losses of HS at optimum and operational separator pressures.

Separator pressure		**460 kPa**		**340 kPa**	
		Exergy loss		**Exergy loss**	
		(kW)	**(%)**	**(kW)**	**(%)**
Exergy at wellhead		**52915**		**52910**	
Exergy losses of main equipments		**36679**	**69.3**	**34859**	**65.9**
	Expansion valve+Separator	3221	6.1	4737	9.0
	Brine	24384	46.1	20330	38.4
	Demister	107	0.2	170	0.3
	Turbine	4252	8.0	4243	8.0
	Generator	1038	2.0	1101	2.1
	Condenser	1321	2.5	1507	2.8
	Cooling tower	1999	3.8	2350	4.4
	Pump1	183	0.3	215	0.4
	Pump2	175	0.3	206	0.4
Reject to atmosphere or river		**308**	**0.6**	**342**	**0.6**
	Reject from cooling water	13	0.0	15	0.0
	Flashing to atmosphere	253	0.5	278	0.5
	CO_2 discharge	42	0.1	49	0.1
Heat loss		**1194**	**2.3**	**1404**	**2.7**
	Pipe (from condenser to cooling tower)	1194	2.3	1404	2.7
Other		**328**	**0.6**	**398**	**0.8**
NCG removal system		**5059**	**9.6**	**5998**	**11.3**
	SJE	2426	4.6	2754	5.2
	LRVP	540		631	
	Inter and after condensers	2093	4.0	2613	4.9
Auxiliary power		**1899**	**3.6**	**2197**	**4.2**
	Parasitic load (pumps, fan etc.)	600	1.1	679	1.3
	LRVP work	1299	2.5	1518	2.9
Net power output		**7447**	**14.1**	**7712**	**14.6**

In Table 6.14, the exergetic efficiency of main components of the plant is given for operational and optimum separator pressure. Table 6.14 shows that the exergetic

efficiencies of the separation, turbine-generator and condenser increase with optimum separator pressure.

Table 6.14. Exergetic efficiencies of main components of HS at optimum and operational separator pressures.

Separator pressure		**460 kPa**	**340 kPa**
Equipment		Exergetic efficiency (%)	Exergetic Efficiency (%)
Expansion valve+Seperator		47.8	52.6
Turbine-generator		63.9	65
Condenser		81.8	82.3
Cooling tower		61.5	61.5
NCG removal system			
	SJE	53.7	56.6
	LRVP	48.8	48.8
	Inter condenser	42.3	42.5
	After condenser	19.3	19.3
GPP overall		14.1	14.6

6.1.2.4. Reboiler System

In Figure 6.20, the flow diagram of RS is demonstrated.

The pressure drop throughout the reboiler is taken as 320 kPa. Exergy balance is conducted to reboiler NCG removal system at 13% NCG fraction and 450 kPa turbine inlet pressure and result are given in Table 6.15 and shown in Figure 6.21.

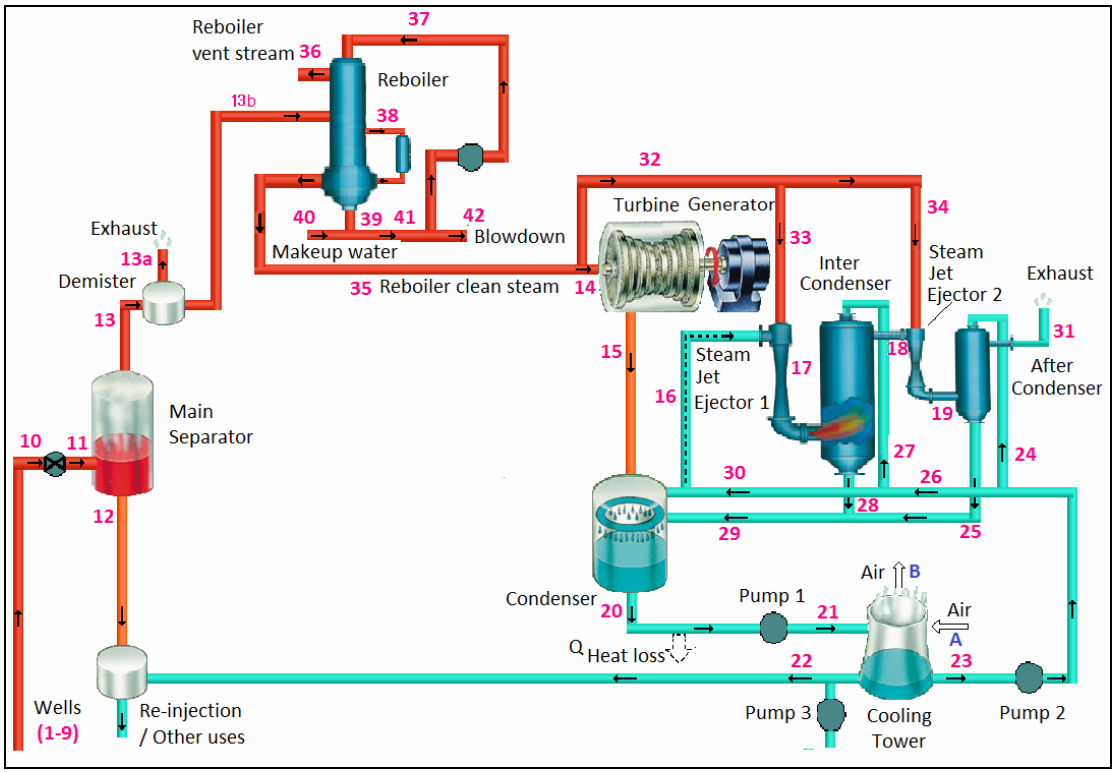

Figure 6.20. The representative model of RS.

Table 6.15. Property values at major locations of RS.

State No	T (°C)	P (kPa)	m (kg/s)	m_f (kg/s)	m_g (kg/s)	m_{CO2} (kg/s)	Enthalpy (kJ/kg)	Specific exergy (kJ/kg)	Energy rate (kW)	Exergy rate (kW)
9	204.7	1800	281.6	278.4	0	3.2	865.5	188.8	243725	53166
10	192.7	1330	281.6	270.7	7.7	3.2	865.5	187.9	243725	52915
11	169.4	780	281.6	257	21.4	3.2	865.5	183.8	243725	51758
12	169.4	780	257	257	0	0	716.6	129.7	184166	33333
13	169.4	780	24.6	0	21.4	3.2	2425	749.8	59558	18415
14	147.9	450	17.5	0	17.4	0.1	2735	760.7	47780	13289
15	45.79	10	17.5	1.6	15.8	0.1	2349	207.1	41037	3618
16	43.74	9	0.1	0	0	0.1	198.4	-103	13	-7
17	113.8	31.24	0.2	0	0.1	0.1	1688	228.1	346	47
18	69.28	30.25	0.1	0	0	0.1	89.24	-49.81	7	-4
19	127.6	105	0.4	0	0.3	0.1	1943	406	796	166
20	45.79	10	569.4	569.4	0	0	191.7	5.924	109154	3373

(cont. on next page)

Table 6.15. (cont.)

21	42.79	95	569.4	569.4	0	0	179.2	4.805	102036	2736
22	29	95	7	7	0	0	121.5	1.096	847	8
23	29	95	551.6	551.6	0	0	121.5	1.096	67019	605
24	29	95	10.5	10.5	0	0	121.5	1.096	1270	11
25	45.79	10	10.7	10.7	0	0	191.7	5.924	2057	64
26	29	95	541.1	541.1	0	0	121.5	1.096	65744	593
27	29	95	4.5	4.5	0	0	121.5	1.096	545	5
28	45.79	10	4.6	4.6	0	0	191.7	5.924	883	27
29	45.79	10	15.3	15.3	0	0	191.7	5.924	2941	91
30	29	95	536.6	537	0	0	121.5	1.096	65197	588
31	98.18	95	0.1	0	0	0	63.86	8.787	8	1
32			0.5	0	0.5	0	2735	760.7	1278	355
33	147.9	450	0.1	0	0.1	0	2401	677.5	333	94
34	147.9	450	0.3	0	0.3	0	2401	677.5	789	223
35	147.9	450	17.9	0	17.9	0.1	2735	760.7	49066	13647
36	169.4	780	6.2	0	3.1	3.1	1448	491.2	8969	3042

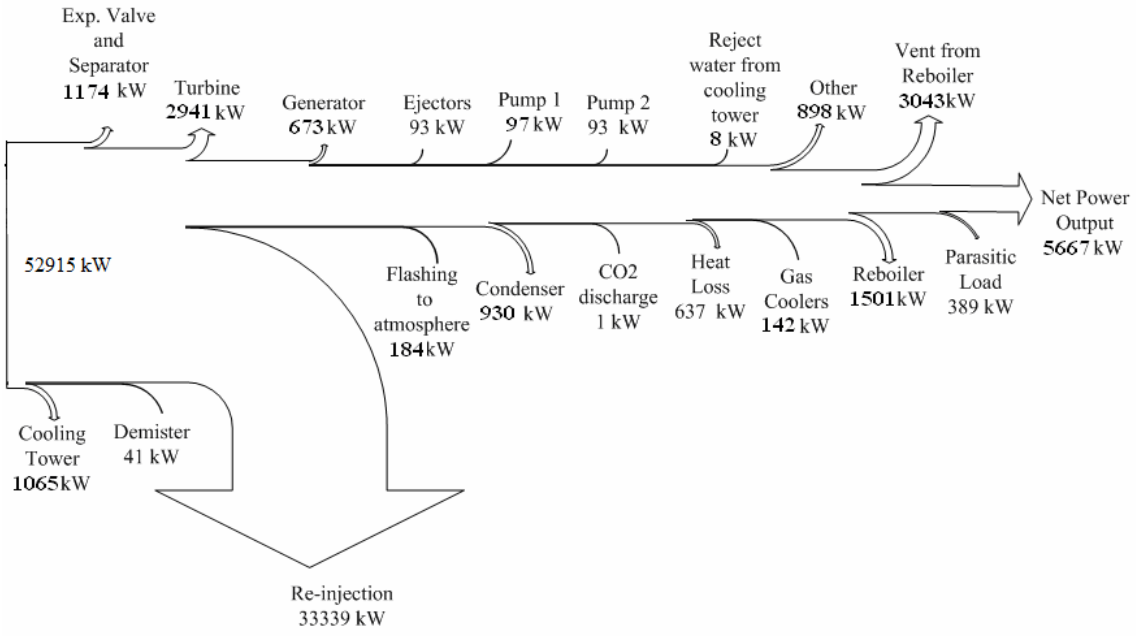

Figure 6.21. Exergy flow chart for RS.

The results of the exergy balance show that the largest exergy destruction occurs on brine with 33339 kW, which amounts 63% of total exergy input (Figure 6.22). The

exergy destruction of brine of RS is higher than the other NCG removal systems because of RS has higher separator pressure.

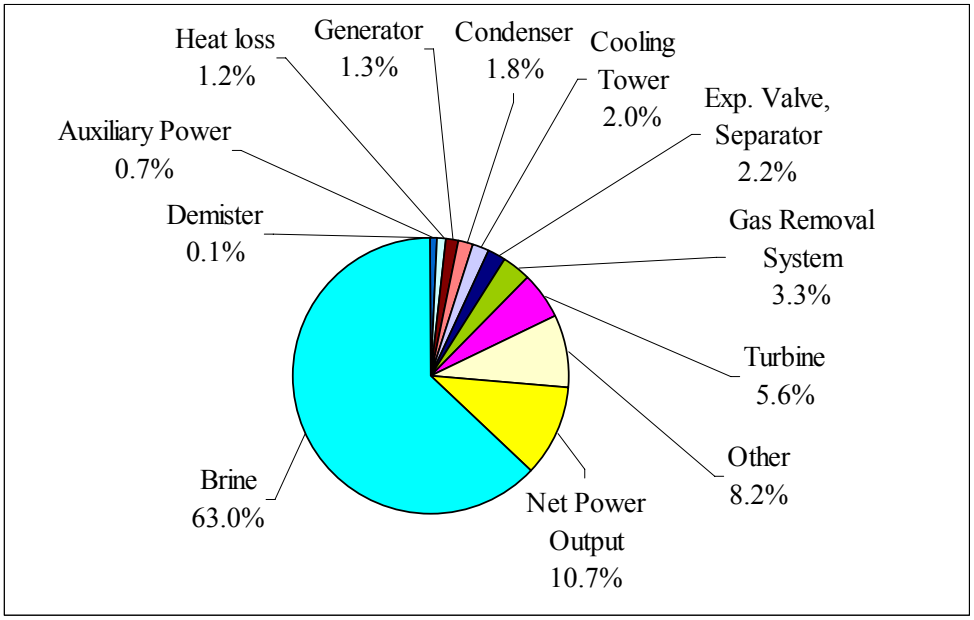

Figure 6.22. Overall exergy balance of RS.

Thermodynamic evaluation according to exergy balance of RS is repeated for optimum separator pressure of RS, determined as 580 kPa. The results are summarized in Table 6.16 and Table 6.17. The overall exergetic efficiency of RS is increased to 11.9% from 10.7% with using optimum separator pressure.

Table 6.16. Exergy losses of RS at optimum and operational separator pressures.

Separator pressure		**460 kPa**		**580 kPa**	
		Exergy Loss		**Exergy Loss**	
		(kW)	**(%)**	**(kW)**	**(%)**
Exergy at wellhead		**52915**		**52919**	
Exergy Losses of main equipments		**40353**	**76.3**	**36774**	**69.5**
	Expansion valve+Separator	1174	2.2	2223	4.2
	Brine	33339	63.0	27987	52.9
	Demister	41	0.1	72	0.1

(cont. on next page)

Table 6.16. (cont.)

	Turbine	2941	5.6	2899	5.5
	Generator	673	1.3	751	1.4
	Condenser	930	1.8	1195	2.3
	Cooling Tower	1065	2.0	1397	2.6
	Pump1	97	0.2	128	0.2
	Pump2	93	0.2	122	0.2
Reject to atmosphere or river		**3236**	**6.1**	**3950**	**7.5**
	Reject from cooling water	8	0.0	10	0.0
	Flashing to atmosphere	184	0.3	227	0.4
	Vent from reboiler	3043	5.8	3711	7.0
	CO_2 discharge	1	0.0	2	0.0
Heat loss		**637**	**1.2**	**835**	**1.6**
	Pipe (from condenser to cooling tower)	637	1.2	835	1.6
Other		**907**	**1.7**	**1225**	**2.3**
NCG removal system		**1735**	**3.3**	**3377**	**6.4**
	Steam Jet Ejectors	93	0.2	135	0.3
	Reboiler	1501	2.8	2903	5.5
	Gas Coolers	142	0.3	339	0.6
Auxiliary Power		**389**	**0.7**	**464**	**0.9**
	Parasitic load (pumps, fan etc.)	389	0.7	464	0.9
Net Power Output		**5667**	**10.7**	**6294**	**11.9**

Table 6.17. Exergetic efficiencies of main components of RS for optimum and operational separator pressure.

Separator pressure	**460 kPa**	**580 kPa**
Equipment	Exergetic efficiency (%)	Exergetic efficiency (%)
Expansion valve+Seperator	34.8	42.9
Turbine-generator	62.6	64.9
Condenser	78.4	78.7

(cont. on next page)

Table 6.17. (cont.)

Cooling tower		61.5	61.5
NCG removal system			
	SJE 1	53.7	59.5
	SJE 2	76.1	83.8
	Reboiler	75	70.5
	Inter condenser	42.3	42.6
	After condenser	50.8	51.4
GPP overall		10.7	11.9

6.1.2.5. Comparison of the NCG Removal Systems

The main results of the exergy analyses of the NCG removal systems are summarized in Table 6.18 for 450 kPa turbine inlet and 10 kPa condenser pressures and 13% NCG fraction. The biggest exergy loss results from brine. While SJES, CS and HS has 46.1% exergy loss on brine, RS has 63%. Because as it is explained in the previous sections, reboiler has 320 kPa higher pressure drop than the others. When the separator pressure increases, the quality of the geothermal fluid decreases. As a result of it, the liquid stream of the fluid increases and RS has 17% higher exergy losses on brine.

SJES has the highest exergy loss on NCG removal system with 17.3% of the total exergy input. HS follows SJES by 9.6%. CS has the lowest exergy losses among the system with 1%. The other equipments having the major exergy losses are turbine (5.2-10.4%), expansion valve and separator couple (2.2-6.1%), cooling tower (2-3.9%), condenser (1.6-3.2%) and generator (1.3-2.5%).

In Table 6.19, at 450 kPa turbine inlet pressure and 13 % NCG fractions the exergetic efficiencies of main components of the plant for different gas removal options are compared. The results indicate that the exergetic efficiency is around 61.5% for the cooling tower and around 63% for turbine-generator couple. Condenser exergetic efficiency is in range of 76.5-87.9%.

Table 6.18. Exergy losses of the NCG removal systems.

Components	CS		SJES		HS		RS	
	(kW)	(%)	(kW)	(%)	(kW)	(%)	(kW)	(%)
Exergy losses of main equipments	**38524**	**72.8**	**34447**	**65.1**	**36679**	**69.3**	**40353**	**76.3**
Expansion valve+Separator	3221	6.1	3221	6.1	3221	6.1	1174	2.2
Brine	24384	46.1	24384	46.1	24384	46.1	33339	63.0
Demister	107	0.2	107	0.2	107	0.2	41	0.1
Turbine	5496	10.4	2767	5.2	4252	8.0	2941	5.6
Generator	1342	2.5	676	1.3	1038	2.0	673	1.3
Condenser	1707	3.2	859	1.6	1321	2.5	930	1.8
Cooling tower	1924	3.6	2063	3.9	1999	3.8	1065	2.0
Pump1	176	0.3	189	0.4	183	0.3	97	0.2
Pump2	168	0.3	181	0.3	175	0.3	93	0.2
Reject to atmosphere or river	**309**	**0.6**	**307**	**0.6**	**308**	**0.6**	**3236**	**6.1**
Reject from cooling water	14	0.0	12	0.0	0.0	15	8	0.0
Flashing to atmosphere	253	0.5	253	0.5	0.5	278	184	0.3
CO_2 discharge	42	0.1	42	0.1	0.1	49	1	0.0
Vent from reboiler							3043	5.8
Heat loss	**1147**	**2.2**	**1233**	**2.3**	**1194**	**2.3**	**637**	**1.2**
Pipe	1147	2.2	1233	2.3	1194	2.3	637	1.2
Other	**300**	**0.6**	**1683**	**3.2**	**328**	**0.6**	**907**	**1.7**
NCG removal system	**556**	**1.0**	**9165**	**17.3**	**5059**	**9.6**	**1735**	**3.3**
Compressors/SJEs	206	0.4	3623	6.8	2426	4.6	93	0.2
LRVP/Reboiler					540	1.0	1501	2.8
Inter and after condensers	349	0.7	5542	10.5	2093	4.0	142	0.3
Auxiliary power	**1844**	**3.5**	**614**	**1.2**	**1899**	**3.6**	**389**	**0.7**
Parasitic load (pumps, fan etc.)	582	1.1	614	1.2	600	1.1	389	0.7
Compressor work/LRVP	1262	2.4			1299	2.5		

Table 6.19. Comparison of exergetic efficiencies of main components of the plant for different gas removal options.

Component	Exergetic efficiency (%)			
	CS	SJES	HS	RS
Expansion valve+Seperator	47.8	47.8	47.8	34.8
Turbine-Generator	63.9	63.9	63.9	62.6
Condenser	76.5	87.9	81.8	78.4
Cooling tower	61.4	61.5	61.5	61.5

The plants with different NCG removal systems are compared to their net power output and overall exergetic efficiency at 450 kPa turbine inlet and 10 kPa condenser pressures for 13% NCG fraction (Table 6.20). Among the systems, CS has the highest net power output (10235 kW), depending on highest overall exergetic efficiency (19.3%). The worst option is SJES with the 5466 kW net power output and 10.3% overall exergetic efficiency.

Table 6.20. Net power output and overall exergetic efficiencies of the plant for different gas removal options.

	CS	SJES	HS	RS
Net Power Output (kW)	10235	5466	7447	5667
Overall Exergetic Efficiency (%)	19.3	10.3	14.1	10.7

In Figure 6.23, overall exergetic efficiency of NCG removal systems depending on NCG fraction at operational turbine inlet pressure of the KGPP is shown. Among the systems, CS has the highest overall exergetic efficiency. RS is the worst option for low NCG fractions, for high NCG fractions at low turbine inlet pressure it becomes more efficient than SJES.

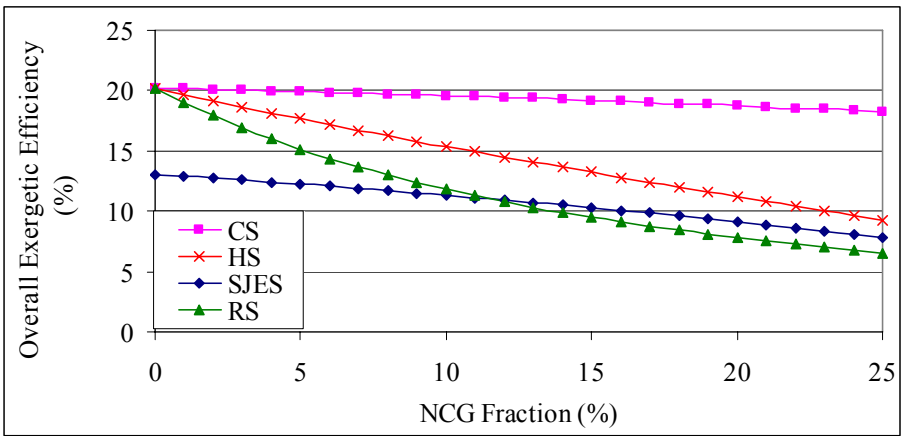

Figure 6.23. Overall exergetic efficiency of NCG removal systems depending on NCG fraction.

Overall exergetic efficiencies of the systems are normalized according to steam ejector NCG removal system for various NCG fractions and turbine inlet pressures. The results are demonstrated in Figure 6.24. As it can be seen from the Figure the exergetic efficiencies of the systems have largest difference at low NCG fractions, but increasing the NCG fraction the efficiencies becomes closer to each other especially for high turbine inlet pressures.

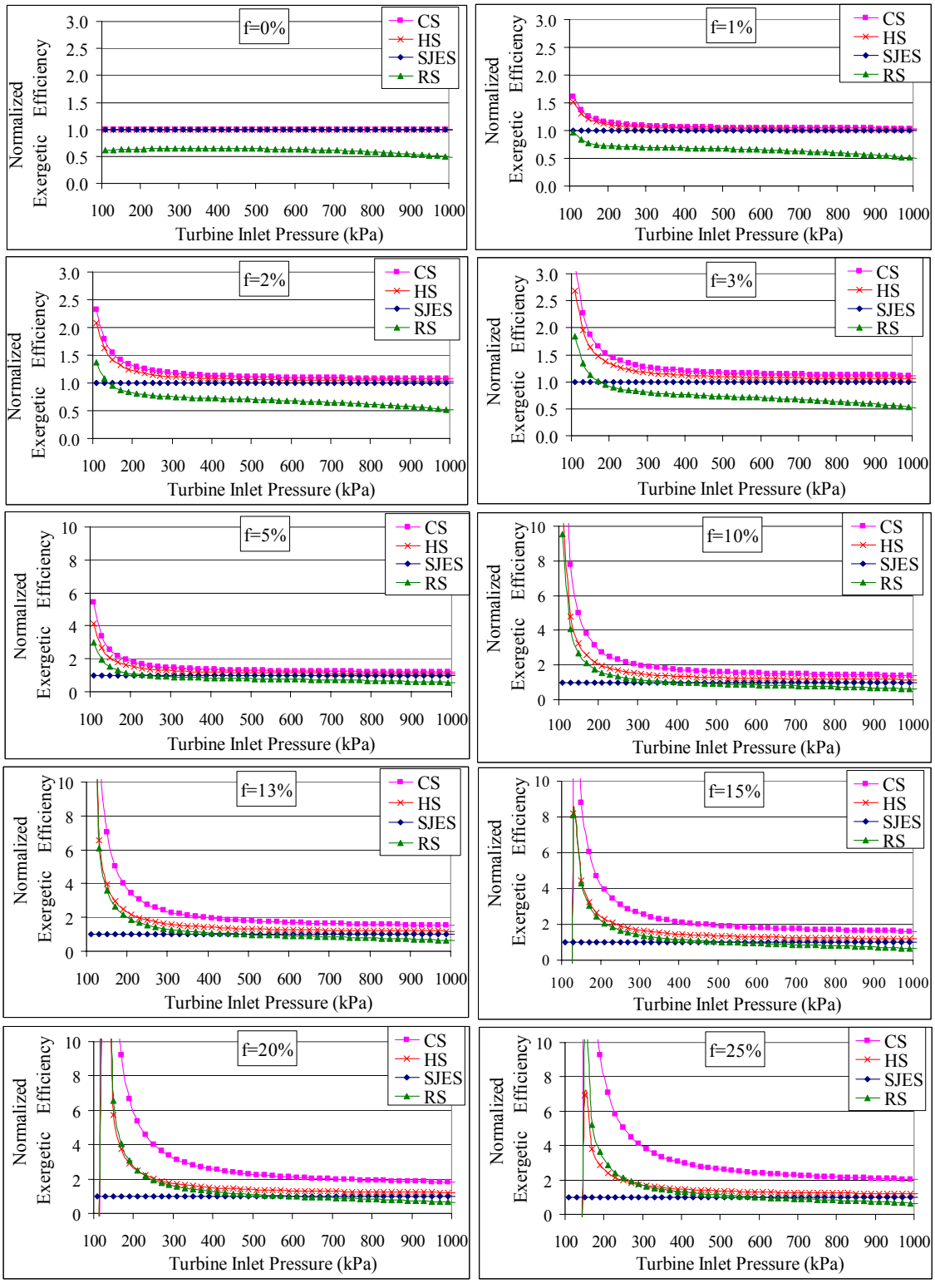

Figure 6.24. Normalized overall exergetic efficiency for various NCG fractions and turbine inlet pressures.

6.1.3. Economical Results

In the Thesis, economic analysis of the four different types of NCG removal systems, which are two-stage CS, SJES, HS and RS, has been conducted. Various methods of comparison exist for economic analysis to be able to show the advantage of one type against to the other. NPV, IRR and SPT methods are used. Addition to these economic comparison methods, the systems are compared according to cost of electricity production per kWh.

Simulations have been conducted for interest rate, tax rate, O&M cost ratio, NCG removal system cost, GPP unit cost, electricity sales price and NCG fraction.

6.1.3.1. Economical Evaluation of NCG Removal Systems

In this section, NCG removal systems are evaluated depending on NPV, IRR and SPT values. Additionally, cost of electricity production of the plant is computed for each NCG removal system option. In the calculations NCG fraction, condenser pressure and wet bulb temperature are taken as 13%, 10 kPa and 12.2 ^{o}C, respectively. Other main economical assumptions and calculated cost are summarized in Table 6.21 for electricity sales price of 0.0733 USD/kWh (equals to 5.5 Eurocent/kWh, which is the government guaranteed tariff according to Law 5346). O&M cost of the plant is assumed as 5% of the total capital investment cost. Interest rate is taken as 15%.

The cash flow of the plant is computed for 20 years economical life with amortization coefficient of 0.1 and tax rate 20%. Electricity sales revenue, O&M cost and amortization cost are taken into account for determination of taxable income. The cash flow of the NCG removal systems is given in Table B.1-4 in Appendix B.

Table 6.21. General results of economical analysis of GPPs.

	Unit	CS	SJES	HS	RS
Separator Pressure	(kPa)	460	460	460	780
Turbine Inlet Pressure	(kPa)	450	450	450	450
Net Power Output	(kW)	10,235	5,466	7,447	5,667

(cont. on next page)

Table 6.21. (cont.)

Annual Electricity Production	(kWh)	80,692,740	43,093,944	58,712,148	44,678,628
GPP Investment Cost	(USD)	15,000,000	15,000,000	15,000,000	15,000,000
NCG Removal System Investment Cost *	(USD)	8,000,000	2,000,000	3,250,000	3,500 000
Total Capital Investment Cost	(USD)	23,000,000	17,000,000	18,250,000	18,500,000
Electricity Sales Revenue	(USD)	5,917,468	3,160,223	4,305,558	3,276,433
O&M Cost	(USD)	1,150,000	850,000	912,500	925,000

* It is assumed depending on Vorum and Fritzler (2000) and Nash (2006).

6.1.3.1.1. Net Present Value

NPV of NCG removal system versus electricity sales price is presented in Figure 6.25 for the electricity sales price range of 0.06-0.12 USD/kWh and 15% interest rate. Among the systems, CS has the highest and mostly positive NPV value. HS follows CS. NPV of RS and SJES are close to each other but these systems start to be profitable for the electricity sales prices are higher than 0.09 USD/kWh.

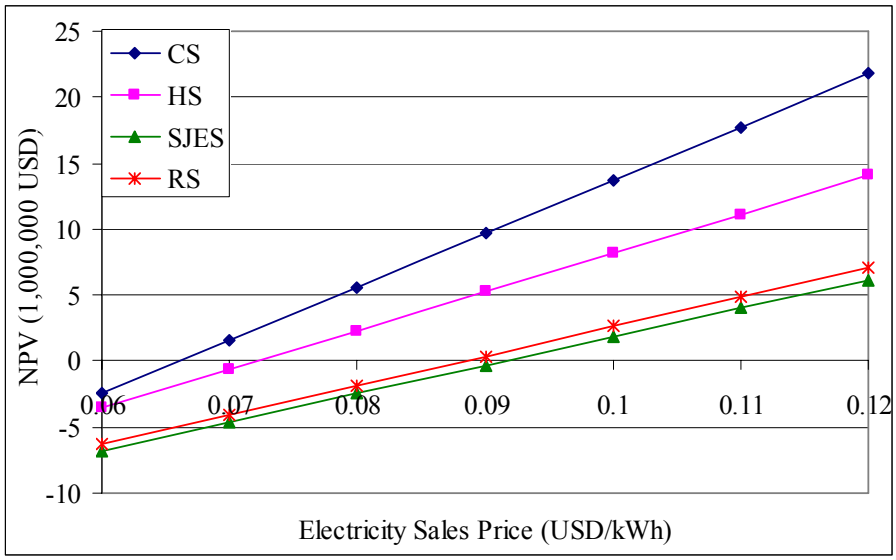

Figure 6.25. NPV of NCG removal systems vs. electricity sales price.

6.1.3.1.2. Internal Rate of Return

IRR method is evaluated for NCG removal system options and the results are demonstrated in Figure 6.26. Similarly of NPV results, CS has the highest IRR. Even SJES is cheaper than RS, it has lower IRR than RS. As an example, IRR is 17.3% for CS, 11.3% for RS, 15.4% for HS and 10.7% for SJES for 0.0733 USD/kWh electricity sales price.

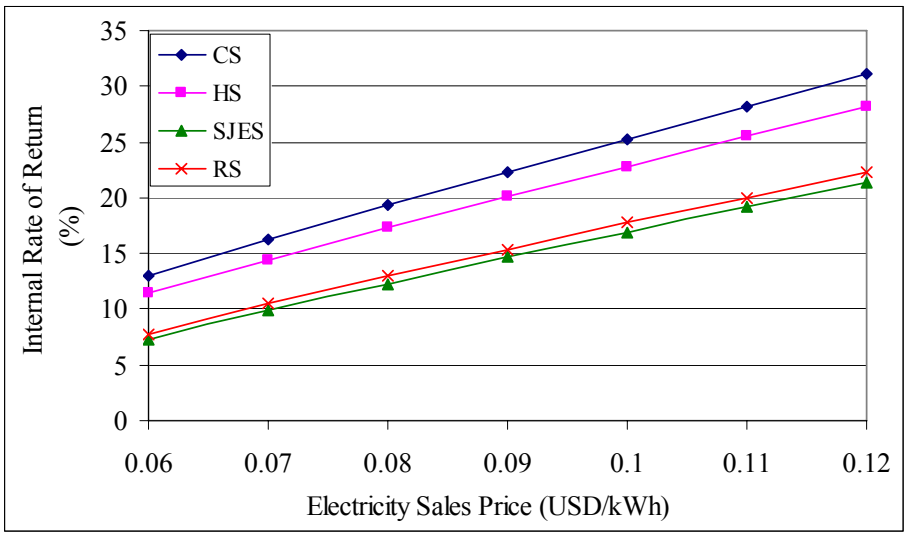

Figure 6.26. IRR of the NCG removal systems.

6.1.3.1.3. Simple Payback Time

The SPT of NCG removal systems is calculated with 15% interest rate, 20% tax rate and 5% O&M ratio. In Figure 6.27 SPT of NCG removal systems versus various electricity sales prices are illustrated. Figure 6.27 provides that, depending on the assumed cost parameters such as investment and O&M costs for all electricity sales prices the SPT of SJES is the highest. CS has the lowest payback time among the NCG removal systems. SPT is 5.69 years for CS, 8.06 years for RS, 6.3 years for HS and 8.43 years for SJES with 0.0733 USD/kWh electricity sales price.

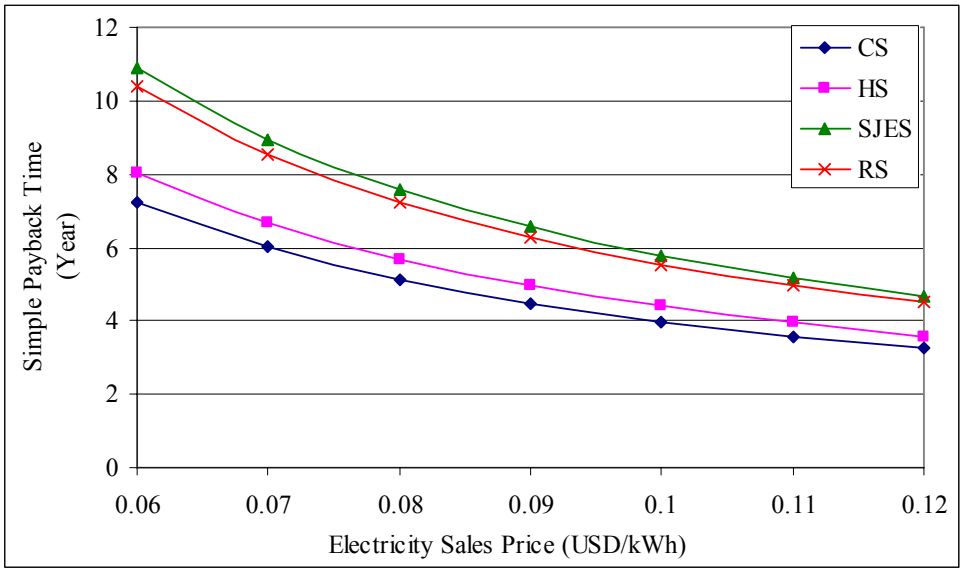

Figure 6.27. SPT of NCG removal systems.

6.1.3.1.4. Cost of Electricity Production

Cost of electricity production versus electricity sales price is shown in Figure 6.28. CS has the lowest electricity production cost per kWh. HS, RS and SJES follow CS. With 0.0733 USD/kWh electricity sales price, electricity production cost per kWh is 0.069 USD for CS, 0.087 USD for RS, 0.074 USD for HS and 0.09 USD for SJES.

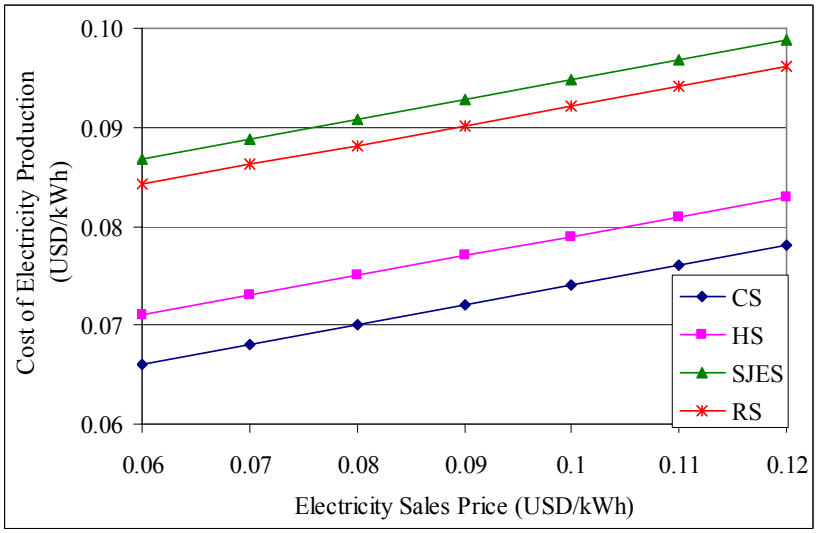

Figure 6.28. Cost of electricity production of NCG removal systems.

These results indicate that, only CS can be selectable option at 13% NCG fraction depending on the assumed economical cost parameters.

6.1.3.2. Simulation of the Parameters of Economical Analysis

Simulation parameters are interest rate, tax rate; O&M cost ratio, NCG removal system cost, GPP unit cost, electricity sales price and NCG fraction.

6.1.3.2.1. Interest Rate

Money has a time value. That means a dollar at the beginning of an investment does not have the same value as a dollar at the end of the investment (even neglecting possible inflation) due to the existence of interest. Therefore, cost of money is directly related to the interest rate and the length of the debt period. Both these parameters (i.e. interest rate & debt length) may vary widely according to conditions and circumstances. The interest or discount rate gives money a time value. To be able to see the effect of the interest rate on the cost of the system, NPV of the system is calculated for various interest rates, which is in range of 10-30% by keeping the other economical parameters as constant. In Figure 6.29, NPV versus electricity sales price for various interest rates is shown of CS.

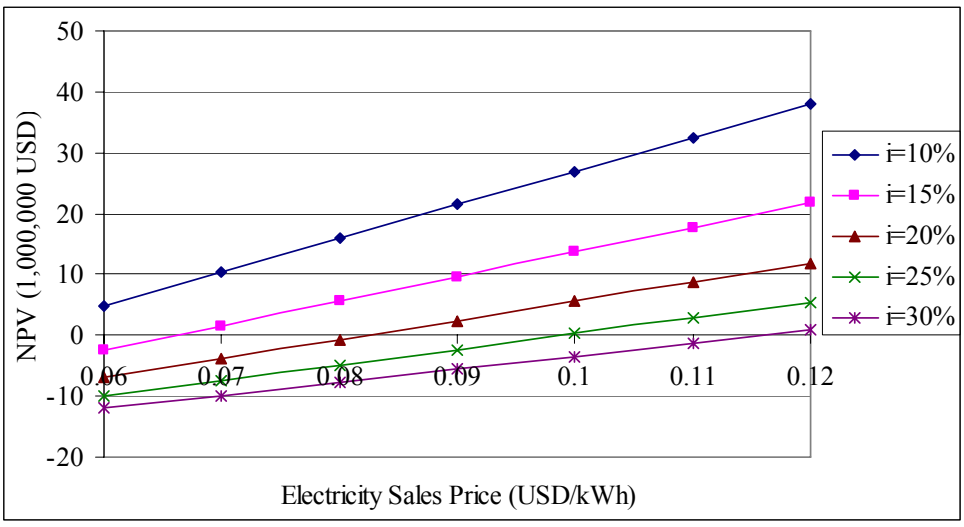

Figure 6.29. NPV of CS vs. electricity sales price changing with interest rate.

It can be seen that from Figure 6.29, NPV decreases with increasing interest rate. The other outcome from the Figure is NPV increases with increasing electricity sales price.

6.1.3.2.2. Electricity Sales Price

The other comparison parameter for the economical analysis of NCG removal systems of flashed-steam GPPs is the cost of electricity production per kWh depending on electricity sales price. The cost of electricity production per kWh of CS is calculated and the results are tabulated on Figure 6.30 for various interest rates and electricity sales price. While the cost of electricity production is 0.0688 USD/kWh for 15 % interest rate and 0.0733 USD/kWh electricity sales price, it is 0.0741 USD/kWh for 0.1 USD/kWh electricity sales price. These results show that, the cost of electricity production increases with increasing electricity sales price. Because revenue and depending on the revenue the tax cost is high for higher electricity sales price.

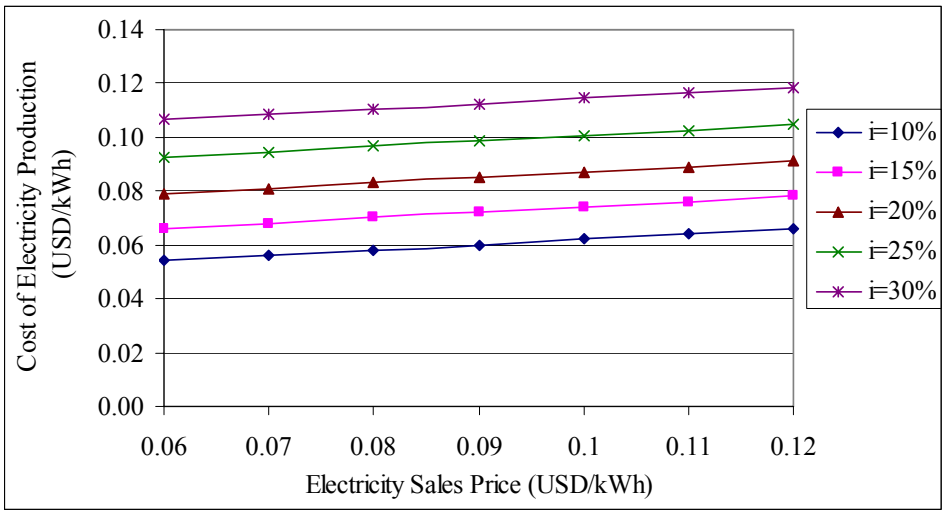

Figure 6.30. Cost of electricity production of CS vs. electricity sales price for various interest rates.

6.1.3.2.3. Tax Rate

One of the parameters of the simulation is tax rate. In the literature different tax rates exist for different countries. While in some references the tax rate is 34% (Vorum

and Fritzler, 2000; Triyono, 2001), for the other references it is 20% (Sener and Uluca, 2009). Therefore, in the simulations the tax rate is taken as 20% and 34%. The same economical analyses methods have been conducted to CS for different tax rates. On Figure 6.31, NPV, cost of electricity production per kWh, SPT and IRR versus electricity sales prices for two different tax rates are exhibited. As it is expected, while NPV and IRR decrease, cost of electricity production and SPT increase with increasing tax rate. As an example, for 0.0733 USD/kWh electricity sales price, NPV of CS decreases to 36,886 USD from 2,910,000 USD with 70% increment in tax rate. While cost of electricity production and SPT increase %8.7 and 14.2%, IRR decreases 13.3% by 70% increment in tax rate.

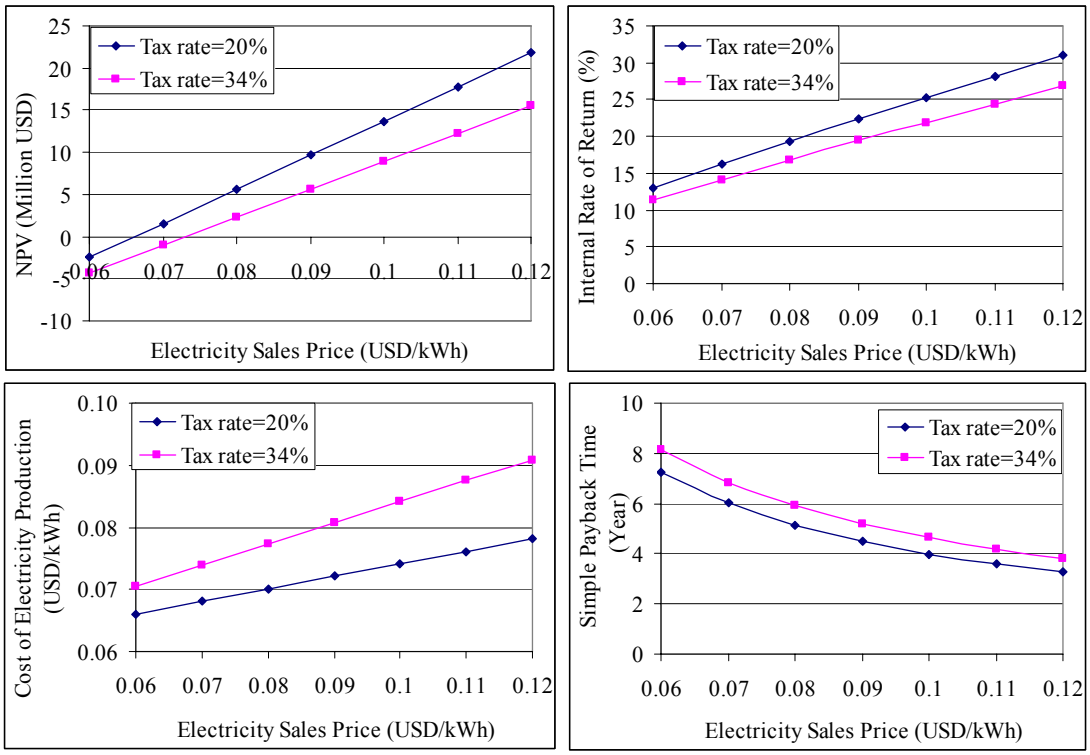

Figure 6.31. Simulation results of CS for tax rate.

6.1.3.2.4. O&M Cost

O&M costs are variable for the GPPs. Upto now O&M costs are assumed as 5% of the total investment cost. Simulations have been conducted to be able to see the effect of the O&M cost in the economical analyses. NPV, cost of electricity production per kWh, SPT and IRR versus electricity sales prices for two different O&M ratio as

5% and 10% are calculated for CS. The results of simulations are plotted on Figure 6.32. While NPV and IRR decreases, cost of electricity production and SPT increases with increasing O&M cost. With 0.0733 USD/kWh electricity sales price, the electricity production cost is 0.069 USD/kWh for 5% O&M ratio. The electricity production cost increases to 0.08 USD/kWh for 10% O&M ratio. Similarly the SPT changes to 7.37 years from 5.69 years by changing O&M cost from 5% to 10% of the investment cost.

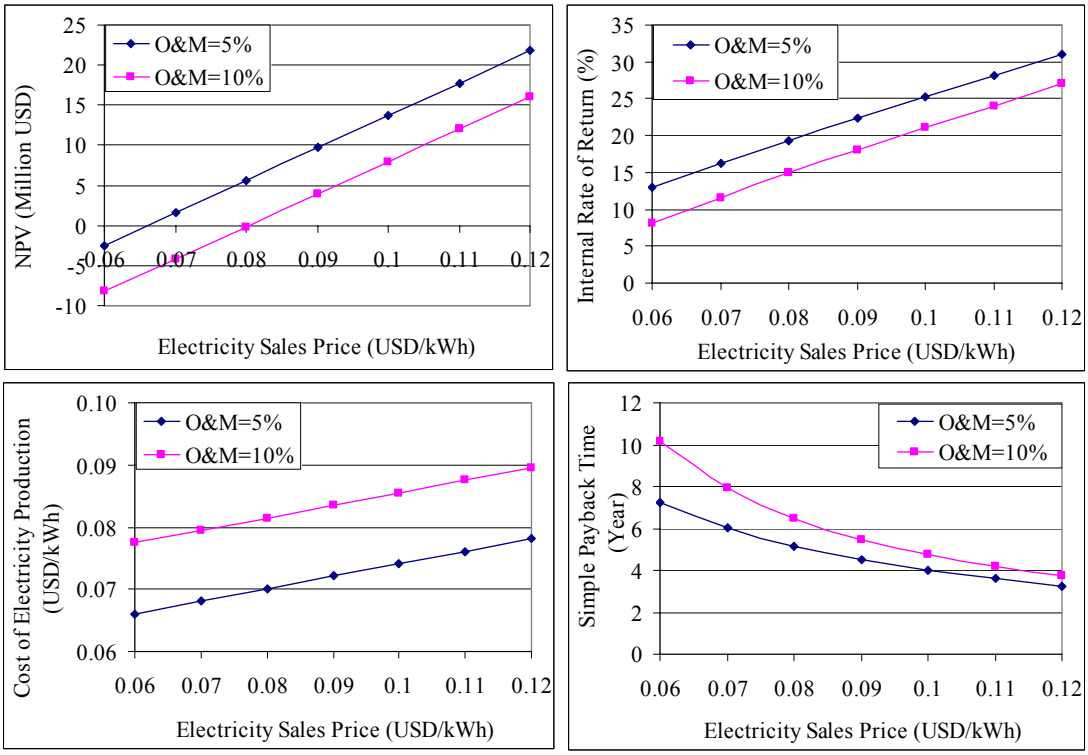

Figure 6.32. Simulation results of CS for O&M ratio.

6.1.3.2.5. NCG Fraction

The other parameter for the simulation is NCG fraction. Upto here, the NCG fraction was taken 13%. To be able to see the effect of the NCG fraction on economical analysis the calculations (NPV, IRR, cost of electricity production and SPT) are repeated for the NCG fraction in the range of 0-25%. The electricity sales price, O&M cost ratio, tax rate are 0.0733 USD/kWh, 5% and 20%, respectively. The GPP investment cost without NCG removal system is 15 Million USD with 12 MW installation capacity for each NCG removal system alternatives. The results, shown in Figure 6.33, indicate that RS has negative values for all NCG fractions. Therefore, it is

not profitable alternative with these assumptions. While until 2% NCG fraction SJES is the best option, after that until 10% NCG fraction HS is the best option with the highest NPV, IRR and lowest SPT and cost of electricity production. But when the NCG fraction is higher than 10%, CS becomes to the most profitable option among the NCG removal systems.

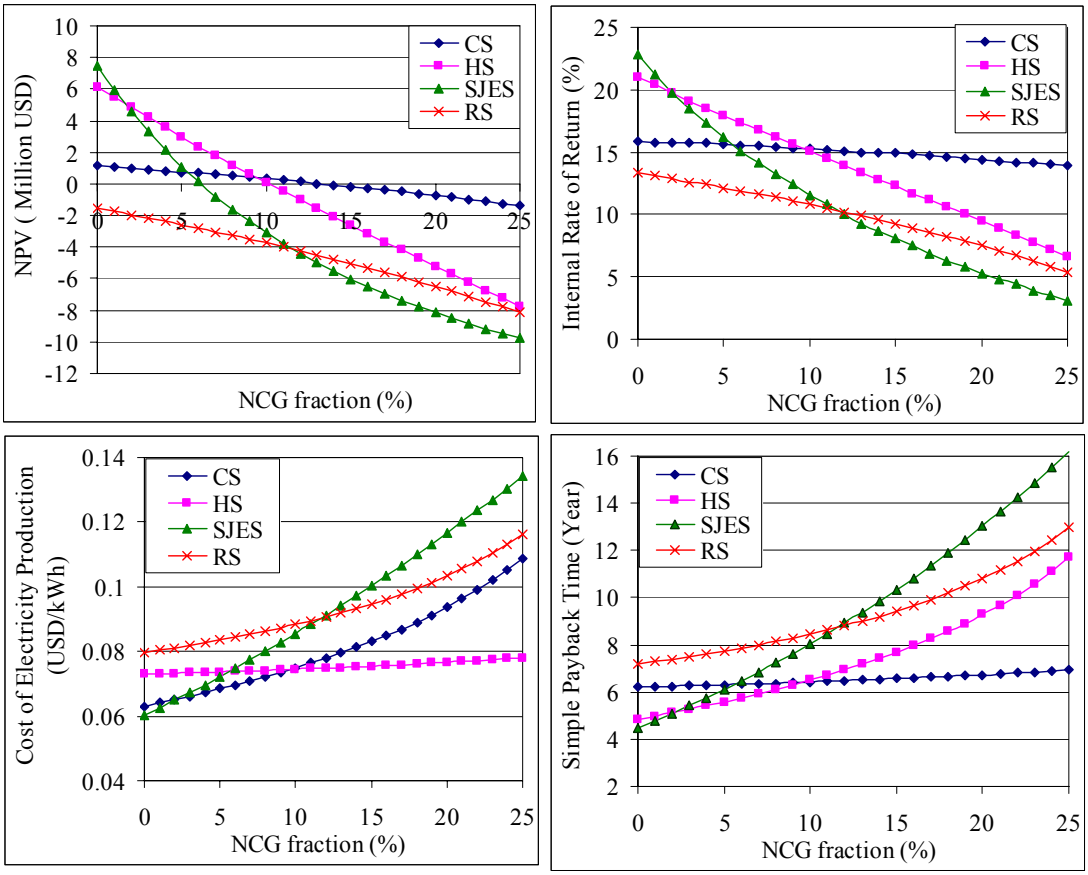

Figure 6.33. Simulations results of CS for NCG fraction.

6.1.3.2.6. Separator Pressure

Effect of the separator pressure on economical analysis of the plant (NPV, IRR, SPT and cost of electricity production) is evaluated by using optimum and operational separator pressures for 13% NCG fraction and results are summarized in Table 6.22. By using optimum separator pressure the net power output of CS increases in the amount of 1251 kW, which represents 12.2% performance improvement of operational separator condition. RS follows to CS with having 627 kW improvement on net power output. While HS has 265 kW net power output improvement, SJES has only 10 kW. Because

optimum separator pressure of SJES is close to operational separator pressure. NPV and IRR of CS have an increment by using optimum separator pressure as 3.48 Million USD and 2.6%, respectively. While, the cost of the electricity production is decreased by the amount of 0.5 USD¢/kWh, SPT is reduced to 5 years from 5.69 years by optimum separator pressure. SJES and RS are not a profitable option having negative sign for NPV, even with optimum separator pressure. The major improvement occurs in NPV with optimum separator pressure for HS. NPV increases to 1.126 Million USD from 0.356 Million USD.

Table 6.22. Simulation of separator pressure.

NCG Removal System	At Separator Pressure	Net Power Output (kW)	NPV (Million USD)	IRR (%)	Cost of electricity production (USD/kWh)	Simple payback time (year)
CS	Operational	10,235	2.91	17.3	0.06875	5.69
	Optimum	11,486	6.39	19.9	0.06307	5
SJES	Operational	5466	-3.92	10.7	0.08951	8.43
	Optimum	5476	-3.89	10.7	0.08938	8.41
HS	Operational	7447	0.356	15.4	0.07365	6.3
	Optimum	7712	1.126	16.1	0.07162	6.05
RS	Operational	5667	-4.52	10	0.09244	8.85
	Optimum	6294	-1.53	13.4	0.07967	7.09

NPV vs. NCG fractions are shown on Figure 6.34 at operational and optimum separator pressures.

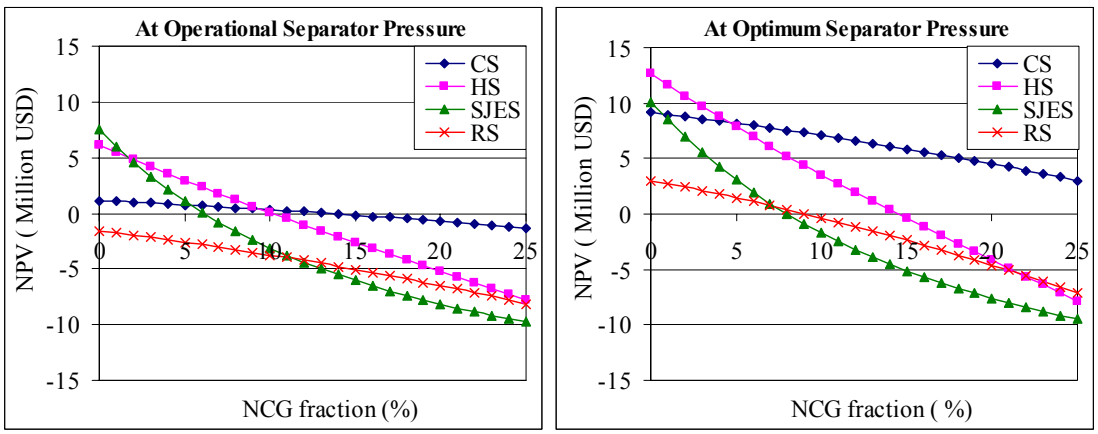

Figure 6.34. Simulation results for separator pressure.

The major outcome from Figure 6.34 is upto 8% NCG fraction all NCG removal system options have positive NPV values. That means all options can be possible to install. Among the systems HS is the most profitable options until 5% NCG fraction. After this point, CS becomes the most profitable options.

6.1.3.2.7. GPP Cost

Initial investment cost of GPP has a vital role in economic analysis. Therefore, simulation has been conducted for investment cost of the power plant. During the iterations of simulation, investment cost of NCG removal systems keep same to the previous cost assumption, unit cost of GPP changes +/- 20%. That means, unit cost of GPP are taken as 1000, 1250 and 1500 USD/kW without NCG removal system cost. The results are given in Table 6.23 at 15% interest rate, 20% tax rate, 5% O&M ratio and 12 MW installed capacity.

Table 6.23. Simulation results of unit cost of GPP.

Economical Parameter	NCG removal system	Unit Cost of GPP (USD/kW)		
		1000	1250	1500
NPV (Million USD)	CS	6.39	2.91	-0.57
	SJES	-0.44	-3.92	-7.41
	HS	3.84	0.36	-3.13
	RS	0.14	-3.34	-6.82
IRR (%)	CS	20.6	17.3	14.6
	SJES	14.4	10.7	7.9
	HS	19.4	15.4	12.3
	RS	15.2	11.3	8.5
SPT (Year)	CS	4.84	5.69	6.58
	SJES	6.64	8.43	10.38
	HS	5.11	6.30	7.58
	RS	6.36	8.06	9.90
Cost of Electricity Production (USD/kWh)	CS	0.062	0.069	0.076
	SJES	0.076	0.090	0.103
	HS	0.064	0.074	0.083
	RS	0.074	0.087	0.100

Table 6.23 indicates that, NPVs of the plants are varied +/- 3.48 Million USD by variation of 3 Million USD on total investment cost of the plant. IRRs are varied as 16% for CS, around 19.5% for HS, 26% for SJES, 25-26% for RS by 20% variation on total investment cost of the plants. SPT of the investment responses to 20% alteration on total investment cost of the plants with the variation of 14.5% for CS, 18% for HS, 20% for SJES, 21% for RS. Cost of electricity productions are changed 0.7 USD¢ for CS, 1 USD¢ for HS, 1.4 USD¢ for SJES and 1.3 USD¢ for RS by 20% variation on total investment cost of the plants.

6.1.3.2.8. NCG Removal System Cost

Upto here, NCG removal system cost are taken 8 Million USD for CS, 3.5 Million USD for RS, 3.25 Million USD for HS and 2 Million USD for SJES (Table 6.21). To be able to see the effect of NCG removal system cost on economical analysis, simulation has been conducted with varies NCG removal system costs. The range for NCG removal investment cost is 1-10 Million USD with the increment of 1 Million USD. The other investment costs of the plant are taken 15 Million USD (12 MW installed capacity) for all options. NPV, IRR, SPT and cost of the electricity production vs. NCG removal system cost are shown on Figure 6.35. The Figure indicates that SJES and RS are not profitable options with negative NPV values. The most profitable option is CS with the highest NPV and IRR values. HS can be profitable upto 4 Million USD of NCG removal system investment cost.

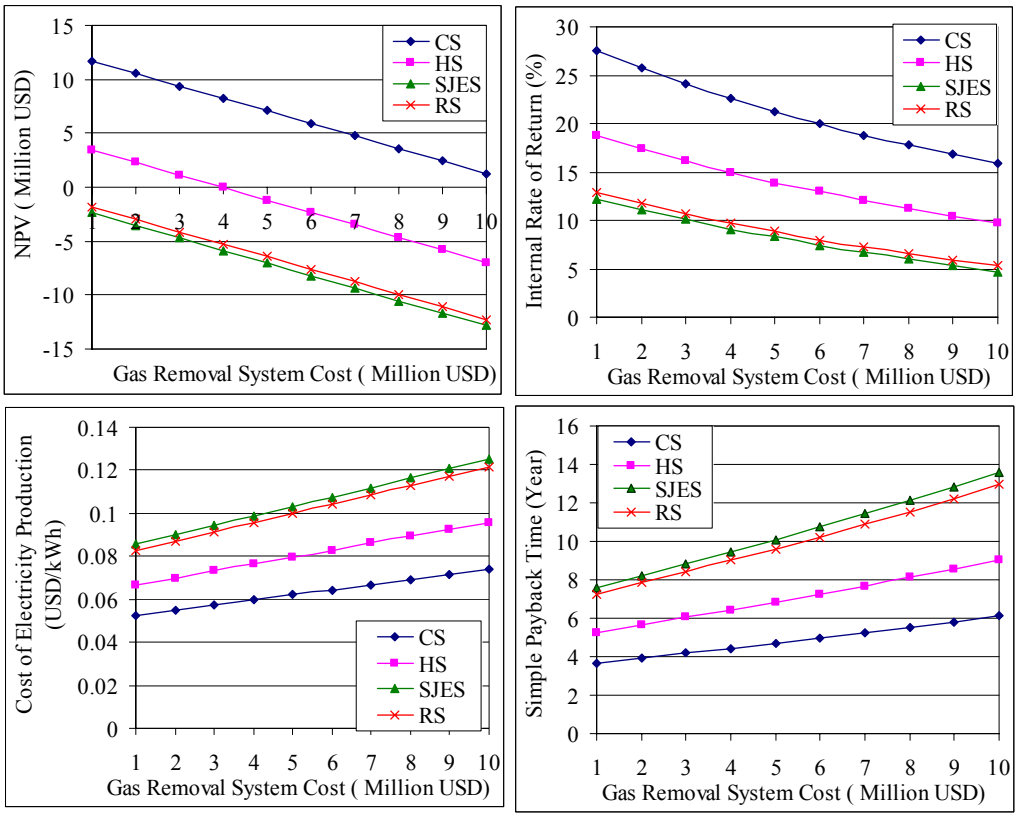

Figure 6.35. Simulation of the plants for NCG removal system investment cost.

6.2. Double-Flash GPPs

The flow diagram of the considered double-flash design of the plant is shown on Figure 6.36.

A secondary flashing unit in which the brine is re-flashed by decreasing its pressure to a lower value is installed to the wellhead to obtain more steam in the double-flash design, The steam coming from the secondary flashing unit is not routed to the existing turbine; it is passed through a different turbine, because its pressure is lower than that obtained from the primary flashing units. After the low pressured turbine, the steam goes to main condenser in the single-flash design.

In the double-flash design, as the first step, the optimum primary separator pressures of NCG removal system options are determined. To be able to determine the optimum primary separator pressures, the net power output of each NCG removal system options are calculated for the primary separator pressures, which are taken as in the range of 340-1300 kPa with the secondary separator pressure of 100 kPa.

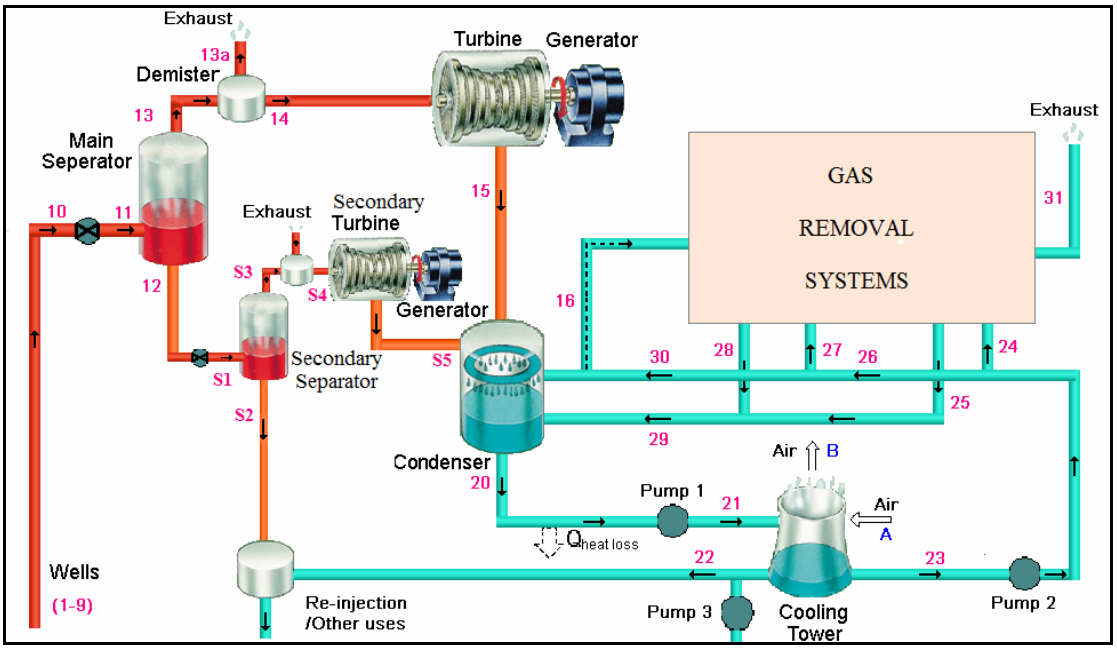

Figure 6.36. Flow diagram of double-flash design.

General assumptions, made for single-flash design, are valid for double-flash design. The net power output vs. primary separator pressure is shown on Figure 6.37 for 13% NCG fraction and 10 kPa condenser pressure. The pressures, at where the net power outputs are maximum, are determined as optimum primary separator pressures. Finally, the optimum primary separator pressure is 500 kPa for CS, 800 kPa for HS, 880 kPa for RS and 1080 kPa for SJES for the double-flash design.

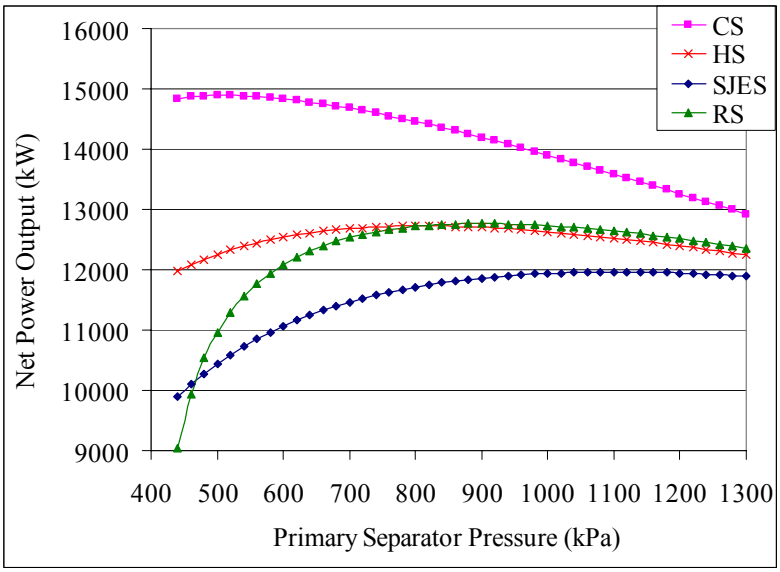

Figure 6.37. Net power output vs. primary separator pressure

As the second step of the double-flash design, the optimum secondary separators are determined by using optimum primary separator pressures of the each NCG removal system options. The net power output of the plant with different NCG removal system options vs. secondary separator pressure is shown in Figure 6.38. The range for the secondary separator pressure is taken as 60-260 kPa. The optimum secondary separator pressure is determined as 100 kPa for CS, 120 kPa for HS, 130 kPa for RS and 150 kPa for SJES.

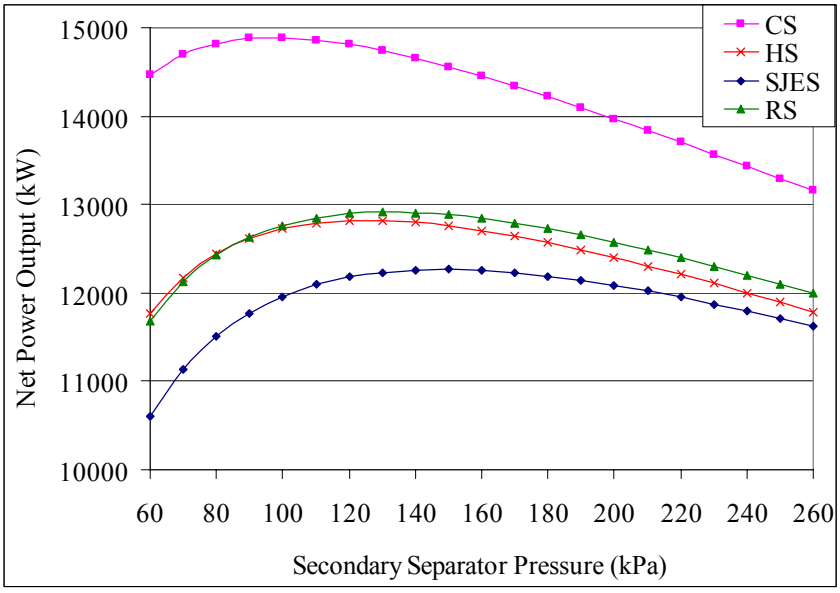

Figure 6.38. Net power output vs. secondary separator pressure.

6.2.1. Compressor System

The optimum primary and secondary separator pressures are determined as 500 kPa and 100 kPa, respectively. The second turbine of the double-flash design produces 5887 kW power. The additional investment cost of the double-flash design is calculated as 7,359,000 USD by 1250 USD/kW unit investment cost for 5887 kW the secondary turbine power output. In the economical analysis, interest rate, tax rate and O&M ratio are 15%, 20% and 5%, respectively. The electricity sales price is 0.0733 USD/kWh. The main results of the single-flash and double-flash design are given in Table 6.24.

Table 6.24. The comparison of the single-flash and double-flash design of CS.

	Single-flash Design	Double-flash Design
Net power output (kW)	10235	14887
Exergy losses from brine (kW)	24384	9463
Overall exergetic efficiency (%)	19.3	28.1
Total investment cost (Million USD)	23	30.36
NPV (Million USD)	2.91	7.827
IRR (%)	17.3	19.6
Cost of electricity production (USD/kWh)	0.069	0.064
SPT (year)	5.69	5.09

Table 6.24 indicates that, net power output of the double-flash plant with CS option is increased to 14,887 kW by 5298 kW net power output of the secondary turbine power output. The increment on the net power output of the plant equals to 45.45% of the net power output of the single-flash design.

6.2.2. Steam Jet Ejector System

Similar analyses have been conducted to double-flash plant with SJES which has 1080 kPa and 150 kPa optimum primary and secondary separator pressures. The comparison of the single-flash and double-flash design of SJES is given in Table 6.25.

Table 6.25. The comparison of the single and double-flash design for SJES.

	Single-flash Design	Double-flash Design
Net power output (kW)	5466	12268
Exergy losses from brine (kW)	24384	12463
Overall exergetic efficiency (%)	19.3	23.2
Total investment cost (Million USD)	17	30.18
NPV (Million USD)	-3.92	0.455
IRR (%)	10.7	15.3
Cost of electricity production (USD/kWh)	0.090	0.074
SPT (year)	8.43	6.33

The net power output is increased to 12268 kW from 5466 kW by a secondary flash. The 7202 kW increment represents 131% of the net power output of the single-flash design. 13.18 million USD additional investment cost changes to SJES investment to profitable with having positive sign NPV.

6.2.3. Hybrid System

By double-flash design, net power output of HS increases in the amount of 5371 kW, results 10% improvement on overall exergetic efficiency of the plant. Total investment cost is 28.83 million USD by around 10.5 million USD additional cost for double-flash design (Table 6. 26).

Table 6.26. The comparison of single-flash and double-flash design of HS.

	Single-flash Design	Double-flash Design
Net power output (kW)	7447	12818
Exergy losses from brine (kW)	24384	10743
Overall exergetic efficiency (%)	14.1	24.2
Total investment cost (Million USD)	18.25	28.83
NPV (Million USD)	0.36	3.617
IRR (%)	15.4	17.2
Cost of electricity production (USD/kWh)	0.074	0.069
SPT (year)	6.3	5.7

6.2.4. Reboiler System

In Table 6.27, single-flash and double-flash design of the plant with RS is compared. As it can be seen from the Table, the biggest improvement occurs on exergy losses from brine. While the exergy losses of the brine are 33339 kW for single-flash design, it reduces to 11335 kW by double-flash design. The net power output of the double-flash design reaches to 12914 kW.

Table 6.27. The comparison of the single and double-flash design for RS.

	Single-flash Design	Double-flash Design
Net power output (kW)	5667	12914
Exergy losses from brine (kW)	33339	11335
Overall exergetic efficiency (%)	10.7	24.4
Total investment cost (Million USD)	28.46	28.46
NPV (Million USD)	-3.34	4.318
IRR (%)	11.3	17.7
Cost of electricity production (USD/kWh)	0.087	0.068
SPT (year)	8.06	5.56

6.2.5. Comparison of NCG Removal Systems

The results on the net power plant increment with double-flash design are summarized in Table 6.28. Thermodynamic performance of single-flash plant can be improved by adding a second flash by 45.5-127.9%.

Table 6.28. Comparison of the net power outputs of the GPP with single-flash and double-flash design at 13% NCG fraction.

NCG Removal System	Single-flash Design (kW)	Double-flash Design (kW)	Increment	
			(kW)	(%)
CS	10235	14887	4652	45.5
SJES	5466	12268	6802	124.4
HS	7447	12818	5371	72.1
RS	5667	12914	7247	127.9

NCG removal system options are compared to each other according to NCG fraction. The optimum primary and secondary separator pressures are used in the comparison. NPV, IRR, cost of electricity production and SPT are calculated and shown on Figure 6.39. NPVs have positive sign for all NCG removal system options upto 15% NCG fraction. That means upto this point all of the NCG removal system options can be

profitable. But among the systems, while until 2% NCG fraction HS is the best option with the highest NPV and IRR, then CS is the best option for all NCG fractions. NPVs of RS and HS are close to each other. There is an intersection at around 8% NCG fraction. Until 8% NCG fraction HS is better than RS. On the other hand, even HS has the minimum cost of electricity production nearly for all NCG fractions, CS has the minimum SPT. In double-flash design, SJES is the worst option with minimum NPV and IRR, maximum cost of electricity production and SPT.

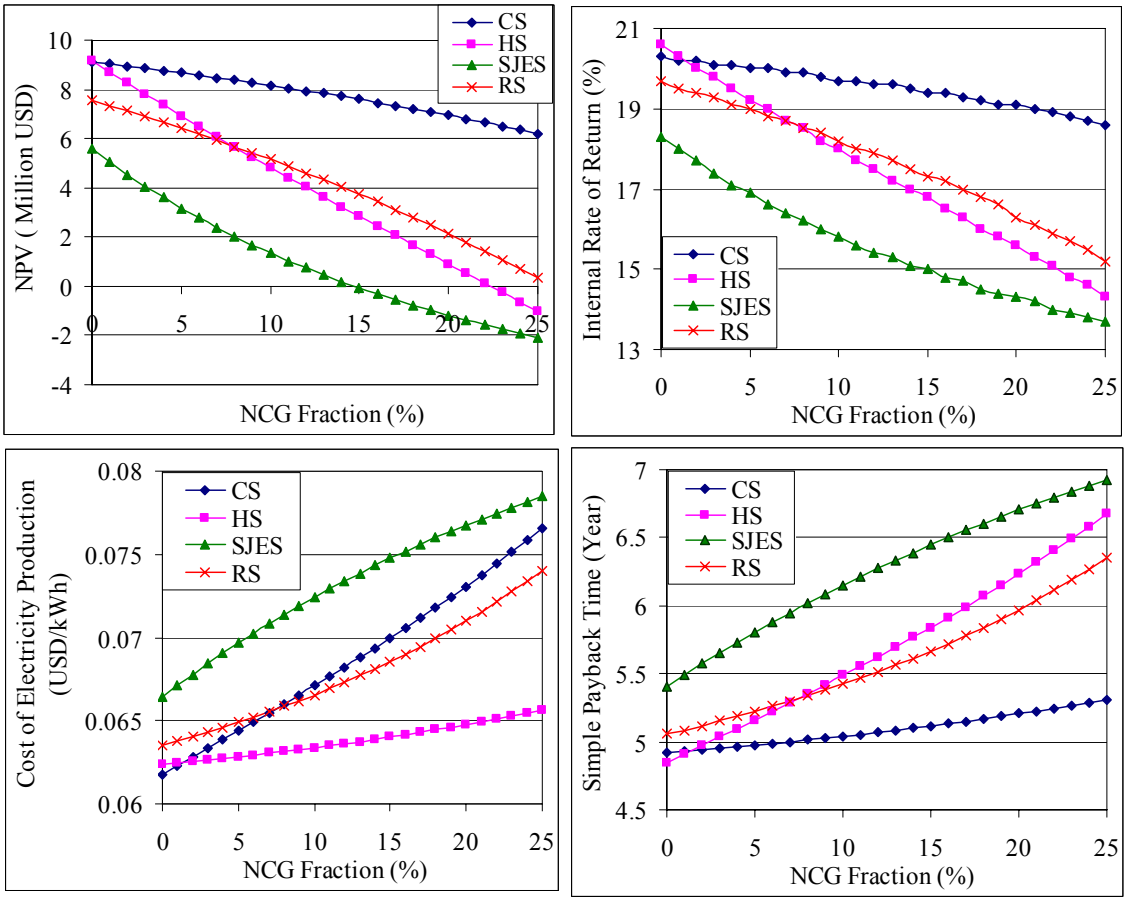

Figure 6.39. Comparison of the NCG removal system for double-flash design with optimum separator pressures.

CHAPTER 7

SUMMARY OF THE RESULTS

The results of modeling and simulation of flashed- steam GPPs are summarized in this chapter. The model is used the data of Kizildere GPP as input parameters. Simulation parameters are wet bulb temperature, separator pressure, condenser pressure, NCG fraction, turbine inlet temperature, interest rate, tax rate, O&M cost ratio, electricity sales price, unit cost of GPP and NCG removal systems.

7.1. Single-Flash GPPs

7.1.1. Mass and Energy Balances

- Optimum condenser pressure for each NCG removal system is determined as 10 kPa.
- Optimum separator pressures are determined as 220 kPa, 340 kPa, 500 kPa and 580 kPa for CS, HS, SJES and RS, respectively.
- The net power output of the plant is computed for 460 kPa, which is operational pressure of Kizildere GPP, and optimum separator pressures of each NCG removal system and results are exhibited in Table 7.1.

Table 7.1. Comparison of the net power outputs of the GPP at operational and optimum separator pressures for 13% NCG fraction.

NCG Removal System	Net Power Output (kW)			
	At Operational Separator Pressures	At Optimum Separator Pressures	Increment	
			(kW)	(%)
CS	10235	11436	1201	11.7
SJES	5466	5476	10	0.2
HS	7447	7712	265	3.6
RS	5667	6294	627	11.1

- 10°C increment in turbine inlet temperature causes approximately 2.3-2.6% increment in net power output.
- Net power output is decreased by 0.18% for CS, 0.37% for SJES and HS and 0.04% for RS by 1°C increment in wet bulb temperature.
- Specific steam consumption is the highest for RS and lowest for CS. As an example at 460 kPa separator pressure; for 2% NCG fraction, RS consumes 47.4% more steam than CS, for 13% NCG fraction it is 97.4%.
- 1% increment in NCG fraction results a decrement on net power output as 0.4% for CS, 2.2% for HS, 2.7% for SJES and 2.5% for RS.
- Based on the results of thermodynamic model, CS is the best gas removal option in terms of the highest net power output and lowest auxiliary power for Kizildere GPP operational conditions. On the other hand, RS is the worst option for entire NCG fraction range. HS is responded late to the change in NCG fraction because the LRVP is more efficient since its performance lies between CS and SJES.

7.1.2. Exergy Balance

- While CS has the highest overall exergetic efficiency of 19.3%, SJES has the lowest overall exergetic of 10.3% for operational condition of Kizildere GPP. The overall exergetic efficiency of HS and RS are 14.1% and 10.7%, respectively.
- SJES has the highest exergy loss on NCG removal system with 17.3% of the total exergy input. HS follows SJES with 9.6%. CS has the lowest exergy losses among NCG removal systems with 1%.
- The other equipment having the major exergy losses are turbine (5.2-10.4%), expansion valve and separator couple (2.2-6.1%), cooling tower (2-3.9%), condenser (1.6-3.2%) and generator (1.3-2.5%).
- The exergy destruction of brine discharge after flashing processes in the separators is 62.9% for RS and 46% for CS, SJES and HS of the total exergy input.

7.1.3. Economical Analysis

- Depending on the assumptions (investment cost, O&M ratio, tax rate etc.) electricity production cost per kWh is 0.069 USD for CS, 0.087 USD for RS, 0.074 USD for HS and 0.09 USD for SJES at 13% NCG fraction.
- IRR is 17.3%, 11.3%, 15.4% and 10.7% for CS, RS, HS and SJES, respectively.
- The SPT is 5.69 years for CS, 8.06 years for RS, 6.3 years for HS and 8.43 years for SJES.
- CS has the highest and most positive NPV value. HS follows CS. NPV of the reboiler and SJES are close to each other but these systems become profitable if the electricity sales prices are higher than 0.09 USD/kWh at 460 kPa separator pressure and 13% NCG fraction.
- According to the results of the economical analysis for 460 kPa separator pressure and 13% NCG fraction, among the NCG removal system options, CS is the best option with highest NPV and IRR, lowest SPT and cost of electricity production. HS and RS follow to CS and SJES is the worst option.
- The best NCG removal system option at 460 kPa separator pressure (Kizildere GPP operational condition) is SJES for 0-2% NCG fraction, HS for 2-10% NCG fraction and CS for 10 higher than 10% NCG fraction with the highest NPV, IRR and lowest SPT and cost of electricity production.
- If the GPP is operated at optimum separator pressures of each NCG removal system Upto 8% NCG fraction all NCG removal system options have positive NPV values. Among the systems HS is the most profitable options until the around of 6% NCG fraction. After this point, CS becomes to the most profitable options.
- The most profitable option is CS with the highest NPV and IRR values. One of the outcomes from the results that HS can be race against to CS, if the investment cost of HS NCG removal system is around 23% of the cost of CS.

7.2. Double-Flash GPPs

- The optimum primary separator pressure is determined as 500 kPa for CS, 800 kPa for HS, 880 kPa for RS and 1080 kPa for SJES for 13% NCG fraction.
- The optimum secondary separator pressure is determined as 100 kPa for CS, 120 kPa for HS, 130 kPa for RS and 150 kPa for SJES.
- The highest net power output is 14887 kW for CS by 4652 kW increment with double-flash design. The increment represents 45.5% of the net power output of the single-flash design. But especially, for SJES and RS the net power increment is very high in the amount of 124.4% and 127.9% of the single-flash design, respectively. The net power output is reached to 12268, 12818 and 12914 kW by double-flash design for SJES, HS and RS.
- By double-flash design NPVs have positive sign for all NCG removal system options up to 15% NCG fraction. That means up to this point all of the NCG removal system options can be profitable. But among them, while until 2% NCG fraction HS has the highest NPV and IRR, then CS has the best options for all NCG fractions. NPVs of RS and HS are close to each other. There is an intersection between them at around 8% NCG fraction. Until 8% NCG fraction HS is better than RS. On the other hand, even HS has the minimum cost of electricity production nearly for all NCG fraction, CS has the minimum SPT. In double-flash design, SJES is the worst option with minimum NPV and IRR, maximum cost of electricity production and SPT.

CHAPTER 8

CONCLUSIONS

A deterministic and static model of flashed-steam (single and double-flash) GPPs is developed and a code written in EES software to examine the effects of NCGs and gas removal systems. The modeled NCG removal system alternatives are compressor system (CS), steam jet ejector system (SJES), hybrid (steam jet ejector and LRVP) system (HS) and reboiler system (RS). Model is firstly run for Kizildere GPP input parameters. Then plant is simulated based on input variables, which are wet bulb temperature, separator pressure, condenser pressure, NCG fraction, interest rate, tax rate, O&M cost ratio and electricity sales price.

- **Wet bulb temperature**

  - Increasing wet bulb temperature causes a decrement on net power output and an increase in auxiliary power consumption with an increase in motive steam flowrate.

- **Separator and condenser pressures**

  - Optimum separator pressure which corresponds to the maximum net power output, is the highest for SJES and lowest for CS at the same NCG fraction and wet bulb temperature. Net power output of the plant decreases with increasing separator pressure with a decrease in steam flowrate feeding the turbine. This makes the situation more dramatic for steam jet ejectors in a feasibility study. To increase the power output, steam flowrate should be increased by drilling more wells which leads the higher cost of field development.
  - Thermodynamic performance of single- flash plant can be improved by 0.2-11.7% running the separator and condenser pressures on their optimum values. GPPs should be urged to operate around design conditions to generate optimum net power.

- **Interest rate, tax rate, O&M cost ratio and electricity sales price**
  - While profitability of the system increases with increasing electricity sales price, it decreases with interest and tax rate and O&M cost ratio.

- **NCG fraction**
  - NCG fraction is the most influencing factor on GPP performance.
  - CS is the most efficient and robust system where the influence of the NCG fraction is limited. On the other hand, SJES and RS are highly affected by increasing NCG fraction since motive steam flowrate to the steam jet ejectors are directly related to NCG fraction. Thus they exhibit as the worst case. HS is responded late to the change in NCG fraction because the LRVP is more efficient since its performance lies between compressors and steam jet ejectors.
  - The net power output and overall exergetic efficiency of single-flash GPP is decreased by
    - 0.4% for CS,
    - 2.2% for HS,
    - 2.5% for RS
    - 2.7% for SJES by 1% increment in NCG fraction.
  - Based on thermodynamic and economical simulations, SJES, HS and CS can be recommended to be used for a NCG fraction range of 0-2%, 2-10% and >10%, respectively.

- **Specific steam consumption**
  - For constant separator pressure and wet bulb temperature, specific steam consumption is highest for steam jet ejectors. The consumption becomes severe at higher NCG fractions.

- **Double-flash**
  - Thermodynamic performance of single-flash plant can be improved by adding a second flash by 45.5-127.9%.

It can be summarized that existance of NCGs in geothermal fluid cause a significant decrease in power production. Consequently, a special care should be taken to the NCG removal system.

Selection of the NCG removal system requires a detailed analysis depending on geothermal field, power plant, environmental and economical parameters. The developed code, provides a quick and easy way to determine the type and/or to evaluate the performance of gas removal systems.

The code would also be a useful tool for the pre-feasibility study of new plants and/or evaluation of the operational conditions of existing plants.

Furthermore, the code can be improved by adding time-varying interactions among variables (dynamic).

REFERENCES

Aksoy, N. Önsöz, *Jeotermal Enerjiden Elektrik Üretimi, TESKON,* Aksoy, N., Eds.; İzmir, 2007, pp. v (in Turkish).

Angulo, R.; Lam, L.; Gamiño, H.; Jiménez, H.; Hughes, E.E. Developments in Geothermal Energy in Mexico-Part Six. Evaluation of a Process to Remove Noncondensable Gases from Flashed Geothermal Steam Upstream of a Power Plant, *Heat Recovery Systems*, 1986, *6-4*, 295-303.

Aqui, A.; Aragones, J.S.; Amistoso, A.E. *Optimization of Palinpinon-1 production field based on exergy analysis-the southern negros goethermal field, Philippines*, Proceedings of World Geothermal Congress, Antalya, Turkey, 2005. Paper No 1312, 1–7.

ASPEN-HYSYS Home Page. http://www.aspentech.com/core/aspen-hysys.cfm (accessed May, 2010).

Awerbuch, L.; Van der Mast, V.; Soo-Hoo, R. Review of Upstream Geothermal Reboiler Concepts, *Geothermal Resources Council Transactions*, 1984, *8*.

Awerbuch,L.; Van Der Mast, V.C. Geothermal reboiler apparatus and method. U.S. Patent 4,534,174, 1985.

Barber Nichols Home Page. http://www.barber-Nichols.com/products/blowers_and_ compressors/turbocompressors/default.asp (accessed May, 2010).

Bertani, R. World geothermal power generation in the period 2001–2005, *Geothermics*, 2005, *34*, 651–69.

Bertani, R. *Geothermal Power Generation in the World 2005–2010 Update Report*, Proceedings of World Geothermal Congress, Bali, Indonesia, April 25-29, 2010.

Birgenheier, David B. et al. *Designing Steam-Jet Vacuum Systems, Chemical Engineering*, July 1993, www.graham-mfg.com/downloads/23.pdf (accessed 2008).

Bloomster, C.H.; Huber, H.D.; Walter, R.A. *GEOCOST: A Computer Program for Geothermal Cost Analysis*, Battelle Pasific Northwest Laboratories, Richland, Washington, 99352, 1975.

Bombarda, P.; Invernizzi, C.M.; Pietra, C. Heat recovery from Diesel engines: A thermodynamic comparison between Kalina and ORC cycles, *Applied Thermal Enginering*, 2010, *30*, 212-219.

Brugman, J.; Hattar, M.; Nichols, K.; Esaki, Y. *Next Generation Geothermal Power Plants*, Technical Report EPRI/RP 3657-01. Research supported in part by Office of Geothermal Technologies, U.S. Department of Energy: CE Holt Co., Pasadena, CA, February 1996.

Cadenas, R. Residual steam to energy: a project for Los Azufres geothermal field, Mexico, *Geothermics*, 1999, *28*, pp 395–423.

Cengel, Y.; Boles, M.A. *Thermodynamics An Engineering Approach* 6th Ed.; McGraw-Hill, 2006.

Cerci, Y. Performance evaluation of a single-flash geothermal power plant in Denizli, Turkey, *Energy*, 2003, *28*, pp 27-35.

Cisarova, K.; Kopal, J.; Kralovcova, J.; Maryska, J. *Simulation of Geothermal Processes*, Proceedings of World Geothermal Congress, Bali, Indonesia, April 25-29, 2010.

Coury, G.E. and Associates. *Upstream H_2S removal from geothermal steam*, Technical Report EPRI, AP-2100, 3.1-3.23. 1981.

Coury, G.E.; Babione, R.A.; Gosik, R.J. *A heat exchanger process for removal of H_2S gas*, Proceedings of 4th Annual Geothermal Conference and Workshop, CA-USA, 1980, 3.18-3.27.

Coury, G. *Geothermal Gas Abatement, Development of Geothermal Energy for Power and Non-Electrical Uses*, Technical report prepared by the United Nations in co-operation with the Government of the Philippines for a project of the United Nations Development Program, PHI/85/003. 1987.

Coury, G.; Guillen, H. V.; Cruz, D. H. *Geothermal noncondensable gas removal from turbine inlet steam*, Proceedings of the 31st Intersociety 3 Energy Conversion Engineering Conference, 1996.

Crest Renewable Energy Policy Project Home Page. http://www.crest.org, 2008 (accessed 2009).

Dagdas, A.; Ozturk, R.; Bekdemir, S. Thermodynamic evaluation of Denizli Kizildere geothermal power plant and its performance improvement, *Energy Conversion and Management*, 2005, *46*, pp 245-256.

DiPippo, R. The Effect of Expansion-Ratio Limitations on Positive-Displacement, Total-Flow Geothermal Power Systems, *Geothermal Resources Council Transactions*, 1982, *6*, pp 343-46.

DiPippo, R. Thermodynamic improvements on the direct-steam plant, *Geothermal Resources Council Transactions*, 1992, *16*, pp 547–552.

DiPippo, R. Second law analysis of flash-binary and multilevel binary geothermal power plants, *Geothermal Resources Council Transactions*, 1994, *18*, pp 505–510.

DiPippo, R. Second law assessment of binary plants generating power from low-temperature geothermal fluids, *Geothermics*, 2004, *33*, pp 565–586.

DiPippo, R. *Geothermal Power Plants Principles, Applications and Case Studies*, Elsevier Science, Oxford, UK, ISBN-10: 1856174743, 2005.

DiPippo, R.; Marcille, D.F. Exergy analysis of geothermal power plants, *Geothermal Resources Council Transactions*,1984, *8*, pp 47-52.

DPT, *Sekizinci Beş Yillik Kalkinma Plani*, Technical Report of Madencilik Özel İhtisas Komisyonu Enerji Hammaddeleri Alt Komisyonu Jeotermal Enerji Çalişma Grubu, DPT. 2609 – ÖİK. 620, 2001.
http://ekutup.dpt.gov.tr/madencil/enerjiha/oik620.pdf (accessed, 2010) (in Turkish).

Durak, S. *Jeotermal Enerjiye İlişkin Yasal Düzenleme ve Destekler*, Procedings of TMMOB Geothermal Congress, ANKARA, 2009, (In Turkish).

Duthie, R.G.; Nawaz, M. Comparison of Direct Contact and Kettle Reboilers to Reduce Noncondensables in Geothermal Steam, *Geothermal Resources Council Transactions*, 1989, *13*, pp 575-580.

Dünya, Huseyin, General Directorate of Mineral Research and Exploration, Turkey, Personal communication, 2008.

EIEI (Elektrik İşleri Etüt İdaresi) Genel Müdürlüğü, *Sanayide Enerji Yönetimi Esasları*, Volume IV, ISBN 975-7566-69-1, 1997 (in Turkish).

El-Wakil, *Geothermal Plant Technology*, McGraw-Hill Inc, NewYork, 1984, 859 pp.

Erdogdu, E. A Snapshot of Geothermal Energy Potential and Utilization in Turkey, *Renewable and Sustainable Energy Reviews*, 2009, *13*, pp 2535-2543.

Erdogmus, A.B. Economic Assessment of Balçova – Narlıdere Geothermal District Heating System. M.Sc. Thesis, Izmir Institute of Technology, Izmir, Turkey, 2003.

F-Chart Software Home Page. http://www.fchart.com/ees/ees.shtml (accessed 2009).

Forsha, M. *High Performance Turbocompressor for Noncondensable Gas Removal at Geothermal Power Plants*, Technical Report of Barber-Nichols Inc. DE-FG07-95ID13391, 1997.

Forsha, M.; Lankford, K. Turbine Driven Compressors for Noncondensable Gas Removal at Geothermal Steam Power Plants, *Geothermal Resources Council, Transactions*, 1994, *18*.

Forsha, M.; Nichols, K. E.; Shull, J. W.; Development and Operation of a Turbocompressor for Noncondensable Gas Removal at Geothermal Power Plants, *Geothermal Resources Council Transactions*, 1999, *23*.

GEA (Geothermal Energy Association) Home Page, *Factors Affecting Costs of Geothermal Power Development*. http://www.geoenergy.org/publications/reports/Factors%20Affecting%20Cost%20of%20Geothermal%20Power%20Development%20-%20August%202005.pdf, 2005 (accessed 2009).

GETEM Home Page. http://www1.eere.energy.gov/geothermal/getem.html (accessed 2010).

Geothermal Institute, *Geothermal Energy Systems*, Course notes of Geothermal Institute, Auckland University, Diploma course in energy technology (geothermal), 1996a, 87 pp.

Geothermal Institute, *Gas extraction system*, Course notes of Geothermal Institute, Auckland University, Diploma course in energy technology (geothermal), 1996b, 75 pp.

Geothermania Home Page. http://geothermania.blogactiv.eu/geothermal_energy/ultra_deep_drilling_technologies/kalina-cycle_2009_08_03/ (accessed 2010).

Gokcen, G.; Ozcan, N.Y. *Yoğuşmayan Gazların Jeotermal Santral Performansına Etkisi: Kizildere Jeotermal Santralı*, Jeotermal Enerjiden Elektrik Üretimi, TESKON, Aksoy, N., Eds.;İ zmir, 2007, pp. 205-18 (in Turkish).

Gokcen, G.G. Yoğuşmayan Korozif Gazların Jeotermal Buhardan Alınması İçin Tasarlanan Yoğuşturma/Kaynatma Modelli Isı Değiştirgeçleri (Reboilerler) Üzerinde Teorik ve Deneysel İncelemeler, Ph.D. Thesis, Ege Universitiy, Izmir, Turkey, 2000, 252 pp (in Turkish).

Gunerhan, G. G. An upstream reboiler design for removal of noncondensable gases from geothermal steam for Kizildere geothermal power plant, Turkey, *Geothermics*, 1999, *28*, pp 739-757.

Gunerhan, G. G.; Coury, G. *Upstream Reboiler Design and Testing for Removal of Noncondensable Gases from Geothermal Steam at Kizildere Geothermal Power Plant, Turkey*, Procedings of World Geothermal Congress, Kyushu-Tohoku, Japan, May 28-June 10, 2000.

Gunerhan, G. *An Upstream Re-Boiler Design for Removal of NCGs from Geothermal Steam*, Geothermal Institute Report, Report No: 96.10, University of Auckland, New Zealand, 1996.

Gupta H.; Roy, S. *Worldwide Status of Geothermal Resource Utilization*, Geothermal Energy, Elsevier, ISBN-13: 978-0-444-52875-9, 2007, pp 199-229.

Hall, N. R. *Gas extraction system*, Lecture notes of Geothermal Utilisation Engineering Geothermal Institute, The University of Auckland, New Zealand in M.G. Dunstall (eds.), 1996.

Hamano, H. Design a Geothermal Power Plant with High Noncondensable Gas Content, *Geothermal Resources Council Transactions*, 1983, *7*.

Hankin, J. W.; Cochrane, G. F.; Van der Mast, V. C. Geothermal Power Plant Design for Steam with High Noncondensable Gas, *Geothermal Resources Council, Transactions*, 1984, *8*.

Hasse, H.; Bessling, B.; Bottcher, R. *OPEN CHEMASIMTM: Breaking Paradigms in Process Simulation*, Proceedings of 16th European Symposium on Computer Aided Process Engineering and 9th International Symposium on Process Systems Engineering, 2006.

HEATMAP Home Page. http://www.energy.wsu.edu/software/heatmap.cfm (accessed 2010).

Holzbecher, E.; Sauter, M. *The Doublet System Simulator*, Proceedings of World Geothermal Congress, Bali, Indonesia, April 25-29, 2010.

Horie, T.; Muto T.; Gray, T. *Technical Features of Kawerau Geothermal Power Station, New Zealand*, Proceedings of World Geothermal Congress, Bali, Indonesia, April 25-29, 2010.

Hughes, E. Removal of hydrogen sulphide from geothermal steam. *EPRI Journal*, 1987, *12-7*, pp 38-42.

Kagel, A. *A Handbook on the Externalities, Employment, and Economics of Geothermal Energy*, Geothermal Energy Association, www.geo-energy.org, 2006, (accessed 2009).

Kalina, A.I. *New binary geothermal power system*. Proceedings of IGW-2003, Russia, p. 49.

Kanoglu M.; Çengel Y.A. Economic evaluation of geothermal power generation, heating, and cooling, *Energy*, 1999, *24*, pp 501-509.

Kanoglu M. Design and Optimization of Geothermal Power Generation, Heating and Cooling. Ph.D. Thesis, University of Nevada, Reno, 1999.

Kanoglu, M.; Dincer, I.; Rosen, M.A. Understanding energy and exergy efficiencies for improved energy management in power plants, *Energy Policy*, 2007, *35*, pp 3967-78.

Khalifa, H. E.; Michaelides, E. *The Effect of Noncondensable Gases on the Performance of Geothermal Steam Power Systems*, Report of Brown University, Contract No EY-76-S-02-4051, November, 1978.

Kim, S.K.; Bae, G.O.; Han, U.; Lee, K.K. *A Parallelized Model For Simulating A Vertical Closed-Loop Geothermal Heat Pump System*, Proceedings of World Geothermal Congress, Bali, Indonesia, April 25-29, 2010.

Kwambai, C. B. *Exergy analysis of Olkaria I power plant, Kenya*, Report of United Nations University Geothermal Training Programme, Reykjavik, Iceland, Report No. 5, 2005.

Kwambai, C.B. *Exergy Analysis of Olkaria I Power Plant, Kenya*, Proceedings of World Geothermal Congress, Bali, Indonesia, April 25-29, 2010.

Lehmann, W. *Liquid ring vacuum pumps and compressors with magnetic drive*, Leak-Free Pumps and Compressors Handbook, 1995, pp. 251-68.

Lund, J.W.; Lienau, P. J.; Lunis, B.C. *Geothermal Direct Use Engineering and Design Guidebook*, Contract Number DE-FG07-90ID 13040, United States of America, 1998, pp. 359-406.

Dickson, M.H.; Fanelli, M. *What is Geothermal Energy?,* Report of Istituto di Geoscienze e Georisorse, CNR , Pisa, Italy, Prepared on February 2004.

Michaelides, E. E. Separation of Noncondensables in Geothermal Installations by Means of Primary Flashing, *Geothermal Resources Council Transactions*, 1980, *4*.

Michaelides, E. E. The influence of Noncondensable Gases on the Net Work Produced by the Geothermal Steam Power Plants, *Geothermics*, 1982, *11-3*, pp 163-174.

Milicich, S.D.; van Dam, M.A.; Rosenberg, M.D.; Rae, A.J.; Bignall, G. *Earth Research 3-Dimensional Geological Modelling of Geothermal Systems in New Zealand- a New Visualisation Tool*, Proceedings of World Geothermal Congress, Bali, Indonesia, April 25-29, 2010.

Mlcak, H.A. *An introduction to the Kalina cycle*. Proceedings of the International Joint Power Generation Conference, PWR, In: Kielasa, L. and Weed, G.E. (editors),30, 11 pp, 1996.

Moghaddam, A.R. *A conceptual Design of A Geothermal Combined Cycle and Comparison with a Single-Flash Power Plant for Well NWS-4, Sabalan, Iran*, Report of the United Nations University Geothermal Training Programme, Reykjavik, Iceland, Report No:18, Pp:391-428, 2006.

Montero, G. *Evaluation of the network of a turbine operated by a mixture of steam and non-condensable gases*, Proceedings of 12th New Zealand Geothermal Workshop,1990, 11, pp 163–174.

Moya, P.; DiPippo, R. *Miravalles Unit 3 Single-Flash Plant, Guanacaste, Costa Rica: Technical and Environmental Performance Assessment*, Proceedings of World Geothermal Congress, Bali, Indonesia, April 25-29, 2010.

NASH, *Gas Extraction Systems for Geothermal Power Plants*, Report of NASH, Gardner Denver Liquid Ring Pump Division, Geothermal WP-1034A-0806, 2006.

Ozturk, H. K.; Atalay, O.; Yilanci, A.; Hepbasli, A. Energy and exergy analysis of Kizildere Geothermal Power Plant, Turkey, *Energy Sources, Part A: Recovery Utilization and Environmental Effects*, 2006, *28*, pp. 1415-1424.

Palen, J.W. *Shell and tube reboilers*, Heat Exchanger Design Handbook 3/A, E.U. Schlünder, et al. Eds.; Hemisphere Publishing Corporation, 1984.

Putten, H.; Colonna, P. Dynamic modeling of steam power cycles: Part II- Simulation of a small simple Rankine cycle system, *Applied Thermal Engineering*, 2007, *27*, pp. 2566-82.

RetScreen Home Page. http://www.retscreen.net/ang/power_projects_geothermal_power.php (accessed 2010).

Rosen, M.; Dincer, I. Exergy as the confluence of energy, environment and sustainable development. *Int. J. on Exergy*, 2001, *1*, pp. 3-13.

Rosen, M.A. Second law analysis, approaches and implications, *Int. J. of Energy Research*, 1999, *23*, pp. 415-29.

Rosen, M.A. Does industry embrace exergy?, *Int. J. on Exergy*, 2002, *2-4*, pp. 221-223.

Sabatelli, F.; Mannari, M. *Latera development update*. CD Transactions of World Geothermal Congress, Florence, Italy, 1995, 3, pp. 1785-1789.

Sener, A.C.; Uluca, B. *Türkiye Elektrik Piyasalari ve Jeotermal Enerjinin Konumu*, Jeotermal Enerji Semineri Kitabi, TESKON, Aksoy, N. Eds.; 2009.

Serpen, U.; Aksoy, N.; Öngür, T.; Korkmaz, E.D. Geothermal energy in Turkey: 2008 update, *Geothermics*, 2009, *38*, pp. 227–237.

Siregar, P. H. H. *Optimization of Electrical Power Production Process for the Sibayak Geothermal Field, Indonesia*, Report of the United Nations University Geothermal Training Programme, Reykjavik, Iceland, Report No:16, Pp. 349-76, 2004.

Spirax Sarco Home Page. http://www.spiraxsarco.com/resources/steam-engineering-tutorials/steam-engineering-principles-and-heat-transfer/steam-consumption-of-heat-exchangers.asp (accessed 2010).

Sugar Engineers Home Page. http://www.sugartech.co.za/vacuum/vacuumpump.php (accessed 2010).

Swandaru, R. B. *Thermodynamic Analysis of Preliminary Design of Power Plant Unit I Patuha, West Java, Indonesia*, Report of the United Nations University Geothermal Training Programme, Reykjavik, Iceland, Report No:7, Pp. 83-119, 2006.

Swandaru, R. B. Modelling and Optimization af Possible Bottoming Units for General Single-flash Geothermal Power Plants. M.Sc. Thesis, Department of Mechanical and Industrial Engineering University of Iceland, 2009.

Tajima, S.; Nomura, M. Optimization of Non-Condensable Gas Removal System in Geothermal Power Plant, *Geothermal Resource Council Transactions*, 1982, *6*, pp. 397-400.

Tanaka, T.; Itoi, R. *Development of Numerical Modeling Environment for TOUGH2 Simulator on the Basis of Graphical User Interface (GUI)*, Proceedings of World Geothermal Congress, Bali, Indonesia, April 25-29, 2010.

Triyono, S. *Thermodynamic and Economic Assessment of Power Plant Expansion from 140 to 200 MW In Kamojang – Indonesia*, Report of Geothermal Training Programme, Report No: 14, The United Nations University, Reykjavik, Iceland, 2001.

TTMD, *Meteorological Data of Turkey*, Technical Publication of Turkish Society of HVAC & Sanitary Engineers, 2000 (in Turkish).

Vorum M.; Fritzler E.A. *Comparative Analysis of Alternative Means for Removing Non-Condensable Gases From Flashed-Steam Geothermal Power Plants*, Report of NREL SR-550-28329, Colorado, The USA, 2000.

Wallace, K.; Dunford, T.; Ralph, M.; Harvey, W. *Aegean Steam: Germencik Dual Flash Plant*, GeoFund, IGA Geothermal Workshop "Turkey 2009", Istanbul, Turkey, February 16-19, 2009.

World Energy Council Home Page http://www.worldenergy.org/publications (accessed 2010).

Yildirim, E. D.; Gokcen, G. Exergy analysis and performance evaluation of Kizildere geothermal power plant, Turkey, *Int. journal of Exergy*, 2004, *1-3*, pp 316-333.

APPENDIX A

AIR TO STEAM RATIO

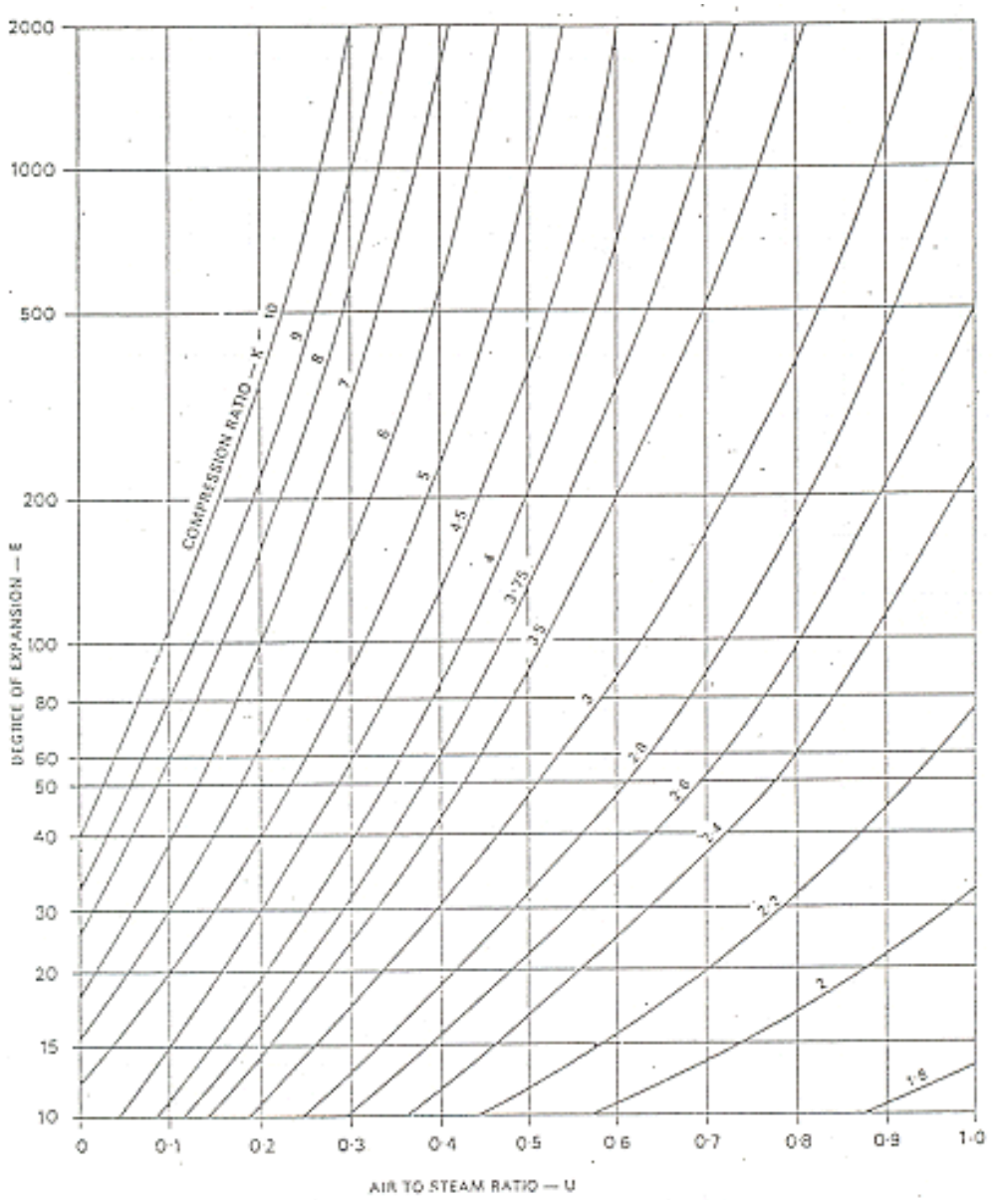

Figure A. 1. Air to steam ratio curve.
(Source: Geothermal Institute, 1996b)

APPENDIX B

CASH FLOW

Table B. 1. Cash flow of CS.

Year	CS					
	Book Value (USD)	Amortization Cost (USD)	Revenue (USD)	O&M Cost (USD)	Tax (USD)	Net Revenue (USD)
0	23,000,000					
1	20,700,000	2,300,000	5,917,468	1,150,000	493,494	4,273,974
2	18,630,000	2,070,000	5,917,468	1,150,000	539,494	4,227,974
3	16,767,000	1,863,000	5,917,468	1,150,000	580,894	4,186,574
4	15,090,300	1,676,700	5,917,468	1,150,000	618,154	4,149,314
5	13,581,270	1,509,030	5,917,468	1,150,000	651,688	4,115,780
6	12,223,143	1,358,127	5,917,468	1,150,000	681,868	4,085,599
7	11,000,829	1,222,314	5,917,468	1,150,000	709,031	4,058,437
8	9,900,746	1,100,083	5,917,468	1,150,000	733,477	4,033,991
9	8,910,671	990,075	5,917,468	1,150,000	755,479	4,011,989
10	8,019,604	891,067	5,917,468	1,150,000	775,280	3,992,188
11	7,217,644	801,960	5,917,468	1,150,000	793,101	3,974,366
12	6,495,879	721,764	5,917,468	1,150,000	809,141	3,958,327
13	5,846,291	649,588	5,917,468	1,150,000	823,576	3,943,892
14	5,261,662	584,629	5,917,468	1,150,000	836,568	3,930,900
15	4,735,496	526,166	5,917,468	1,150,000	848,260	3,919,207
16	4,261,946	473,550	5,917,468	1,150,000	858,784	3,908,684
17	3,835,752	426,195	5,917,468	1,150,000	868,255	3,899,213
18	3,452,177	383,575	5,917,468	1,150,000	876,778	3,890,689
19	3,106,959	345,218	5,917,468	1,150,000	884,450	3,883,018
20		3,106,959	5,917,468	1,150,000	332,102	4,435,366

Table B. 2. Cash flow of SJES.

Year	SJES					
	Book Value (USD)	Amortization Cost (USD)	Revenue (USD)	O&M Cost (USD)	Tax (USD)	Net Revenue (USD)
0	17,000,000					
1	15,300,000	1,700,000	3,160,223	850,000	122,045	2,188,178
2	13,770,000	1,530,000	3,160,223	850,000	156,045	2,154,178
3	12,393,000	1,377,000	3,160,223	850,000	186,645	2,123,578
4	11,153,700	1,239,300	3,160,223	850,000	214,185	2,096,038
5	10,038,330	1,115,370	3,160,223	850,000	238,971	2,071,252
6	9,034,497	1,003,833	3,160,223	850,000	261,278	2,048,945
7	8,131,047	903,450	3,160,223	850,000	281,355	2,028,868
8	7,317,943	813,105	3,160,223	850,000	299,424	2,010,799
9	6,586,148	731,794	3,160,223	850,000	315,686	1,994,537
10	5,927,533	658,615	3,160,223	850,000	330,322	1,979,901
11	5,334,780	592,753	3,160,223	850,000	343,494	1,966,729
12	4,801,302	533,478	3,160,223	850,000	355,349	1,954,874
13	4,321,172	480,130	3,160,223	850,000	366,018	1,944,204
14	3,889,055	432,117	3,160,223	850,000	375,621	1,934,601
15	3,500,149	388,905	3,160,223	850,000	384,263	1,925,959
16	3,150,134	350,015	3,160,223	850,000	392,042	1,918,181
17	2,835,121	315,013	3,160,223	850,000	399,042	1,911,181
18	2,551,609	283,512	3,160,223	850,000	405,342	1,904,880
19	2,296,448	255,161	3,160,223	850,000	411,012	1,899,210
20		2,296,448	3,160,223	850,000	2,755	2,307,468

Table B. 3. Cash flow of HS.

Year	HS					
	Book Value (USD)	Amortization Cost (USD)	Revenue (USD)	O&M Cost (USD)	Tax (USD)	Net Revenue (USD)
0	18,250,000					
1	16,425,000	1,825,000	4,305,558	912,500	313,612	3,079,446
2	14,782,500	1,642,500	4,305,558	912,500	350,112	3,042,946
3	13,304,250	1,478,250	4,305,558	912,500	382,962	3,010,096
4	11,973,825	1,330,425	4,305,558	912,500	412,527	2,980,531
5	10,776,443	1,197,383	4,305,558	912,500	439,135	2,953,923
6	9,698,798	1,077,644	4,305,558	912,500	463,083	2,929,975
7	8,728,918	969,880	4,305,558	912,500	484,636	2,908,422
8	7,856,027	872,892	4,305,558	912,500	504,033	2,889,024
9	7,070,424	785,603	4,305,558	912,500	521,491	2,871,567
10	6,363,382	707,042	4,305,558	912,500	537,203	2,855,854
11	5,727,043	636,338	4,305,558	912,500	551,344	2,841,714
12	5,154,339	572,704	4,305,558	912,500	564,071	2,828,987
13	4,638,905	515,434	4,305,558	912,500	575,525	2,817,533
14	4,175,015	463,891	4,305,558	912,500	585,833	2,807,224
15	3,757,513	417,501	4,305,558	912,500	595,111	2,797,946
16	3,381,762	375,751	4,305,558	912,500	603,461	2,789,596
17	3,043,586	338,176	4,305,558	912,500	610,976	2,782,081
18	2,739,227	304,359	4,305,558	912,500	617,740	2,775,318
19	2,465,304	273,923	4,305,558	912,500	623,827	2,769,231
20		2,465,304	4,305,558	912,500	185,551	3,207,507

Table B. 4. Cash flow of RS.

Year	RS					
	Book Value (USD)	Amortization Cost (USD)	Revenue (USD)	O&M Cost (USD)	Tax (USD)	Net Revenue (USD)
0	18,500,000					
1	16,650,000	1,850,000	3,276,433	925,000	100,287	2,251,146
2	14,985,000	1,665,000	3,276,433	925,000	137,287	2,214,146
3	13,486,500	1,498,500	3,276,433	925,000	170,587	2,180,846
4	12,137,850	1,348,650	3,276,433	925,000	200,557	2,150,876
5	10,924,065	1,213,785	3,276,433	925,000	227,530	2,123,903
6	9,831,659	1,092,407	3,276,433	925,000	251,805	2,099,627
7	8,848,493	983,166	3,276,433	925,000	273,653	2,077,779
8	7,963,643	884,849	3,276,433	925,000	293,317	2,058,116
9	7,167,279	796,364	3,276,433	925,000	311,014	2,040,419
10	6,450,551	716,728	3,276,433	925,000	326,941	2,024,492
11	5,805,496	645,055	3,276,433	925,000	341,276	2,010,157
12	5,224,946	580,550	3,276,433	925,000	354,177	1,997,256
13	4,702,452	522,495	3,276,433	925,000	365,788	1,985,645
14	4,232,207	470,245	3,276,433	925,000	376,238	1,975,195
15	3,808,986	423,221	3,276,433	925,000	385,642	1,965,790
16	3,428,087	380,899	3,276,433	925,000	394,107	1,957,326
17	3,085,279	342,809	3,276,433	925,000	401,725	1,949,708
18	2,776,751	308,528	3,276,433	925,000	408,581	1,942,852
19	2,499,076	277,675	3,276,433	925,000	414,752	1,936,681
20		2,499,076	3,276,433	925,000	29,529	2,380,961

VITA

Nurdan YILDIRIM ÖZCAN, borned in 1977 in Kutahya-TURKEY. She graduated from Dokuz Eylul University at Mechanical Engineering Department in 1999. Then, she got M.Sc. degree in 2003 at Mechanical Engineering Department of Izmir Institute of Technology. Between the year of 2000-2010, she worked as a research assistant at Mechanical Engineering Department of Izmir Institute of Technology. She is working as a Project Manager in a private company in Izmir. She joined a six-month "United Nations Geothermal Training Programme" in 2002 at Reykjavik, Iceland, received an Iceland government and United Nations University fellowship. In 2005, she attended a nine-month "Diploma Course on Environmental and Applied Fluid Dynamics Department" at Von Karman Institute for Fluid Dynamics, Belgium, received a NATO fellowship. She studies mainly on geothermal energy, geothermal district heating system modeling, heat pump systems and geothermal power plants. She is married and has a three-year old daughter.

The publications of her are listed below:

Journals:

1. "Piping Network Design of Geothermal District Heating Systems: Case Study for a University Campus", *International Journal of Energy (in press)*.
2. "Thermodynamic Assessment of Gas Removal Systems for Single-flash Geothermal Power Plants", *Applied Thermal Engineering*, Issue 29/2009, Pages 3246–53.
3. "Effect of Non-Condensable Gases on Geothermal Power Plant Performance. Case Study: Kizildere Geothermal Power Plant-Turkey", *International Journal of Exergy*, Volume 5, Issue 5-6/2008, Pages 684-95.
4. "District heating system design for a university campus", *International Journal of Energy and Buildings*, Volume 38, Issue 9/2006, Pages 1111-19.
5. "Modelling of Low Temperature Geothermal District Heating Systems", *International Journal of Green Energy*, Volume 1, Number 3/2004, Pages 365-79.